

INVERSE SIMULATION FOR CARDIAC ARRHYTHMIA

Der Fakultät für Mathematik
der Otto-von-Guericke-Universität Magdeburg
zur Erlangung des akademischen Grades

doctor rerum naturalium
(Dr. rer. nat.)

am 07.02.2018 vorgelegte Dissertation

von Diplom-Mathematiker FLORIAN KEHRLE

Florian Kehrle

Diplom-Mathematiker

Institut für Mathematische Optimierung
Otto-von-Guericke-Universität Magdeburg
Gebäude 02
Universitätsplatz 2
39106 Magdeburg
Germany

florian.kehrle@ovgu.de

Mathematics Subject Classification (2010): 90C26; 90C90; 92C50

Zusammenfassung

Das Ziel der vorgelegten Arbeit ist die Entwicklung einer algorithmischen Methode zur inversen Simulation von Herzrhythmusstörungen. Konkret wird die mathematische Anwendung des offenen klinischen Problems der Differenzierung von verschiedenen atrialen Tachykardien untersucht. Die folgenden Beiträge werden zum Stand der Technik geleistet.

- Es wird ein gänzlich neues Konzept zur Modellierung atrioventrikulärer (AV) Vorgänge entwickelt, um die elektrischen Prozesse im menschlichen Herzen sowohl im Ganzen als auch im Detail besser beschreiben zu können. Daher werden die Funktionsweise des Herzens sowie die komplexen Leitungseigenschaften zwischen Vorhof und Herzkammer untersucht.
- Hierzu werden mehrere Modellierungstechniken aus verschiedensten Blickwinkeln analysiert, die sowohl statistische als auch first principle Methoden auf zellulärer Basis beinhalten. Das Hauptaugenmerk liegt jedoch auf phenomenologischen Modellen, welche die elektrischen Vorgänge des AV Knotens prognostizieren können. Diese spezielle Art mathematischer Modelle kann leicht "vorwärts" berechnet werden falls alle patientenabhängigen Modellparameter bekannt wären. In unserem Fall einer inversen Simulation entsteht jedoch ein Nicht-Standard Optimierungsproblem. Die verknüpfte kombinatorische und nichtlineare Struktur, in Verbindung unterschiedlicher Dimensionen auf mehreren Block-Ebenen, erschweren diese Problemklasse.
- Dieses inverse Simulationsproblem wird durch den Vergleich der Zielfunktionswerte und anschließender Optimierung angegangen, ausgehend von einem regelmäßigen Signaleingang. Dadurch ist unser neu entwickelter Algorithmus in der Lage die meisten Merkmale des AV Knotens einfacher, exakter und effektiver zu beschreiben. Wir haben es weiterhin geschafft die Komplexität des vorliegenden Diskriminierungsproblems innerhalb der genutzten Modelle und Algorithmen drastisch zu reduzieren. Diese Optimierungen führen zu einer enormen Laufzeitbeschleunigung, die ein diagnostisches Ergebnis innerhalb weniger Sekunden garantiert.
- Als Teil dieser Arbeit haben wir die wohl weltweit größte Datenbank mit verifizierten Testfällen der betreffenden Herzrhythmusstörungen erstellt. Die numerischen Ergebnisse beinhalten eine ausführliche Validierung der präsentierten mathematischen Methoden und Algorithmen. Diese werden sowohl auf der gesammelten Datenbasis getestet, als auch gegenüber medizinischen Experten, sowie anderen computerbasierten Algorithmen.
- Wir haben einen speziell zugeschnittenen Lösungsalgorithmus entwickelt, implementiert und evaluiert. Dieser übertrifft Standardverfahren um mehrere Größenordnungen in Bezug auf Laufzeit, Sensitivität und Spezifität. Das Resultat beinhaltet ein kom-

plettes Softwarepaket, inklusive mobiler Applikation, welches imstande ist, einem Arzt direkt am Krankenbett eines Patienten diagnostische Unterstützung zu geben.

Die Relevanz des vorliegenden Problems wird durch die große Anzahl der Fehldiagnosen, die in aktueller Literatur beschrieben werden, weiter verdeutlicht. Ein wichtiges Resultat der vorliegenden Arbeit ist mit Sicherheit, dass die hier entwickelten mathematischen Werkzeuge in der Lage sind dieses medizinische Problem in Gänze zu lösen. Infolgedessen schafft die mathematische Grundlage ein besseres Verständnis der Mechanismen im AV Knoten, die zu einem korrekt diagnostizierten und potentiell geheilten Patienten führen könnten.

Abstract

This dissertation aims at developing an algorithmic approach to the inverse simulation for cardiac arrhythmia. More specifically, the open clinical problem of differentiating various atrial tachycardias is examined as mathematical application. The following contributions to the state of the art are accomplished.

- An entirely new concept to model atrioventricular (AV) dynamics is developed in order to describe the electrical processes in the human heart more complete and better in detail. Thus, the functionality of the heart is explored as well as the complex conduction characteristics between atria and ventricles.
- Various modeling techniques from different perspectives are analyzed to approach the specific problem. Statistical as well as first principle methods on a cellular basis are investigated. The main focus however, lies on phenomenological models which are able to predict the electrical conduction phenomena of the AV node. This kind of mathematical model can be easily simulated forward if all patient-specific model parameters were known. In our context of an inverse simulation though a non-standard optimization problem arises. The combined combinatorial and nonlinear nature together with variable dimensions on different block levels make this problem class difficult.
- This inverse simulation problem is solved by the comparison of objective function values assuming a regular input and a subsequent optimization. Thus, our newly developed algorithmic concept is able to explain most of the AV node characteristics easier, more precise and effective. We further managed to drastically reduce the complexity of the existing discrimination problem which leads to an enormous run time acceleration and providing a diagnostic result within just a few seconds.
- As part of the thesis we established the worldwide largest database with verified cases of the considered cardiac arrhythmia. The numerical results include a detailed validation of the presented mathematical models and algorithms on this data set, against physicians, as well as other computerized algorithms.
- We develop, implement and evaluate a specifically tailored solution algorithm that outperforms standard approaches by orders of magnitude with respect to run time, sensitivity and specificity. In consequence, our software package, including a mobile app, is able to assist a physician with a diagnostic result right at the patients bedside.

The large number of misinterpretations reported in recent literature further proves the relevance of the present problem. One important result of this thesis is clearly that the developed mathematical tools are able to solve this medical application problem from start to finish. In consequence, the mathematical basis creates a better understanding of the AV node mechanisms, which could lead to correctly diagnosed and potentially cured patients.

Contents

0	Introduction	1
1	The Human Heart	5
1.1	A Historical Introduction to Cardiac Electrophysiology	5
1.2	Anatomy and Normal Physiology	9
1.3	The Cardiac Conduction System	11
1.3.1	Cardiac Conduction Overview	11
1.3.2	Cardiac Rate Control	14
1.3.3	Summary	15
1.4	Cellular Level	15
1.5	Electrocardiogram	19
1.5.1	Standard 12-lead ECG	20
1.5.2	Reading an ECG	21
1.6	Cardiac Arrhythmias	23
1.6.1	Classification of Cardiac Arrhythmias	23
1.6.2	Sinus Node Abnormalities	25
1.6.3	Atrial Abnormalities	25
1.6.4	Atrioventricular Abnormalities	27
1.6.5	Ventricular Arrhythmias	29
1.6.6	Methods of Treatment	30
2	AV Nodal Characteristics in Supraventricular Tachycardias	35
2.1	Differentiation of Regular Atrial Tachycardias from Atrial Fibrillation	35
2.1.1	Reasons for the Misinterpretation of AFib and AFlut	36
2.1.2	Misinterpretation Examples Documented in Literature	37
2.2	Classical AV Block Type Definitions	38
2.2.1	Type I Block	39
2.2.2	Type II Block	42
2.2.3	Advanced Second-Degree AV Block	43
2.3	Multilevel AV Block (MAVB)	44
2.4	Combined Multilevel Concept for Second-Degree AV Block	46
3	Modeling Atrioventricular Dynamics	49
3.1	Statistical Approaches	50
3.1.1	RR Interval Periodicity	50
3.1.2	Heart Rate Variability and Poincaré Plots	51

3.2	First Principle Models	52
3.2.1	Hodgkin-Huxley Model	52
3.2.2	Noble Model	54
3.2.3	Ion Pumps, Exchangers, and Calcium Dynamics	56
3.2.4	AV Node Models	57
3.2.5	Discussion	60
3.3	Phenomenological Models of the AV Junction	62
3.3.1	Classical AV Block Type Models	63
3.3.2	AV Nodal Recovery Curve Models	66
3.3.3	Combined Multilevel Model	70
4	Algorithms & Implementation	73
4.1	Signal Processing Methods for ECG Analysis	73
4.1.1	Filtering ECG Signals and R Wave Detection	74
4.1.2	Established ECG Interpretation Algorithms	75
4.1.3	Signal Processing Methods for Discriminating AFlut from AFib	77
4.1.4	Discussion	78
4.2	HEAT Software Package	80
4.2.1	Overview	80
4.2.2	Data Acquisition	82
4.2.3	Solution Space	83
4.2.4	Combined Multilevel Algorithm	88
5	Numerical Results	103
5.1	Verification Requirements	103
5.1.1	Heidelberg University Hospital Data Set	104
5.1.2	Objective Functions	104
5.1.3	Receiver Operating Characteristic	106
5.2	Validation of Statistical Approaches	108
5.2.1	RR Interval Periodicity	108
5.2.2	Heart Rate Variability and Poincaré Plots	108
5.3	Validation of Phenomenological Approaches	110
5.3.1	Classical AV Block Type Models and the First Multilevel Approach	110
5.3.2	Recovery Curve Approach	111
5.4	Detailed Validation of the HEAT Algorithm	113
5.4.1	HEAT Validation Against Other Data Sets	113
5.4.2	Validation Against Heidelberg University Hospital Data Set	119
5.4.3	Validation Summary	123
6	Summary	127

A Models & Algorithms 131

B Solutions 133

Bibliography 141

Nomenclature 155

List of Figures 158

List of Tables 159

List of Acronyms 161

Chapter 0

Introduction

In 1628, Dr. William Harvey (1578–1657) laid the foundation for the modern view of the cardiovascular system with his publication “*On the Motion of the Heart and Blood in Animals*” [51]. He is most famous for discovering the circulation of blood in the body and its connection to the heart’s motion. Previously, the theory of Galen of Pergamon¹ was prevalent that the venous and arterial systems are separated. It was believed, that liver and heart are producing blood out of food for the separated systems of veins and arteries, while organs somehow “consuming” the blood. For today’s point of view, this theory sounds rather strange although it was valid for almost 1500 years until Harvey disproved it.

He started with a simple but clever question: “*How much blood is pumped into the body with every heart beat?*”² To solve this question, he used a very systematic approach with a combination of careful observations of the biological system, formulation of hypotheses, modeling the system, calculations, and conclusions. He actually calculated the total amount of blood that would be produced depending on Galen’s theory. Even with very low estimations of heart beat and pumping capacity he came to a value of 7 to 15 liters of blood per half hour, which could obviously not be possible. On the one hand, that is more blood than the whole body consist of, and on the other hand, this enormous amount should be produced out of food. [7]

The calculation was only the beginning and one disproof of the general assumption about the blood flow, while his publication contained a lot more interesting and important achievements. This specific discovery, however, was probably the *first significant application of mathematics in biology*. And as Dr. Harvey about 400 years ago, we want to contribute to the field of medical science in this thesis and investigate, so far, unclear biological processes with the help of existing and newly developed mathematical tools. Therefore, we use nowadays mathematical methods, modeling, and optimization, to explore the dynamics of the human heart and especially the complicated AV characteristics during arrhythmia.

Motivation

Cardiovascular diseases are the number one cause of death throughout the world. In 2015, over 17 million people were killed by this cause, which corresponds to 3 in every 10 deaths. Of those, estimated 7.4 million people died of coronary heart disease and 6.7 million from stroke. Since 2000, cardiovascular diseases gained dramatically and are responsible for over 2 million more deaths today [158]. One type hereof are cardiac arrhythmias like atrial fibrillation and atrial flutter. These are the most common arrhythmias in humans and, on a

¹Claudius Galenus, 129–200 AD

²Original formulation: “...and how much blood it will project into the aorta upon each contraction” [51], Chapter IX

more detailed level, also belong to the top 10 causes of deaths, especially in older people. In 2015, atrial fibrillation and atrial flutter were solely responsible for 5.4% of all deaths, which are 19265 people for Germany [27]. Although, atrial fibrillation is the most frequent arrhythmia in adults atrial flutter is under recognized in clinical practice. Especially in the growing number of people over 50 years, the incidence of atrial flutter is particularly high. According to Granada et al. [49], there are estimated over 200000 *new* flutter patients per year in the US. Transferred to Germany, this would be about 57000 new flutter patients per year. For these reasons, our main focus lies in the open clinical problem to distinguish regular atrial tachycardias including atrial flutter (AFlut)³ from atrial fibrillation (AFib).

Over the past decades, there have been a lot of improvements in cardiology, especially in the field of cardiac electrophysiology. A better understanding of the heart's activities and new treatment methods have been developed successfully. But still, several electrophysiological processes are not completely understood. Despite all progress, both in expert's knowledge as in sophisticated analysis tools, large numbers of misinterpretations are reported in recent literature. Especially in cases of irregular ventricular response to regular atrial activation, AFlut is often wrongly diagnosed as AFib. If we have a closer look at the misinterpretation rates reported the problem gets even clearer. Incorrectly differentiated AFlut from AFib by physicians or algorithms are reported from 15% and go up to 80% for atypical atrial flutter. Even in low estimations, there are assumed to be lots of undetected AFlut patients. [75, 57, 14, 78, 131]

In consequence, misdiagnosed patients could be supplied with a wrong, and if worst comes to the worst, with an even harmful treatment. This is because both arrhythmias have to be treated differently. For AFib the state of the art treatment is still antiarrhythmic therapy. While AFlut on the other hand, can be treated and cured with a success rate of over 95% by a 3D mapping guided catheter ablation [128]. To further illustrate the importance, wrongly given antiarrhythmic agents come with severe side effects to the point of stroke risk and increased mortality rate. On the contrary, the correctly diagnosed and cured patients could have an enormous improvement in their quality of life.

Contributions

In 2000, a leading expert in electrophysiology Douglas P. Zipes noted that the atrioventricular (AV) node is still "a riddle wrapped in a mystery inside an enigma" [100]. With this dissertation, we claim to have improved the knowledge about these processes and dynamics in the AV node, especially in the diseased heart, by using state-of-the-art mathematical methods in combination with existing and newly developed mathematical models. We managed to build a novel algorithmic approach that is able to explain most of the AV node characteristics easier, more precise and effective. This is based on our specifically designed *combined multilevel* concept of the conduction mechanisms in the AV node. Therefore, we managed to reduce the complexity of the highly nonlinear nature of the present problem drastically. Thus, it is possible to receive a diagnostic result within just a few seconds and solely based on the input data of only a few RR intervals. This fact offers many advantages compared to other approaches, which is also denoted in detail.

³Unless noted otherwise, we include regular atrial tachycardias in the abbreviation of AFlut for simplicity reasons.

The entire approach is put to the acid test at the worldwide largest database with verified cases of the considered cardiac arrhythmia that we managed to establish. Furthermore, our algorithm is validated at other data sets from literature, compared against physicians, as well as other algorithms. In conclusion, we developed, implemented and evaluated this specifically tailored solution algorithm that outperforms standard approaches by orders of magnitude with respect to run time, sensitivity and specificity. In consequence, our software package, including a mobile app, is able to assist a physician with a diagnostic result right at the patients bedside.

Thesis Overview

Chapter 1 gives a basic introduction to **The Human Heart**. We start with a historical view on the field of cardiac electrophysiology, followed by a closer look at the anatomy and physiology of the human heart, its conduction system and the different cardiac cell types. How to read an ECG and finally several kinds of arrhythmias are shown, as well as their treatment possibilities in specific.

Chapter 2 reveals the **AV Nodal Characteristics in Supraventricular Tachycardias**. We describe the difficulties that arise in discriminating regular atrial tachycardias from atrial fibrillation. The incidence of the classical AV block types is shown, based on the medical literature, followed by an exact definition of the specific types of second-degree AV blocks. The basic idea of the Multilevel AV Block (MAVB) as well as various medical verification examples are presented. Based on these researched facts, a new *combined multilevel concept* for second-degree AV blocks is developed in order to describe the electrical processes more complete and better in detail.

Chapter 3 gives detailed insight about different approaches of **Modeling Atrioventricular Dynamics**. At first, statistical approaches for discriminating AFlut from AFib are described. Then, there is an extensive section about first principle models, from the first cardiac cell model to modern AV node models. Here, it is also discussed in which cases these models do work properly and why they are not advisable in our considered problem. After these very detailed models on cellular basis we focus on a higher level of abstraction, namely on phenomenological models of the AV junction. In this section, the first exact mathematical definitions of the classical AV block types are given to our knowledge. In addition, the foundation of the newly developed combined multilevel approach is laid with the mathematical description of the multiple block levels. Besides, several methods of another phenomenological approach is described in detail with the AV nodal recovery curve.

Chapter 4 presents **Algorithms & Implementation** to solve the existing discrimination problem for cardiac arrhythmias. A short introduction to signal processing methods is given which can be used to filter the ECG signal and detect R waves for example. Established ECG interpretation algorithms are analyzed, while we also compare the various algorithmic approaches against each other as regards diagnostic skills and necessary input data. Finally, all components of our newly developed **Heidelberg Electrocardiogram Analysis Tool (HEAT)** software package are examined in detail which specifies “the heart” of this dissertation. The software includes various user handling options in form of a desktop PC version as well as a mobile app by which a physician is able to receive a diagnosis result right at the patients bed

side. Furthermore, there are various options implemented from R wave detection to several diagnostic skills, as well as algorithmic optimizations. We also define the solution space for the used model and algorithm on the medical basis of the previous chapters, which helps to reduce the complexity of the problem enormously. At the end of this chapter, the particular HEAT algorithm is illustrated in detail which is able to detect regular atrial tachycardia including atrial flutter and to solve present discrimination problem.

In **Chapter 5** the ideas, mathematical models, and algorithms, which are presented and developed in this thesis are tested in real world application data to get detailed **Numerical Results**. Therefore, we built up a huge data set of intracardiac electrograms of supraventricular tachycardias and also use well known data sets as an additional validation. Then, we define various objective functions that are used to receive the best possible result. Further verification methods are explained before we validate and compare the HEAT algorithm to literature studies made with physicians as well as to other approaches and algorithms. Finally, these numerical results and the additional detailed validation at the our own data set proves the quality of our research.

Chapter 6 In the final chapter, the results and contributions of this thesis are once again overviewed as a **Summary**. This includes a final comparison overview of our software package against other approaches and applied on other data sets. Here, we also give an impression of the medical achievements that has been investigated.

Chapter 1

The Human Heart

In the first chapter, we want to provide a basic introduction to the human heart, its functionality as well as pathological variations. This means that we have to take a closer look at the medical branch of cardiology, including the anatomical structure and the physiology of the heart. Our main focus however, lies in the field of *cardiac electrophysiology* as a “science of elucidating, diagnosing, and treating the electrical activities of the heart”¹.

We start with a historical introduction in cardiac electrophysiology to get access to the field. The anatomical structure of the heart, as well as its physiology is described in the second section, followed by the electrical connections of the cardiac conduction system. After a closer look at different cardiac cell types and how they operate, we give a brief introduction in ECG analysis and the difficulties of ECG diagnostics. Finally, we show different kinds of arrhythmias, in particular the tachycardias of atrial flutter and atrial fibrillation, and their different kinds of treatment.

1.1 A Historical Introduction to Cardiac Electrophysiology

From an Electric Current to the Electrocardiograph

In 1786, the Italian anatomist Luigi Galvani accidentally made an important discovery for a major invention of the medical discipline, what would later become cardiac electrophysiology. At a dissection of a frog, its leg came in touch with two dissimilar metals. In combination with the salty water in the legs, he created an electric circuit (which he was not aware of at this time). Galvani thought, he found something he called *animal electricity* and noted that “all the muscles of the legs seemed to contract again and again as if they were affected by powerful cramps” [44]. Later, his name was given to the *galvanometer*, an instrument for creating and measuring electric current, which became a precursor to the *electrocardiograph*.

With his discoveries, Galvani made important contributions to the knowledge of electrophysiology. Nevertheless, the foundation for modern electrophysiology was laid by the Italian physicist and mathematician Carlo Matteucci in 1842. At a pigeon’s heart, he showed that electric current attends at each heart beat [99]. Just one year later the German physiologist Emil Du Bois-Reymond confirmed Matteucci’s findings, while examining frogs, and described an action potential (AP) that accompanies muscular contraction [30]. For this discovery, Du Bois-Reymond is known as pioneer in experimental electrophysiology. In 1856, Rudolph von Kölliker and Heinrich Müller were the first, who actually succeeded, recording a cardiac action potential. They also confirmed that an electric current is present at every contraction of the heart [151].

¹Definition of Wikipedia, The Free Encyclopedia

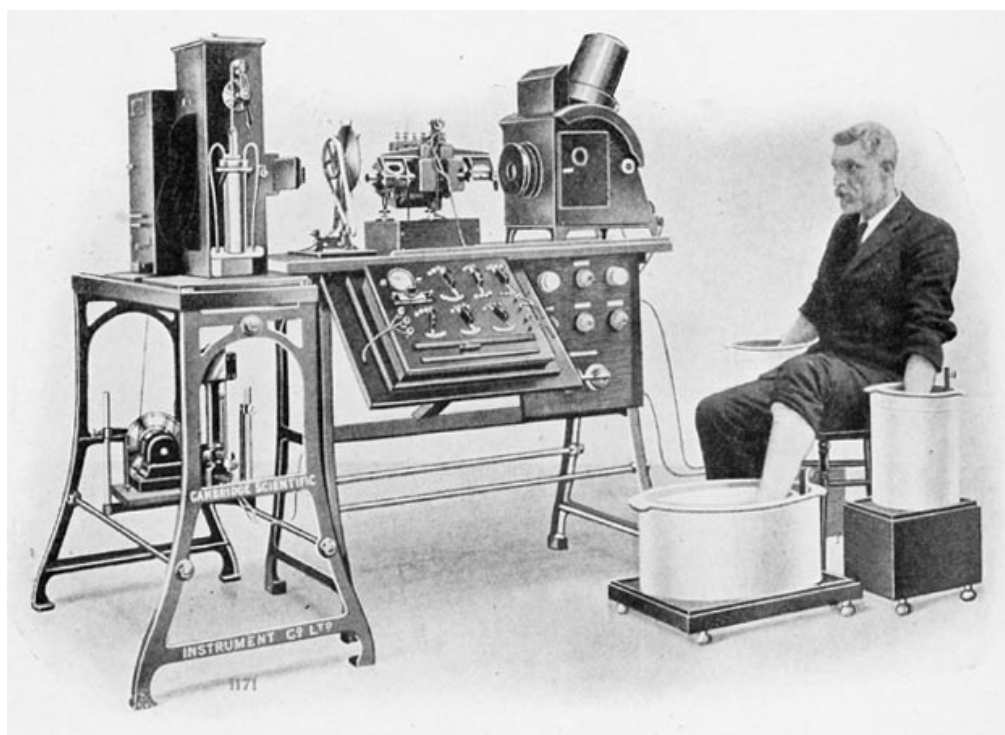


Figure 1.1: Willem Einthoven using the first table-model electrocardiograph manufactured by the Cambridge Scientific Instrument Company in 1911. His hands and one foot are immersed in jars of salt solution. On the right hand side is the arch lamp, in the center on the table the string galvanometer and below the switching board for the leads. Left to the camera comes the timer (rotating wheel with spokes) and on the left hand side the falling-plate camera.²

The first human electrocardiogram (ECG) was published by the British physiologist Augustus D. Waller in 1887 [152]. Two years later he presented his technique to record an ECG at the *First International Congress of Physiologists* in Basel, performing an ECG ablation at his dog. At this congress the Dutch Willem Einthoven saw Waller demonstrate his experiment. Inspired by this performance, Einthoven spent the 1890s focusing on the heart's electrical activity. He introduced the term electrocardiogram (although he later said that Waller used it before him) and improved the electrometer. In 1902, Einthoven published the first ECG recorded on a modified and more sensitive string galvanometer [34], which is known as the invention of the *electrocardiograph*, see also Figure 1.1. This invention was by any doubt, the most important improvement for diagnostics in cardiac electrophysiology, to discover the heart and its diseases. [137, 43]

²From "A History of Electrocardiography", by Burch and De Pasquale, p. 33 [15]. This image is in public domain because its copyright has expired.

The Beginning of Heart Beat Analysis and ECG Diagnosis

The real analysis of the heart and diagnosis of its diseases, came with the technical appliances in this area. Altogether, cardiology is one of the most technology dependent fields in medicine for diagnosing patients. This goes back to 1819, when the French physician René Laennec made the invention of the stethoscope [80]. But the actual starting point for cardiac diagnostics has been the electrocardiograph. First fundamental discoveries were made by the inventor Einthoven that each contraction comes with five electrical deflections. He labeled these P, Q, R, S, and T [33], which are still used today as declarations for the deflections in an ECG. Furthermore, Einthoven introduced the three-lead ECG, which was used the first decades of the 20th century, using only three bipolar electrodes placed in a triangle, known as *Einthoven Triangle*. He received the Nobel Prize in 1924, “for his discovery of the mechanism of the electrocardiogram”³ [137]. In 1934, Frank Norman Wilson added six additional chest leads, based on his idea of unipolar leads, which made the ECG description more detailed [160]. Emanuel Goldberger refined Wilson’s unipolar concept in 1942 and added the limb leads augmented voltage left (aVL), augmented voltage right (aVR) and augmented voltage foot (aVF) [47, 48]. Taken together the 12-lead-ECG was created, which still is the main concept today. A more detailed explanation of the ECG, as well as analyzing techniques are given in Section 1.5.

In 1906, Einthoven published a paper showing normal and abnormal ECG’s. He described, arrhythmias like ventricular premature beats, complete heart blocks, atrial flutter, and for the first time atrial fibrillation [35]. However, some arrhythmias were known earlier, they could poorly be detected by the sphygmograph⁴ and, e.g., atrial fibrillation wasn’t noted at all. The findings of Einthoven were probably the crucial point, for the importance of the electrocardiograph in medical practice. The British cardiologist Thomas Lewis wrote about the new possibilities of the electrocardiogram: “You will know how blind we have been to things which, once seen, are so apparent...the awakening was a sudden one”[89]. Lewis was the first one to realize the clinical use of the electrocardiograph, for which Einthoven dedicated his Nobel Prize to Lewis in 1924. Additionally, he played a major role identifying the sinus node as origin of the electric impulse in the heart. [56]

Beside the findings of arrhythmias, the knowledge about a blocking in the conduction system increased. The actual AV node was discovered by Tawara in 1906 [144]. Nevertheless, already in 1899, Karel Frederik Wenckebach pioneered at an experiment with frogs, in finding the progressive conduction lengthening, which lead to a conduction block [154]. This type of AV block is later known as Wenckebach phenomenon. In 1905, John Hay discovered at pressure recordings a second block type in the AV node [52]. Woldemar Mobitz recaptured both findings in 1924 [105], based on the electrocardiogram and classified the different AV blocks as Mobitz type I and type II. Most of these theoretical investigations go back to the first half of the 20th century and led to an increasing importance of the electrocardiograph and its application in medical examination. As a result it created an entirely new clinical discipline in cardiology, the *cardiac electrophysiology*. [2]

³Official prize motivation by nobelprize.org

⁴A machine which recorded the pulse and blood pressure

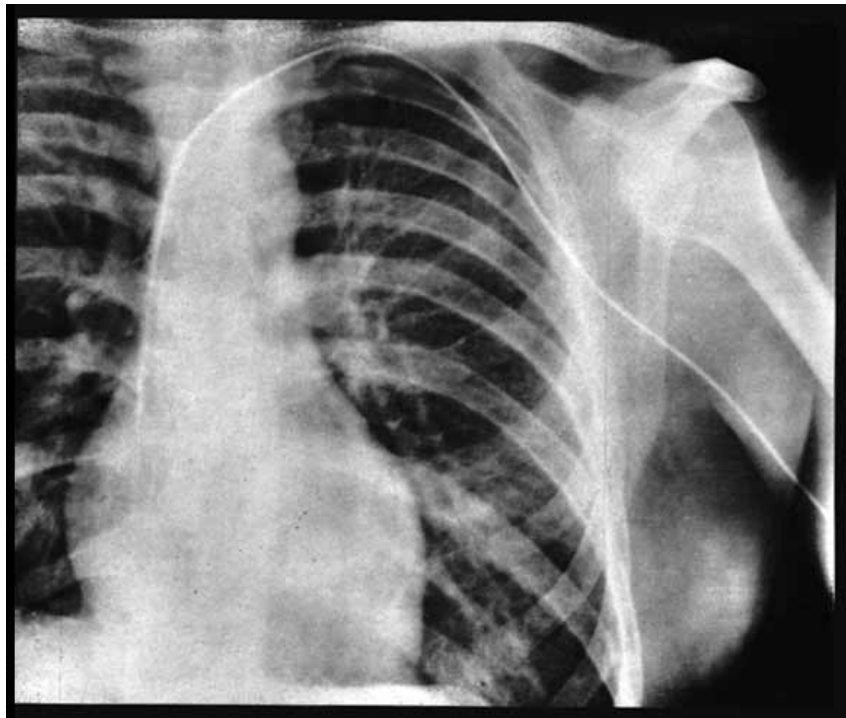


Figure 1.2: X-ray of Forßmann putting a catheter up his left arm to the right atrial chamber.⁵

Technological Improvements and Methods of Treatment

For ECG diagnosis just as for the methods of treatment, a further and major breakthrough was the development of the catheter technique. In 1929, the young intern Werner Forßmann performed the first right heart catheter examination at himself, by putting a catheter 65 centimeters up his left arm to the heart and looking at it on an X-ray screen (see Figure 1.2). He published the successful approach [41], for which he gained a lot of attention in the following, although he got offended and even fired for some time by his superior Sauerbruch. Later, the Americans André Frédéric Cournand and William Richards picked up and continued his work, for which the three scientists finally got rewarded by a delayed Nobel Prize in 1956. [54]

The start of computerized ECG analysis goes back to Hubert v. Pipberger. In 1959, his group were the first to describe the digital conversion of an ECG by a computer, testing a series of almost 1000 ECG's [148]. This was enhanced by Stallmann and Pipberger two years later by the automatic computer recognition of ECG waves [139]. With this work and his continuing effort, Pipberger set the basis for an objective ECG analysis and a standardization in ECG interpretation. [120]

⁵From "Über die Sondierung des rechten Herzens", by Forßmann, p. 2 [41]. This image is in public domain because its copyright has expired.

The foundation for a (non-drug) treatment of cardiac arrhythmias, was laid in 1899, by Jean-Louis Prevost and Frédéric Battelli, both professors at the university of Geneva. They applied large electrical voltages on a dog's heart and discovered that this can stop ventricular fibrillation [119]. In 1947, Claude Beck was the first to successfully defibrillates a human heart during cardiac surgery [12]. The rise of catheter ablation and its combination with the programmed stimulation technique, led to a much better understanding of the electrophysiology of the heart. Due to the intravascular catheters, which could be placed nearly everywhere in the heart, such things as refractory period of atrium, AV conduction, a variety of tachycardias, and much more, could be explored in detail. While drug therapy for arrhythmias became more and more popular in the 1970s, non-drug treatment improved as well [66]. In 1978, Michel Mirowski et al. built an implantable defibrillator, which could detect heart rhythm changes from normal to abnormal ventricular fibrillation and prevent sudden cardiac death by bringing the heart back to sinus rhythm [104]. Finally, the catheter technique led to a method, which could not only diagnose, but treat (and cure) some of the arrhythmias. Today, the *catheter ablation* is the state-of-the-art treatment technique for most supraventricular tachycardias [84].

However, technology is a major factor as a tool of treatment in the progress of electrophysiology, a crucial point lies in the underlying mechanisms. In this thesis, we use mathematical methods with the purpose to improve the understanding of those mechanisms and to provide tools for more accurate diagnoses, by using modern computer technology.

1.2 Anatomy and Normal Physiology

The heart is a muscular hollow organ that pumps about 5 to 6 liters of blood per minute through the cardiovascular system of the human body. It is located between the right and left lung in a spot called *mediastinum*, within the chest cavity. A typical male heart weights about 300 to 350 g and has the approximate dimensions of $12 \times 8 \times 6$ cm. [114]

Heart Structure and Blood Circulation

Having a closer look on the inside, see also Figure 1.3, the heart consists of four main chambers, two superior *atria* (*A*) and two inferior *ventricles* (*V*). The atria are used to receive blood from the veins, whereas the ventricles are larger and stronger to pump blood into the arteries of the body. Besides, the right hand side is responsible for the circulation of the deoxygenated blood from the body (inferior and superior *vena cava*), to the lungs (left and right *pulmonary arteries*). Therefore, this part of the cardiac conduction system is referred to as *pulmonary circulation*. The chambers on the left hand side, however, control the *systemic circulatory loop*. Here, the oxygenated blood from the lungs (left and right *pulmonary veins*) is conducted to the left atrium and pumped into the aorta by the left ventricle, which leads to all the extremities of the body.

The different states of the cardiac muscle cells of any chamber are either contracted (*systole*), to push blood out, or relaxed (*diastole*), to allow the blood to flow in. The arterial pressure in systole and diastole phase are, by the way, stated while measuring the blood pressure.

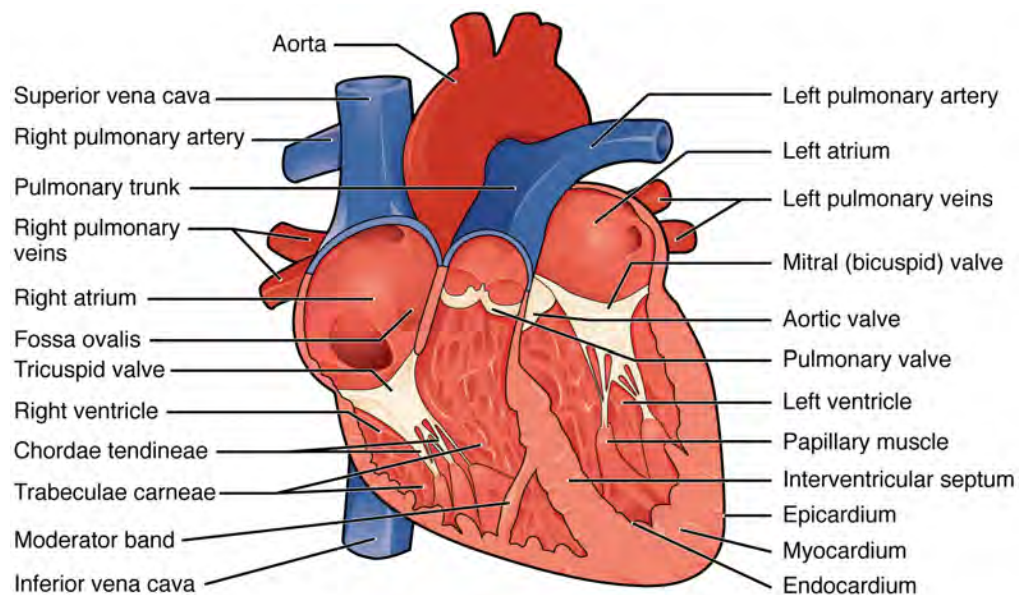


Figure 1.3: Internal anatomy of the human heart. Blue components indicate deoxygenated blood pathways and red components indicate oxygenated pathways.⁶

When all heart chambers are in diastole, it is called *relaxation phase*. Within this phase the ventricles fill up to 75% of their volume, before they get fully filled after atrial systole. [59, 70]

Heart Valves

Separating the four heart chambers, the *septum* is an extension of surrounding connective tissue and also contains the heart valves. Those determine the one-way direction of the blood flow. There are the *atrioventricular valves*, naturally located between both atria and ventricles. Furthermore, the *semilunar valves* with a different, half-moon shape, which open to the aorta and the pulmonary arteries. The AV valves are attached by strong strings on the ventricular side to the papillary muscles, called *chordae tendineae*. Those are necessary, because the blood pressure on the atrial side, is much lower than on the ventricular one and these strings prevent the valves from being pushed back into the atrium. The semilunar valves shut only with the blood pressure from the arteries and therefore don't need those additional strings. The snap shut of the heart valves, creates the typical two heartbeat sounds, one can hear using a stethoscope. [70, 59]

⁶From "Anatomy & Physiology", by OpenStax College, 2015 [114]. Licensed under *Creative Commons Attribution License (by 4.0)*.

Heart Layers

On the outside, the heart is surrounded by the *pericardium*. This connective tissue is constructed like a sac, which contains of two, toward each other movable layers. Between those layers is the lubricating *serous fluid* that reduces friction when the heart contracts. Inside the pericardium lies the actual, three-layer *heart wall*, which also surrounds each chamber. The *epicardium* constitutes the outermost level of the heart wall and is continuous with the pericardium. The middle layer is composed of muscle cells, which are responsible for the contraction of the heart chambers. This *myocardium* is by far the thickest layer, whereat its thickness depends on the required muscular strength. Hence, the myocardium surrounding the left ventricle is much thicker than on the right hand side. The innermost layer is called *endocardium* and provides smooth blood flow. [70, 59]

1.3 The Cardiac Conduction System

In the previous section, we described the blood flow through the heart, triggered by the contraction of the myocardium. Now, we give an insight to the electrical connections and the workflow of the cardiac conduction system. This is followed by the general cardiac rate control with the automatic control mechanisms and the conduction velocity of the different heart regions.

1.3.1 Cardiac Conduction Overview

For a regular blood flow through the heart, some source of energy is required. Basically, all cardiac muscle cells are capable to initiate an electrical stimulus, even without any nerve impulse. This so-called *autorhythmicity* distinguishes them from all other muscle cells in the human body. Nevertheless, this ability is developed differently and only some myocardial cells are responsible for electrical conduction, whereas the major part are contractile cells. In any case, for a fast and well-coordinated process of the electrical activity of atrial and ventricular chambers, a structured cardiac conduction system is essential. [59, 66, 5]

Sinus Node and Atrial Stimulation

Within the cardiac system, there are several areas an impulse passes through. As primary electrical stimulus act the *pacemaker cells* in the sinoatrial (SA) or sinus node. It initiates a regular electrical pattern at a healthy heart, called *sinus rhythm*. These pacemaker cells, just like other specialized conduction cells, are slightly different compared to the contractile cells, as their ability to contract is underdeveloped. A more detailed view on both cell types is given in Paragraph 1.4. The sinus node is located at the top of the right atrium, as can be seen in Figure 1.4. [59, 70]

From the sinus node, the stimulation spreads throughout the right atrium, and over the *Bachmanns Bundle* to the left atrium, for their contraction. The theory of three *internodal tracts* or *pathways*⁷, carrying the conduction to the AV node, has been subject of controver-

⁷Anterior, middle or Wenckebach, and interior or Thorel pathway

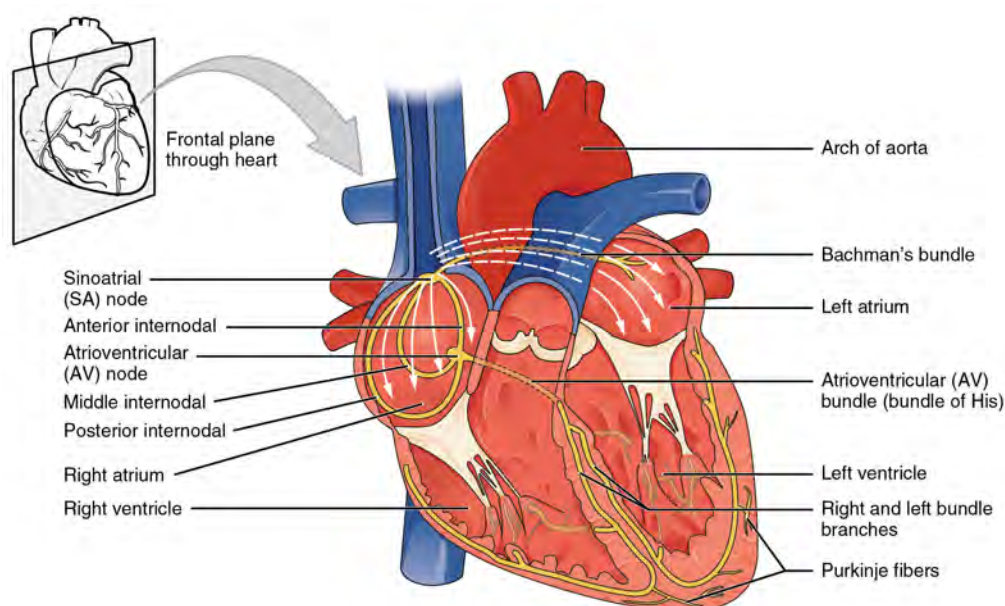


Figure 1.4: The electrical conduction system of the heart.⁹

sial debates over the last decades [59]. This idea of specialized routes with a physiological difference, goes back to 1907, when Wenckebach described such a pathway [156]. A second one was specified by Thorel in 1909 [145, 146] and a third by James in 1963 [63]. The tracts were functionally confirmed in dog hearts, where a block of all three pathways generally results in a junctional rhythm⁸ [85]. However, no histological difference was found in the atrial cells [103, 3].

In 1910, after a meeting of the German Pathological Society, Mönckeberg and Aschoff published three criteria, which define conducting tracts [107, 6]. The cells should be histologically distinct from others. Secondly, they pointed out the ability to follow the tracts through serial sections. And thirdly, the tract cells are supposed to be insulated by a fibrous sheath from the non-contractile myocardium. As stated by Meredith [103], it is probably more an issue of definition. While no presence of insulated atrial tracts have been found [4], there appears to be a similar arrangement of rapidly conducting atrial fibers in those areas [67].

Atrioventricular Node

The AV node was first described in 1893 by Wilhelm His [68]. Sunao Tawara confirmed the existence of this critical component within the cardiac conduction system in 1906 [144]. It

⁸Abnormal heart rhythm created by the AV node region, see Paragraph 1.3.2

⁹From "Anatomy & Physiology", by OpenStax College, 2015 [115]. Licensed under *Creative Commons Attribution License (by 4.0)*.

is the second junction of contractile cells, located at the apex of the *triangle of Koch*, which lies in the lower septum of the right atrium [76]. Its major function is to prevent the stimulation from spreading out directly into the ventricles. It delays the electrical impulse and therefore permits the atria to pump the blood into the ventricles, before their contraction. On the other hand, the AV node is responsible to prevent the ventricles from a too frequent contraction at extremely high sinoatrial stimulation rates, e.g., within atrial fibrillation (see Section 1.6). Hence, the conduction time of the electrical activity through the AV node can vary or a signal can even be completely blocked. [96, 163, 59]

Furthermore, the AV node has the ability to act as a secondary pacemaker, further discussed in Paragraph 1.3.2. According to Mönckeberg and Aschoff, both AV and SA node, do not fulfill the criterion of the insulation from surrounding myocardial cells. This is caused by the fact that both nodes have to interact somehow with the adjacent muscular tissue. Therefore, the AV node consists of two areas of different cell types, a compact AV node, about 5 to 7 mm × 3 to 4 mm in size, which is surrounded by a *transitional zone*. This zone works as connection between the compact node and the atrial myocardium. The *transitional cells* are in fact a crossing in morphology and function between compact node cells and atrial working cells. [163, 5, 126]

Unfortunately, it is still not completely clear, how to bring some of the electrophysiological and anatomical data together. An example is the *dual pathway physiology*, for which Moe et al. provided evidence for the first time in 1956 [106]. It has been demonstrated that a sudden lengthening within the atrioventricular conduction can be induced, via programmed electrical premature stimulation. Referring to the sudden conduction delay, it was supposed that there is a so-called *slow* and a *fast pathway* present. This phenomenon is especially common during AV nodal reentry tachycardia (AVNRT) (see also 1.6). Basically, there are two anatomical distinct input areas within the AV junction, which has been dedicated to the fast (anterior AV septum), respectively slow pathway (inferior nodal extension). But, recent visualizations of the conduction via optical mapping has shown that the signal travels broadly through this zones rather than through special pathways. Hence, no specific cell type could be assigned to fast or slow pathway. It was assumed previously that the transitional cells potentially built the fast pathway, due to a faster conduction velocity. The visualization techniques exposed, however, that the dual pathway phenomenon is probably more a question of distance rather than conduction velocity. [163, 58, 101, 96]

Bundle of His, Bundle Branches, and Purkinje Fibers

The *bundle of His*¹⁰ directly ties in with the AV node in the cardiac conduction system. In contrast to the AV node, which lies in the atrial muscular tissue, the bundle of His is the first part of the ventricular conduction pathway [101]. It spreads into a left and right bundle branch, also called *Tawara branches*. The bundle of His and the Tawara branches can be seen as a good example for the specialized conduction tracts and in fact do fulfill all criteria defined by Mönckeberg and Aschoff [3].

The two branches take the signal to the *Purkinje fibers*, which are myocardial conductive fibers, located all around both ventricles. The Purkinje fibers spread the signal to the my-

¹⁰Also referred to as *atrioventricular bundle*

Location	Conduction Velocity [$\frac{m}{s}$]	Pacemaker Rate [$\frac{beats}{min}$]
SA node	< 0.1	60 – 100
Atrial myocardium	1.0 – 1.2	–
AV node	0.02 – 0.05	40 – 55
His bundle	1.2 – 2.0	40 – 55
Bundle branches	2.0 – 4.0	25 – 40
Purkinje network	2.0 – 4.0	25 – 40
Ventricular myocardium	0.3 – 1.0	–

Table 1.1: Conduction velocity and pacemaker rate of the cardiac conduction system. Data compiled from [70]. All values are approximate estimations.

ocardial contractile cells and guarantee a synchronized contraction of the ventricles, from the top to the bottom. [59, 67]

1.3.2 Cardiac Rate Control

As mentioned before, the general or *primary pacemaker* of the heart is the SA node. In healthy condition, depending on age and level of fitness of a person, the heart rate is about 60 to 80 $\frac{beats}{min}$. In cases of a loss of the primary pacemaker however, other components of the cardiac conduction system are capable to produce an impulse. These are so-called *ectopic pacemakers*, which is in particular the AV junction as *secondary* and the His-Purkinje system as *tertiary pacemaker*. If the atrioventricular junction or the His-Purkinje system have to take action to generate an impulse, naturally the rate decreases to not interfere in a regular beat by mistake, see Table 1.1. A closer look to the different kinds of blocks in cases of cardiac arrhythmias is given in Section 1.6. [59, 67]

Conduction Time and Velocity

A *normal* conduction time and velocity of the different passages within the cardiac conduction system, is obviously not easy to determine. Both depend on many different factors of the test person and of course there is the difficulty of measurement in the specific areas. Nevertheless, we want to give an indication for the conduction times and velocity in normal rhythm, measured via intracardiac electrogram according to Josephson and Katz [67, 70]. For this electrogram, an electrode catheter is placed at the desired position in the heart, usually through the veins from the upper or lower extremity. The chosen access depends on the desired recording position.

From the first atrial activity in the sinus node region to the AV node junction, a signal takes about 30 to 50 ms. The total atrial activation lasts for 80 to 100 ms. After that, the AV node delays the signal about 125 ms on the way to the His bundle. From the His bundle region to the ventricular excitation, the time duration is about 55 ms. [67, 70, 59]

1.3.3 Summary

Although, lots of the cardiac conduction system has been explored very well, there is still some work to do. Especially the AV node is in focus of current researches, because the knowledge about its conduction is crucial for a better treatment of different diseases. Despite the 100 year history of investigating the AV node, still some of its activities are not completely understood. Only with the help of *microelectrode recording* combined with *optical mapping techniques*, many physiological properties could be enlightened recently [163]. Although mathematical models and diagnosis algorithms improved in the last years, there is still some truth in a citation of a leading expert in electrophysiology Douglas P. Zipes in 2004 ([162], p. 204): "...the AV node is the Cinderella of mathematical cardiology, being the only major cell type or major structure of the heart that has not yet been characterized within a framework of an accurate mathematical model." Our claim is, to improve the understanding of the AV node, supported by enhanced as well as new designed mathematical models and established in relevant clinical case studies.

1.4 Cellular Level

To get a full insight in the processes of the heart, it is necessary to understand the connection of the heart rhythm in total, but also the processes of a single cardiac cell. For this purpose, and after the general overview on the cardiac conduction system, we now take a closer look at the events on a cellular level.

General Mammalian Cells

Basically, a cell in the human body is composed of three parts. These are *intracellular*¹¹ as well as *extracellular fluid*, which both contain free ions like sodium (Na^+), potassium (K^+), calcium (Ca^{2+}), or chloride (Cl^-). Between inner and outer fluid, there is a *membrane*, acting as selective permeable boundary. The membrane offers a series of valves or *ion channels*, which let certain ions flow in or out. This effect changes the electrical potential and is the foundation for the communication between cells. [136, 70]

The condition of a cell membrane in a state where there would be no ion flow, is called *equilibrium potential*. To calculate this potential, supposing the membrane is only permeable to a single ion, one can use the equation described by Nernst:

$$E_m = \frac{RT}{zF} \ln P \frac{a_o}{a_i}, \quad (1.1)$$

where

- E_m is the membrane potential,
- R is the universal gas constant,
- T is the temperature in Kelvin,

¹¹Also called *cytosol*

- z is the charge of the ion,
- F is the Faraday constant,
- P is the permeability of the membrane to the ion,
- a_o, a_i is the extracellular, respectively intracellular concentration, which can be seen as the activity gradient across that ion.

The *Nernst equation* for potassium gives a good prediction for the *resting potential* for most regions of the heart. However, a more accurate estimation can be calculated by the *Goldman-Hodgkin-Katz equation*, which describes the general case of a membrane that is permeable to several ions. In the following equation, the membrane permeable to sodium, potassium, and chloride is described [70, 59]:

$$E_m = \frac{RT}{zF} \ln \left(P_K \frac{[K^+]_o}{[K^+]_i} + P_{Na} \frac{[Na^+]_o}{[Na^+]_i} + P_{Cl} \frac{[Cl^-]_i}{[Cl^-]_o} \right) \quad (1.2)$$

In Section 3.2, we take a closer look at various cardiac cell models and especially at a description of the AV node on a cellular basis.

Cardiac Cells

Cardiac cells are more or less of cylindrical shape with a size of 10 to 40 μm times 50 to 200 μm . Basically, there are two significantly differing cell types in the human heart, even though mixtures of these occur. The first one is of muscular kind, so-called *cardiac myocytes*, which are responsible for the contraction of the heart chambers. On the other hand, there are specialized *pacemaker cells* in specific areas of the heart, as in the SA or AV node. Those have for example a slower conduction velocity, due to their smaller size. Fast *conducting cells* like the Purkinje fibers have a morphology similar to myocardial cells, but lack of contractile proteins and even have a slow pacemaker ability. The differences in the cell types, can especially be seen in the varying *action potentials*, which we discuss in the following paragraph and can be seen in Figure 1.5.

The intercellular connection is applied by different types of junctions, called *intercalated discs*. Primarily, those are responsible for a mechanical connection between myocytes. The fast cell-to-cell transmission of an electrical impulse though, is provided by *gap junctions*. Both specialized junction types are fundamental for a simultaneous contraction of the cells in the different regions of the heart. [70, 59]

Cardiac Action Potentials

If you examine intra- and extracellular fluid individually, both have a neutral electrical charge. Between both fluids, however, there is an imbalance hereof. Looking from the interior membrane at a non-activated cell, the resting potential is negative. During this resting state, some valves allow an one-way exchange of ions (K^+ out, Na^+ in), while specialized ion pumps, which work the other way around, preserve the negative potential. If an impulse

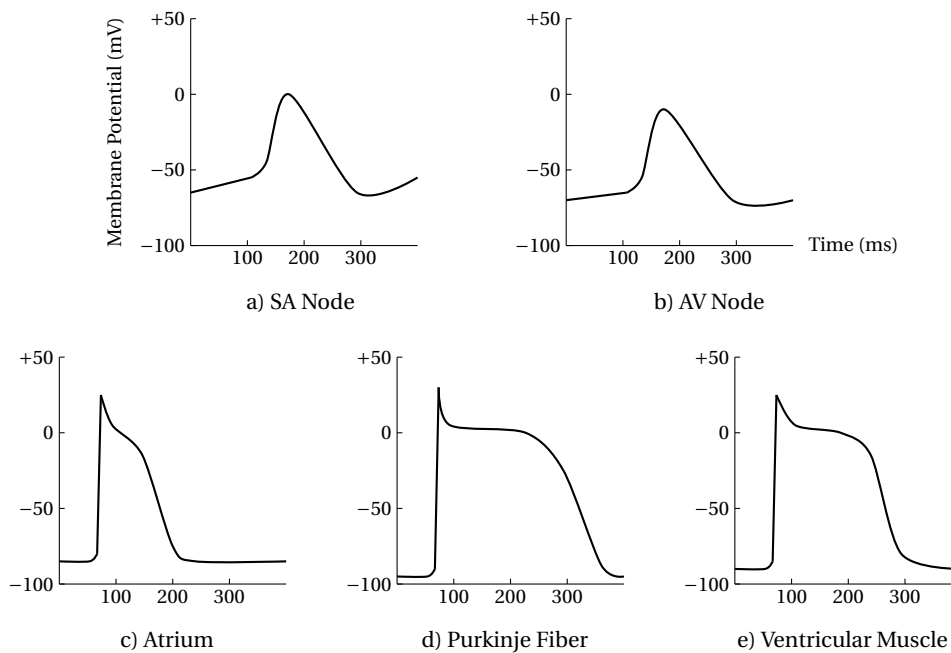


Figure 1.5: Action potentials in the different regions of the heart. Adapted from [70, 59].

reaches the cell and a certain charging threshold is crossed, the cell membrane depolarizes and an action potential is initialized.

Cardiac action potentials are quite different and more complex in contrast to those in common muscular cells. For instance, the duration up to 300 ms, is much longer compared to just a couple of milliseconds in a skeletal muscle cell. Furthermore, there are significant differences within the cardiac cell types as well as the different regions of the heart. In Figure 1.5, the varying action potentials from a SA nodal cell to the a ventricular myocyte is shown. The combination of all cardiac action potentials is then displayed in a typical ECG. [70, 59]

Action potentials of the contracting cells resemble each other. They basically consist of five phases, which only differ in duration and intensity depending on their location. In the atria they are a bit more compressed compared to the ventricular ones, but both have a resting potential of approximately -90 mV. Figure 1.6 exemplary describes an action potential of such a cardiac myocyte. The process is initiated, if an impulse reaches the cell and a certain threshold is passed by the influx of positive ions. The rapid depolarization (phase 0) is caused by the opening of the Na^+ channels. This is followed by a short repolarization (phase 1), where the Na^+ channels close and the voltage-gated K^+ and slow Ca^{2+} channels open up. Within the long plateau phase (phase 2), the potential slowly declines to zero, which ends with the closing of the Ca^{2+} channels. The main difference between the cell types can be seen at the duration of the plateau phase. The potassium fully repolarizes the cell (phase 3), which results back in the negative resting potential (phase 4). Most of the time, while the

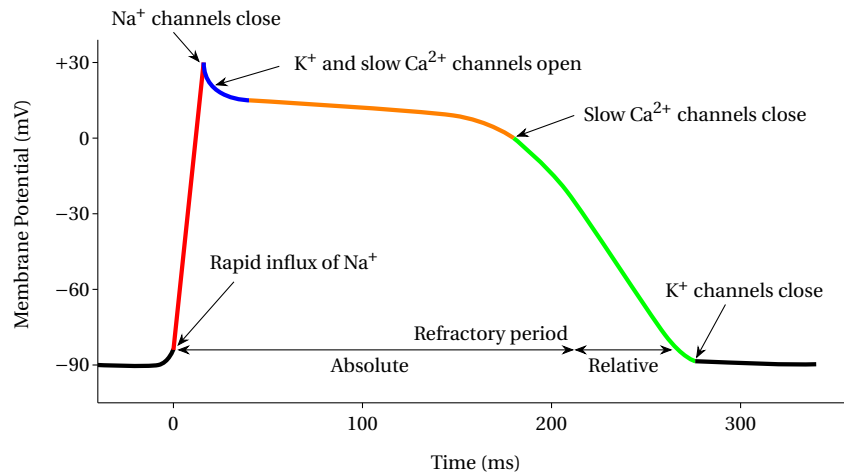


Figure 1.6: Action potential of a cardiac muscle cell. The different colors symbolize the five different phases an action potential passes through. Adapted from [70, 59] and further described in the text.

cell is not in resting potential, it cannot respond to another impulse. This *refractory state* is further explained in the next paragraph. [70, 59]

SA or AV nodal pacemaker cells, on the other hand, depolarize by a rapid calcium influx via open Ca^{2+} channels (phase 0). The depolarization is slower than in working myocytes. The pacemaker cells lack of phase 1 and plateau phase 2 and immediately repolarize by an outflux of potassium (phase 3). When the cell is fully repolarized, there is not a stable resting potential, due to open Na^+ channels. The potential rises approximately between -60 mV and -40 mV until it crosses the threshold and the process starts over again, see Figure 1.7. This phenomenon appears in the SA, respectively AV node, or His-Purkinje system as discussed in Paragraph 1.3.2, and is the background for a regular contraction of the heart. [70, 59]

Refractory Period

Refractoriness in physiology specifies the time period, in which a cell is incapable of repeating a certain action. Simplified, it can be considered as the recovery time of a cell, after previous stimulation. In electrophysiology, there are three different types for the term *refractory period*, which is the *absolute* (or effective), *relative*, and the *functional* refractory period. All three definitions can be applied to any component in the cardiac conduction system. [67]

Absolute refractory period (ARP) correlates the most with the physical definition of refractory period, as it describes the duration, in which a cell cannot be stimulated under any circumstances.

Relative refractory period (RRP) marks the end of the absolute refractory period. The tissue can now be stimulated under certain conditions, but reacts on a stimulation with a

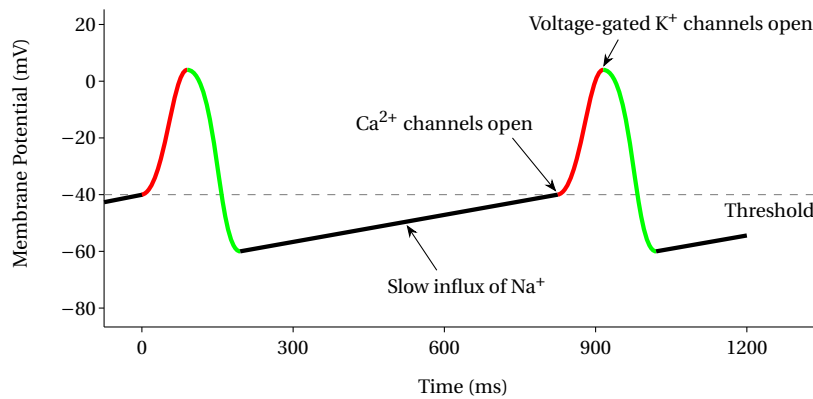


Figure 1.7: Action potential of a sinoatrial pacemaker cell with three different phases of depolarization, immediate repolarization and the characteristic unstable *resting potential*. Adapted from [70, 59] and further described in the text.

prolonged conduction, compared to the basic drive.

Functional refractory period (FRP) is a specific electrophysiological term, as described by Josephson [67]. It is the shortest interval of two consequently conducted impulses through a specific tissue that can be measured. The FRP can be seen as a combination of refractory period and conduction time. So it defines the output interval of two successive signals, in contrast to the absolute or relative refractory period, which give the longest input interval.

1.5 Electrocardiogram

An electrocardiogram (ECG) measures the electrical activity in the heart at each cardiac cycle. There are different methods to capture an ECG, depending on the current patient status or the disease to be studied. Foremost, the basic method is a *surface ECG* while resting, which is even possible in case of emergency. Here, often only a few seconds are recorded, to get a current and fast diagnosis. For partially occurring rhythm disorders that cannot be diagnosed adequately with a short resting ECG a *long-term ECG* can be used, recording, e.g., 24 hours with a portable device. The *cardiac stress test*, checks the response of the heart under physical stress, which mainly exposes coronary heart diseases.

In the recent years, *implantable monitoring devices* got more and more established, in particular because of their reduced size. Those are able to record up to three years, 24 hours a day, identifying infrequent heart beat irregularities after fainting spells for example. The most detailed, but extensive method is the previously mentioned *intracardiac electrogram*. This is recorded as required, at the high right atrium (HRA), the coronary sinus (CS), the His bundle (HIS), or the right ventricular apex (RVA). The intracardiac electrogram is crucial in cases of a catheter ablation treatment.

Lead	Potential Difference Between	Zero
I	Right arm and left arm	RA
II	Right arm and left leg	RA
III	Left arm and left leg	LA
aVR	Right arm and V lead by connecting left arm and left leg electrodes	V
aVL	Left arm and V lead by connecting right arm and left leg electrodes	V
aVF	Left leg and V lead by connecting left arm and right arm electrodes	V

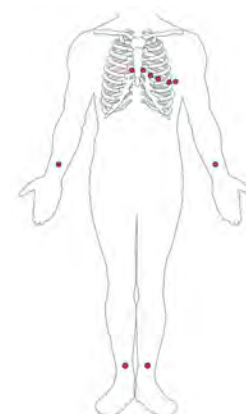


Table 1.2 & Figure 1.8: Standard limb leads and placement of the 12-lead ECG electrodes.¹²

1.5.1 Standard 12-lead ECG

The standard ECG is taken on the body surface via electrodes, which are placed at various spots around the body, see Figure 1.8. The tracing of the voltage difference between two or more of these electrodes is displayed in an ECG and called *lead*. By convention, a wave of depolarization that travels toward a recording electrode, results in a positive deflection and likewise in a negative deflection, for propagating away from it. Thus, for the repolarization process it is the other way around, because of its opposite polarity. Due to the fact that an ECG measures only potential differences, it can neither provide any information about the absolute level of membrane potential, nor discriminate between fully depolarized or repolarized cells.

The first and simplest type of recording, is the three-lead ECG according to Einthoven. It uses bipolar leads, called lead I, II, and III, which record the potential difference between only two electrodes. The electrodes are placed at the right arm (RA), the left arm (LA) and the left leg (LL) and derived against each other. In each case, one of the electrodes measures the potential, while the other one is defined as “zero”. The three-lead ECG can be enhanced according to Goldberger, when respectively two of the limb electrodes are interconnected to an *indifferent V lead* (zero potential) and derived against the third, *exploring* electrode. These are named *augmented unipolar* limb leads or in particular for being the exploring reference at the right arm augmented voltage right (aVR), respectively aVL for the left arm, and aVF for the (left) foot. All standard limb leads are described in Table 1.2.

For more details, six chest leads according to Wilson can be added, which are also unipolar and follow the same principles as the unipolar limb leads. Taken together, ten electrodes are necessary to complete the nowadays most common *12-lead ECG*, including an additional ground electrode on the right foot, which is a safety feature and helps to eliminate extraneous electrical interference. [70, 137, 160, 47, 48]

¹²Table data compiled from [70]. Figure from “Anatomy & Physiology”, by OpenStax College, 2015 [115]. Licensed under *Creative Commons Attribution License (by 4.0)*.

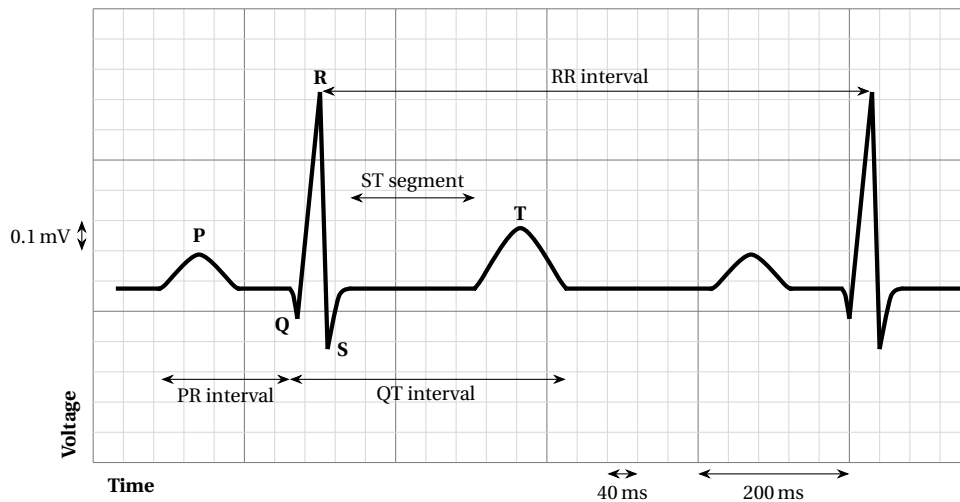


Figure 1.9: Exemplary ECG of a normal cardiac cycle at an approximate heart rate of $80 \frac{\text{beats}}{\text{min}}$. The writing speed is $25 \frac{\text{mm}}{\text{s}}$ at $10 \frac{\text{mm}}{\text{mV}}$.

1.5.2 Reading an ECG

An idealized example of normal activity in the heart can be seen in Figure 1.9, in an exemplary ECG output. As discussed in the previous paragraph, the leads give different views on the heart, e.g., lead I as if you are looking from the top, lead II from the lower right side, and lead III from the lower left side. On an ECG print, one can also see the intensity of the electrical signal, expressed in the vertical dimension and the velocity of propagation in the horizontal plane. By convention, the common recording speed is either $25 \frac{\text{mm}}{\text{s}}$ or $50 \frac{\text{mm}}{\text{s}}$, though other recording speeds can occur. In the former case, each major horizontal division on standard ECG paper equals 0.2 s, while the major vertical lines represent 0.5 mV. A standard 12-lead ECG print of a patient in sinus rhythm is illustrated in Figure 1.10.

P wave The P wave represents atrial depolarization initiated by the SA node. Its duration, which indicates the propagation time over the atria, is around 80 to 100 ms. The atrial repolarization is typically overlain by the QRS complex and thus not displayed on the ECG.

PR interval The entire PR interval takes about 120 to 200 ms and includes the depolarization from SA to AV node, along the bundle of His and bundle branches to the Purkinje network. Because of the small size of these structures, the activity in the areas from the AV node, can only be recorded via intracardiac electrogram but not on a surface ECG. With this method, however, the atrial-His (AH) as well as the His-ventricular (HV) interval can be measured. Furthermore, the rather long duration of the *PQ segment*, can be explained by the conduction delay in the AV node.

QRS complex The depolarization of the action potentials in the ventricular myocardium is

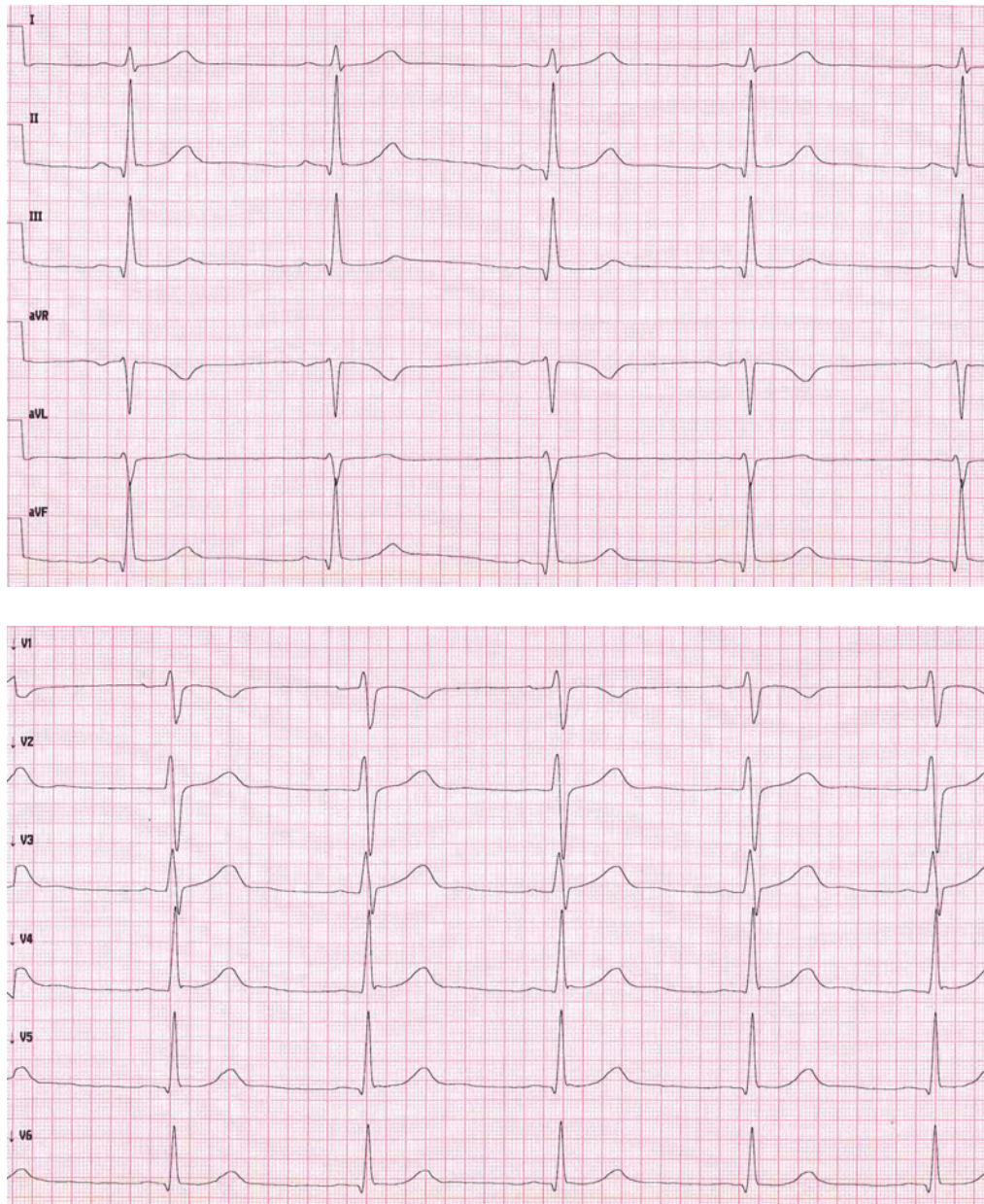


Figure 1.10: Standard 12-lead surface ECG print of a male athlete, recorded at a paper speed of $50 \frac{\text{mm}}{\text{s}}$. The patient is in sinus rhythm at a heart rate of $58 \frac{\text{beats}}{\text{min}}$, a PR interval of 155 ms, a QRS complex of 101 ms, and a QT interval of 427 ms.

displayed in the shorter (<120 ms) but higher amplitude of the QRS complex, in particular in the R wave. The fast upstroke of the R wave, where most of the myocardial cells are stimulated, is surrounded by the negative deflection of Q and S wave, in some leads. The preceding Q wave is caused by the electricity that usually spreads from left to the right interventricular septum (mostly visible in lead III and aVR). At the end of the ventricular activation process, the depolarization wave propagates from the apex to the basis of both ventricles, which causes the negative S wave in the according leads.

ST segment After the QRS complex, the ventricular cells are completely depolarized, which means the action potential is in plateau phase 2. Hence, no potential differences can be measured on the body surface and the ST segment equals the baseline. It seems kind of strange that the state of fully depolarized cells equals the one in resting potential after repolarization, but it clarifies the concept of an ECG.

T wave The repolarization of the ventricles is represented by the T wave. This process is much slower than then depolarization and also happens in opposite direction. Therefore, the T wave is displayed positive with respect to the baseline (in most leads), in spite of the fact that the cell becomes more negatively charged.

QT interval Is the total time the ventricular action potential duration, including full depolarization and repolarization. The period is roughly 350 to 400 ms.

U wave In some cases a small deflection can be seen following the T wave, called U wave. It is still not clearly understood what its cause is, but a possible explanation is the repolarization of the Purkinje fibers or the papillary muscles. [70]

1.6 Cardiac Arrhythmias

In this section, we want to give an overview of cardiac arrhythmias and classify the many different kinds. Our main focus, however, lies in the disturbances that happen in the AV node, with the intention to create a mathematical model that depict as accurate as possible the atrioventricular conduction. With this support, we especially try to predict and discriminate between supraventricular tachycardias, only by the means of a few RR intervals. For this purpose, those arrhythmias like atrial flutter or atrial fibrillation are examined more closely as well. At the end of the chapter, the different treatment modalities are explained, to further illustrate the importance on this topic.

1.6.1 Classification of Cardiac Arrhythmias

A normal heart beat is described at a rate of 60 to 100 $\frac{\text{beats}}{\text{min}}$ and called (*normal*) *sinus rhythm*. Cardiac arrhythmias can be classified in different ways, which is by the heart rate, by the location of their appearance, as well as the underlying arrhythmogenic mechanism. The term arrhythmia, by the way, is also used for a healthy variation of the sinus rhythm, which does not have to be perfectly regular (see *respiratory sinus arrhythmia* in Paragraph 1.6.2). In the following, we give an overview of different pathological mechanisms, as well as a description of the major clinical arrhythmias. [70]

Bradycardias

A too slow or weak heart beat, less than $60 \frac{\text{beats}}{\text{min}}$, is called *bradycardia*. However, this is not necessarily pathological and high-performance athletes may also have a heart rate lower than normal, called *athletic heart syndrome*. This syndrome helps to prevent tachycardia during training and comes along with an enlarged heart in combination with a very slow resting heart rate.

The usual reason for bradyarrhythmias is either a slow pacemaker activity or a blocked impulse conduction. The slow pacemaker is common in elderly and also often additionally caused by drugs like β blockers or others. Blocked impulses can happen anywhere in the cardiac conduction system from sinus node to the ventricles, although they are most likely in the atrioventricular junction. However, one has to be aware that conduction blocks can either be a cause of disease as well as a protective mechanism. For bradycardias, they are the cause for a too slow heart rate, while on the other hand the same mechanisms help to protect from a too frequent stimulation of the ventricles, in case of atrial flutter for example. [70, 59]

Tachycardias

Contrariwise, if the heart beats faster than $100 \frac{\text{beats}}{\text{min}}$, it is defined as a *tachycardia*. There are more different kinds of tachycardias than bradycardias, hence these are usually subcategorized in two areas by their origin. On the one hand, there are *supraventricular tachyarrhythmias* that can arise from the SA node up to and including the AV node. While *ventricular tachyarrhythmias* on the other hand, are defined as abnormal patterns of electrical activity, originating within ventricular tissue. Both can be caused by accelerated pacemaker activity, triggered depolarizations, and reentrant arrhythmias. Although, accelerated pacemaker activity of the SA node is often just a normal response to non-pathological external influences on the heart (see also *sinus tachycardia* in Paragraph 1.6.2).

Early or late afterdepolarizations are generally caused by a calcium overload of one or more cells. This leads to an additional depolarization during cell repolarization (phase 3) or resting (phase 4), without any external stimulation of the cell. The effect is a common cause for *premature contractions*, which describes an early or extra beat that can happen in the atria, the AV junction, or the ventricles.¹³ Individually appearing, premature contractions are harmless and do not need any special treatment. A series, however, is a tachycardia that can spread from one cardiac region over the whole conduction system.

Two or more propagated signals, which are triggered by one single impulse, are described as *reentry* mechanism. On the one hand, reentrant arrhythmias can be caused by a functional problem, like defective signal conduction due to inhomogeneous action potential duration or abnormal refractoriness. Furthermore, reentry tachycardias can originate from an anatomical mechanisms, e.g., due to scared tissue or accessory conduction pathways. A mixture of both can also occur. [70, 67, 59]

¹³There are many different terms for this phenomenon, namely *premature* contraction, systole, depolarization, complex as well as extrasystole, and each in different combinations with their point of origin. To avoid confusion, we use as the case may be, premature atrial, junctional, or ventricular contraction.

1.6.2 Sinus Node Abnormalities

Sinus Bradycardia A slowing of the SA node pacemaker below $60 \frac{\text{beats}}{\text{min}}$ is defined as sinus bradycardia. It often comes with an increased vagal tone¹⁴, but also drugs can be the cause. In general, healthy adults have a resting sinus rate of 60 to $70 \frac{\text{beats}}{\text{min}}$, however, especially in well trained athletes a rate down to $40 \frac{\text{beats}}{\text{min}}$ is not uncommon. Hence, a sinus rate less than $60 \frac{\text{beats}}{\text{min}}$ is not necessarily pathological.

Sinoatrial Block When the SA node delays or completely fails the depolarization of the atria, it is called SA block. A first-degree SA block is difficult to diagnose, because it is not visual in an ECG, while second- and third-degree (see Paragraph 1.6.4 for a detailed explanation) can be recognized. It can be caused by similar reasons as a sinus bradycardia, like increased vagal tone, drugs, or else.

Sick Sinus Syndrome This term is not entirely clear defined, but is more an umbrella term for a dysfunction of the SA node. It is sometimes used to describe sinus bradycardia, SA block, but also a combined arrhythmia of very slow and fast heart rates appearing in the SA node, which is more precisely called *bradycardia-tachycardia syndrome*.

Sinus Node Reentry A rather uncommon arrhythmia, caused by a reentrant circuit within the tiny SA node.

Sinus Tachycardia This describes a normal and harmless increase of the heart rate that happens for example through physical exercise or emotional stress. The maximum sinus rate varies with the age. A rule of thumb is $220 \frac{\text{beats}}{\text{min}}$ minus the patient's age, although this is of course highly variable from one to another individual.

Respiratory Sinus Arrhythmia Rise and fall of the sinus rhythm frequency, caused by the clearance of an increased blood flow into the right heart chambers. The heart increases its beat reflexively. This is mainly observed in young people and in general, there is no treatment applied. [70, 67, 59]

1.6.3 Atrial Abnormalities

Premature Atrial Contractions (PACs) A sign for a premature atrial contraction is an early depolarization of the P wave. It is normally followed by a QRS complex without any prolongation of the PR interval, if the AV junction is not refractory anymore. PACs are often propagated into the sinus node, so that the normal rhythm is reset. They are frequently found in patients and do not need any special treatment in general.

Atrial Tachycardia Due to the different terms and declarations for atrial tachycardia and atrial flutter that came up in the 1990s, Saoudi et al. [127] tried to make clearer definitions according to electrophysiological mechanisms and anatomical bases. Hence, they defined atrial tachycardias by a *regular* atrial rhythm, which does not originate in

¹⁴“The effect produced on the heart when only the parasympathetic nerve fibers are controlling the heart rate.”
Definition of http://www.encyclopedia.com/doc/106-vagal_tone.html

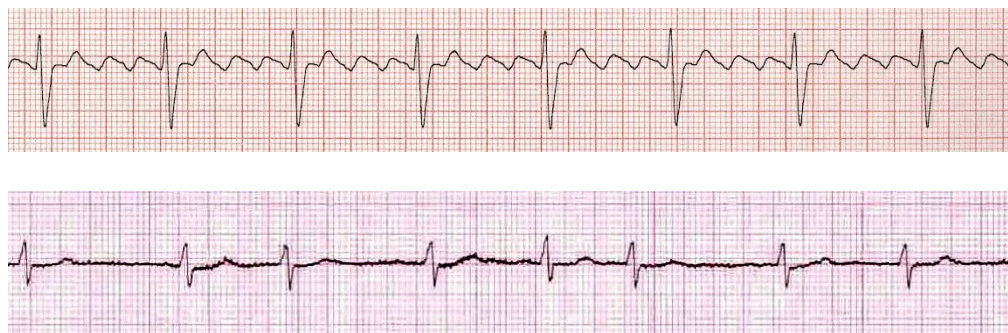


Figure 1.11: ECG example of typical atrial flutter with the characteristic sawtooth pattern and a 4:1 AV block at the top. At the bottom, the ECG shows a series of atrial fibrillation with an irregular ventricular response, showing no evidence of organized or basically any atrial activity.¹⁶

the SA node, at an *atrial* rate of $> 100 \frac{\text{beats}}{\text{min}}$. The tachycardia can either be focal (see next item) or macroreentrant, which include typical atrial flutter or other atrial reentrant causes.

Focal Atrial Tachycardia A tachycardia that originates in a small bounded region, caused by triggered depolarizations or abnormal automaticity.

Atrial Flutter As a very common type of arrhythmia, the rate of AFlut is defined at a range of 220 to $320 \frac{\text{beats}}{\text{min}}$.¹⁵ This tachycardia can be subdivided in *typical* as well as *atypical* flutter. Typical atrial flutter is triggered by a counterclockwise macroreentrant rhythm, which can be identified at a sawtooth-like pattern in the ECG, see Figure 1.11 at the top. Additionally, clockwise rotating flutter is also described as *typical* or *reverse typical*, which can be recognized at notched flutter waves in the inferior leads and at inverted P waves in V_6 . Both types are usually located in the same anatomical region that lies within the lower right atrium, called isthmus. The term atypical flutter is actually used for any kind of flutter that can not be described by the typical types. Those include several other macroreentrant tachycardias, originating in the left atrium for example, or occurring due to incisions from prior surgery. Atypical flutter forms are often harder to identify in the ECG.

Atrial Fibrillation The most prevalent pathological arrhythmia is AFib, which is characterized by a very rapid and totally chaotic contraction of the atrium for at least 30 s. The atrial rate usually exceeds $350 \frac{\text{beats}}{\text{min}}$ and a rate up to $600 \frac{\text{beats}}{\text{min}}$ is not uncommon. In general, the ECG shows disorganized RR intervals with no distinct P waves, but varying oscillations in the baseline, called *F waves* (see bottom ECG in Figure 1.11). It is

¹⁵The atrial range is defined according to Josephson [67]. Specifications by others, may vary a little.

¹⁶Both images adapted from “Life in the Fastlane”, by FOAM - Free Open Access Meducation, 2017 [93] and [92]. Licensed under *Creative Commons Attribution-NonCommercial-ShareAlike 4.0 International License*.

further classified in *paroxysmal*, *persistent*, *longstanding persistent*, and *permanent* AFib. Paroxysmal is defined as recurrent episodes, which are spontaneously terminating within 7 days. Persistent is a continuous AFib, ongoing for more than 7 days, while longstanding persistent lasts for over 12 months. For Patients that are classified of permanent AFib, it has been decided not to restore the sinus rhythm for any reason. It is generally accepted that AFib is often developed by a focal trigger. Furthermore, the chaotic atrial pattern is supported by a specific, susceptible tissue that develops overlying high frequent reentrant “rotors”. The observation that the focal trigger is often located in an area near the pulmonary veins (PVs), has been an important breakthrough for the diagnosis and treatment of AFib. Since then, the pulmonary vein isolation (PVI) treatment has been developed, which is further discussed in Paragraph 1.6.6. While especially the irregular RR intervals indicate a diagnosis for AFib, it has also been observed at very high frequencies that a kind of “pseudo-regular” ventricular contraction can occur [73, 46]. In general, AFib is not immediately life threatening, but can indicate life threatening diseases like stroke or heart failure. [70, 67, 59, 163, 127]

1.6.4 Atrioventricular Abnormalities

We count conduction abnormalities to the AV junction arrhythmias, which arise in the AV node, the bundle of His, or the bundle branches.

Premature Junctional Contractions (PJC) These systoles can develop anywhere within the AV junction and can be recognized in the ECG at normal QRS complexes without preceding P wave. Instead, there can be a retrograde P wave, which means it is inverted in lead II, III and aVF, preceding or following the QRS complex. This negative wave comes with the opposite direction of depolarization in the atria. PJC are not as frequent as premature atrial or ventricular contractions.

Wolff-Parkinson-White Syndrome An accessory pathway that allows the conduction from the atria directly to the ventricles is called Wolff-Parkinson-White (WPW) syndrome. This additional connection can actually be located anywhere along the AV junction, but often lies in an area referred to as *bundle of Kent*. It causes a preexcitation of the ventricles and can be recognized at a very short PR interval (< 0.12 s) or at a *delta wave*. The latter is characterized by a slower rise at the beginning of the QRS complex. The conduction can be possible in both directions and therefore often causes so-called *accessory pathway tachycardias*. These usually occur when the normal AV conduction signal travels retrograde to the atria, via the accessory pathway, creating a reentry circuit.

AV Nodal Reentry Tachycardia Over 50% of the supraventricular tachycardias come from an AV nodal reentry tachycardia (AVNRT). In contrast to an accessory pathway tachycardia, the AVNRT originates by a functional reentry circuit within the AV node and not by an anatomical bypass. In most of those patients ($> 90\%$), the prior mentioned *dual pathway physiology* is the cause. In those cases, the normal signal runs over the fast pathway, which is conducting bidirectional, and a PAC triggers the tachycardia.

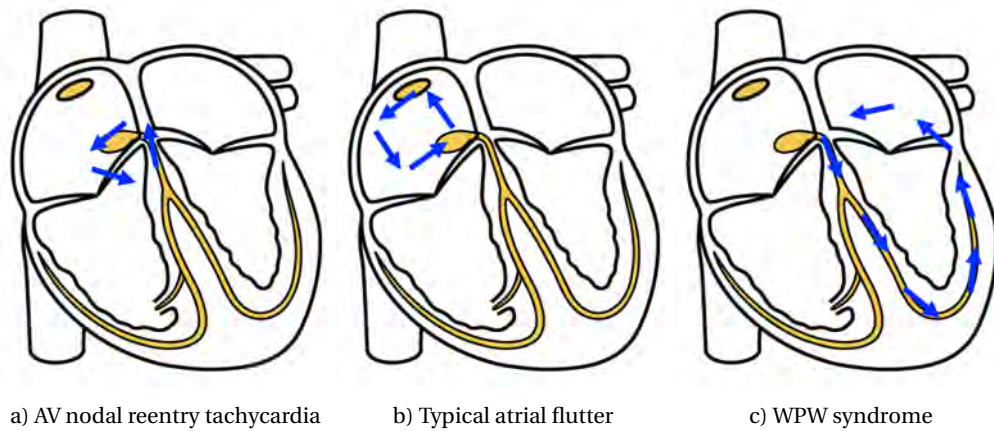


Figure 1.12: Various reentry locations and dimensions of three exemplary supraventricular tachycardias. See text for a further description.

While the fast pathway is still refractory at the arrival of the early signal, it is conducted through the slow pathway, creating a reentry circuit. A tool of modern electrophysiology to analyze this phenomenon, or other characteristics of the AV conduction, is *programmed stimulation*. Via incremental electrical pacing during sinus rhythm with a progressive shortening of the cycle length for example, one can induce AVNRT as well as different AV block types. In Figure 1.12, the different reentry locations and dimensions can be seen for AVNRT, typical atrial flutter, and WPW syndrome.

First-, Second-, and Third-Degree AV Block There are three different kinds of impulse block types that can actually happen anywhere in the cardiac conduction system. However, these blocks are rather common within the AV junction and therefore often simply described as *AV block*. In the following, we use the terms *first-degree*, *second-degree*, and *third-degree* block, specified, among others, by Josephson et al. [67]. The first-degree block is not a real gap, but a prevalent, prolonged conduction, compared to the normal conduction in sinus rhythm. The second-degree block is further separated into type I and type II, which are defined by a regular or irregular intermittent conduction, first introduced in detail by Mobitz in 1924 [105]. Type I describes an progressive prolongation of the PR interval, leading to a skipped beat before the prolongation starts over again. Furthermore, it follows a certain pattern like 4 : 3 or 5 : 4, see Figure 1.13 AV Block the left hand side. Although, there can also be alternating patterns as well as a shortening instead of a prolongation of the conduction time. The type II leads to a skipped beat, but without an alternation in conduction time or pattern. The second type is exemplary described in Figure 1.13 on the right hand side. More detailed and other conduction properties of the various second-degree AV block types are shown in Chapter 2. Finally, a third-degree block characterizes a complete blockade without any signal transmission. In this case, other parts of the cardiac conduction system has

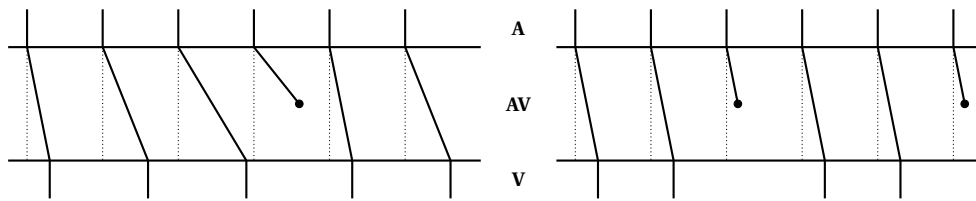


Figure 1.13: Conduction graph from the atria to the ventricles with two different types of AV blocks. On the left hand side a type I block with 4 : 3 blocking and a 3 : 2 type II block on the right hand side.

to fill in as pacemaker, as specified in Section 1.3.2. [67, 70, 59]

1.6.5 Ventricular Arrhythmias

Premature Ventricular Contractions (PVCs) Extra impulses that originate below the AV junction are recognized on the ECG as abnormal wide QRS complexes (> 120 ms), as they do not propagate over the ventricles synchronously. Premature ventricular contractions do usually not reach into the atria and therefore are not accompanied by a P wave. However, they can make the AV junction refractory and block the subsequent impulse from the SA node. PVCs can occur individually or in pairs (each systole following a sinus beat). Three or more extra beats in a row are in general described as non-sustained (< 30 s) or sustained (> 30 s) tachycardia. Single ventricular extra beats are a common electrophysiological phenomenon and usually not treated. Frequent premature ventricular contractions, however, can highly increase the risk for ventricular fibrillation and sudden cardiac death.

Ventricular Tachycardia (VT) Characteristic for ventricular tachycardias are a series of wide QRS complexes at a fast heart rate ($> 100 \frac{\text{beats}}{\text{min}}$). Different underlying mechanisms such as reentry or abnormal automaticity can be the trigger. The correct diagnosis is very important, because a ventricular origin of the disease can lead to acute cardiac failure. An indication for a ventricular tachycardia is a *captured beat* that is regularly conducted via the AV node and “captures” the misconducted signal from the ventricle. It can be seen in an ECG at an ordinary QRS complex between the wide ones. Furthermore, so-called *fusion beats* occur, when sinus and ventricular beat are depolarized simultaneously. These are recognized at narrower QRS complexes.

Ventricular Flutter The electrical activity in ventricular flutter usually appears as a form of sine wave at a rate of 150 to $300 \frac{\text{beats}}{\text{min}}$. In general, no specific morphology like QRS complexes, P, or T waves can be identified. It comes along with limited pumping capacity due to short filling time of the ventricles.

Ventricular Fibrillation This most dangerous cardiac arrhythmia comes with a very fast an totally disorganized ventricular activity. In the ECG, only chaotic oscillations can

be identified. The pumping function is disrupted with no time for a mechanical heart action. In contrary to atrial fibrillation, the ventricular counterpart is acute life-threatening and needs to be treated within seconds. Both, ventricular tachycardia and ventricular flutter, often degenerate into ventricular fibrillation. Sudden cardiac death can be prevented by an implantable defibrillator. [70, 67, 59]

1.6.6 Methods of Treatment

Lots of different methods have been developed to treat the various kinds of arrhythmic heart diseases. A milestone in cardiac device development for example, was the invention of the *implantable pacemaker* in the 1950s. With this device, it was suddenly possible to control the heart rate in a very effective way in patients with a complete heart block, who previously would have suffered a sudden cardiac death at a very high chance. Nowadays, pacemakers are not only capable of recording, but analyzing different kinds arrhythmia and even respond in a specific way. Furthermore, it has been experienced with the effect of drugs on arrhythmia since the beginning of the 20th century. A expansive medical treatment with these agents, however, started to spread in the late 1960s and 1970s. In the meantime, the endocardial *catheter mapping* and *programmed stimulation* lead to a much better understanding of origin and kind of the arrhythmia. Although a drug based treatment is still common, the *catheter ablation* is the state-of-the-art technique to deal with many of the supraventricular tachycardias. Medicinal as well as catheter ablation treatment are examined more closely in the following paragraphs.

For atrial fibrillation, there is an additional surgical treatment option, introduced by James Cox in 1987. The *Cox maze procedure* was designed to interrupt all possibilities of the atria to fibrillate or flutter, by incisions made into the heart tissue, at a open heart surgery. After some improvements, the standardized Cox maze III procedure was actually quite successful in eliminating AFib permanently. However, the method did not gain a widespread application, due to its complexity and risks. Today, the less invasive Cox-Maze IV procedure uses a kind of surgical ablation technique, which has a similar success compared to the previous cutting method and therefore is an option in some cases of AFib.

Despite the medical and technological progress, the exact diagnosis and best treatment option for arrhythmias is still a complex challenge for cardiologists and electrophysiologists. Our main focus lies in the discrimination of AFib and AFlut, or more precisely, between the chaotic, irregular atrial contractions of AFib and all atrial tachycardias, which are defined by a regular atrial rhythm. As will be seen in the following, this is of particular importance due to their different treatment modalities. [162, 67, 87, 59, 17]

Medicinal Treatment

There are different principles for a drug based treatment to control the heart rate during arrhythmias. In 1970, a classification of antiarrhythmic drugs was introduced by Singh and Vaughan Williams [159, 133], which basics, combined with some revisions, are still valid today. In general, the different antiarrhythmic agents interfere with the ion channels of the cells, to affect their action potentials in various ways. Based on the specific channels they

use, these are grouped into different classes from I to V. On the one hand, they are able to lengthen the action potential and therefore stabilize the rhythm. This is done, either via a prolongation of the repolarization or a slowing of depolarization phase. Hence, this so-called *chemical cardioversion* restores a sinus rhythm. On the other hand, there are blocking agents, which can lower the number of impulses that are conducted through the AV node. These are used as rhythm control agents, however, they do not restore a regular atrial rate.

On the downside, the medical treatment can come along with drastic side-effects. Special attention has been paid to the *Cardiac Arrhythmia Suppression Trial (CAST)* that was performed within two studies (CAST I and CAST II) between 1986 and 1998 at over 1700 patients [61, 62, 32]. This double-blinded, randomized study was initiated to test the effects of several specific antiarrhythmic agents at patients after a myocardial infarction. The drugs in fact reduced PVCs for example, but were accompanied by a drastically increased mortality rate due to sudden cardiac death, which in consequence even led to the termination of the study. As a result, a rethinking process started in the use of antiarrhythmic agents, especially in patients after a myocardial infarction.

In atrial fibrillation, a medicinal treatment is still the main therapy option. However, the decision of the preferred drug, needs to be taken at each patient individually. It has been shown in multiple trials that rate control agents, which restore a regular sinus rate, are not superior to a rhythm control via blocking agents, in matters of lifetime, stroke, or bleeding. For typical forms of atrial flutter, a long-term anti-arrhythmic drug therapy is usually not indicated. This is one the one hand because of a limited efficiency to restore the rhythm permanently, but in particular due to the high success and low complication rate of radiofrequency catheter ablation for these patients, as can be seen in the following. [17, 46, 163, 162]

Electrical Cardioversion and Defibrillation

The main task of *implantable cardioverter defibrillators (ICDs)* is to detect and immediately stop mostly ventricular tachycardias, which are acute life threatening. In patients with an ICD, the cardiac activity is monitored by an algorithm. In the case of ventricular fibrillation for example, a high-voltage electric shock is released, to bring the heart back to a normal rhythm. The reliability and accuracy of the underlying algorithm is obviously very important. Most algorithms are based on the interval length of successive R or P waves for their analysis. The importance of a correct diagnosis is further increased by the extremely painful shock. For this reason, many patients complain about a loss of life quality due to the permanent fear of a shock. In this matter, a new, promising method is in development, where multiple low-voltage shocks are used instead of a high-voltage one [64]. Furthermore, atrial defibrillation via implantable device is also possible in cases of AFib. The treatment is not established though, mostly because of a lack of patient acceptance to this method.

The *electrical cardioversion*¹⁷ procedure is basically a kind of defibrillation, but with synchronized and lower electrical shocks, externally applied on a sedated patient. Synchronized in this context means that the shock is initiated simultaneously to the R wave, which reduces the risk of ventricular fibrillation. The success rate of this procedure, to get the heart back

¹⁷Also known as direct-current cardioversion.

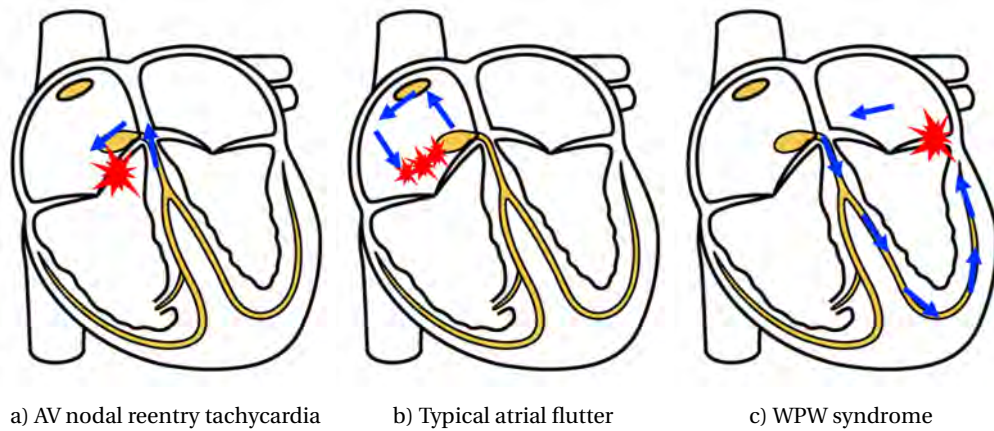


Figure 1.14: Approximate area of application of a catheter ablation therapy of three exemplary supraventricular tachycardias. See text for a further description.

to sinus rhythm, is very high, but the treatment is in most cases not permanent. Hence, cardioversion is usually applied to younger patients with non-chronic supraventricular tachycardias. [87, 59, 66, 130]

Catheter Ablation

In the last decades the catheter ablation technique evolved enormously from an experimental to a widespread performed treatment. In general, the procedure uses heating or freezing to destroy the tissue that causes the arrhythmia. The catheters are usually inserted through the blood vessels over arm or groin area. The most common method is the radiofrequency ablation (RFA), because of its efficacy and safety. Further alternatives are direct-current (DC) ablation, with energy coming from a defibrillator or cardioverter, laser ablation, ultrasound, or cryoablation, which uses freezing. These technologies have also been applied within operative procedures, but the catheter technique has almost made this step obsolete in treating supraventricular tachycardias. In this connection, AFib is basically the only remaining arrhythmia, where surgery can be an option for specific patients. As a matter of course, the various kinds of tachycardias need to be *ablated* differently, which also implies the importance to find the accurate location of the arrhythmogenic tissue. In Figure 1.14, the different areas are shown where the ablation treatment is approximately applied in the case of AVNRT, typical atrial flutter, and WPW syndrome.

The success rates of ablation are often denoted in a highly varying range, especially in cases of AFib. On the one hand, this comes from the various therapy approaches, which are more or less successful in the specific areas where the arrhythmia originates. Furthermore, the many studies observed a very different time period for recurrence cases. Nevertheless, for typical AFlut or other macroreentrant atrial tachycardias, catheter ablation is most effective. Here, the tissue that is initiating the fast rhythm is eliminated by the ablation, which

intercepts the reentrant circuit and brings the conduction back to normal. In a big study with 363 patients of Schmieder et al. [128], 90% of the patients were free of AFLut permanently after a single procedure. A recurrence rate less than 10% has been evaluated, of which most cases could be cured with a second or third ablation. Several other studies come to a similar result in treating typical AFLut with ablation (see [97, 16, 66]).

To find the best treatment option for AFib is challenging though. It includes several goals from a primal rate control, via keeping a permanent sinus rhythm, to prevention from further AFib series as well as embolisms. Based on the findings, and now common assumption that AFib usually arises from a focal trigger and needs the specific, susceptible tissue to propagate, the ablation method gained attention as treatment option. Here, the procedure aims either at an elimination of the trigger or at a modification of the supporting tissue. It has been observed that an increased number of AFib arises in the area of the pulmonary veins. The result was the pulmonary vein isolation (PVI) procedure, where the wrong stimulating tissue is destroyed (or *isolated*). It covers on the one hand, the separation of the PVs as possible trigger. On the other hand, it also alters the arrhythmogenic tissue, if the trigger is in another, surrounding location. For all the good results, which have been achieved by the PVI, it is still far from being as successful as the AFLut ablation.

A very extensive report has been made in 2012, by a worldwide task force of experts¹⁸ [17]. Among other things, they do provide a classification with indications, when to use catheter or surgical ablation of AFib. It is based on many previous studies that have been published, considering safety, efficacy, as well as the number and quality of the clinical trials. They actually suggest catheter ablation, in patients with symptomatic AFib, or patients with a refractory or intolerance for Class I or III antiarrhythmic drugs. Nevertheless, they also come to the conclusion that in spite of the many studies that already exist in this context, there is still a large, prospective and randomized clinical trial for AFib ablation missing. This trial should consider long-term stroke risk, heart failure, and mortality rate of AFib ablation, in comparison to a drug therapy.

Moreover, as we focus on the differentiation of AFib and AFLut, there is a high recurrence rate of regular atrial tachycardias (ATs) after an AFib ablation, which lies at up to 50%. Again, these recurrent cases have been ablated in a very successful way (> 90%). Needless to say, the correct diagnosis at this point is essential. In this context, we want to mention that a high rate of misinterpretation of surface ECG's has been shown. For example, Shiyovich et al. [131] examined the diagnosis of surface ECG's made by physicians with respect to AFib and AFLut differentiation. They discovered that AFLut is often misinterpreted as AFib, in typical case over 50%, but especially in atypical flutter (up to 80%). The difficulties on this topic are further examined in Chapter 2. [17, 66, 163]

Summary

As seen above, the exact differentiation between the two tachycardias is imperative, with respect to their treatment modalities. In AFLut, ablation is usually the superior option, not only

¹⁸Including the American College of Cardiology (ACC), the American Heart Association (AHA), the Asia Pacific Heart Rhythm Society (APHRS), the European Cardiac Arrhythmia Society (ECAS), the European Heart Rhythm Association (EHRA), the Society of Thoracic Surgeons (STS), and the Heart Rhythm Society (HRS).

because the effectiveness of antiarrhythmic therapy is very variable, expensive, and comes with side effects. In the best case, patients can actually be cured with a few current impulses, resulting in highly improved quality of life. In AFib however, the preferred therapy option is still a big challenge. Whether catheter ablation, surgical ablation, or antiarrhythmic drug treatment is the best option, has to be decided individually for each patient.

Chapter 2

AV Nodal Characteristics in Supraventricular Tachycardias

This chapter will give a better understanding of the AV nodal conduction characteristics that arise within supraventricular tachycardias. We take a more detailed look on the different second-degree AV block types and their properties to create an accurate mathematical model of the AV conduction, later on. As described in the previous Chapter, Wenckebach (type I block) [154, 155] and Hay (type II block) [52] were the first ones to discover those second-degree AV block types, at the conduction of the A-C interval of the jugular pulse and even before the electrocardiogram was introduced. In 1924, Mobitz classified the two different block types more specifically, which basically still applies today [105]. However, to find standard definitions for certain block types is not straightforward at all, because on the one hand, the physiology is still not completely understood. On the other hand, the definitions are not being used universally in literature, several terms are used for the same phenomenon, or diagnostic errors has been presented and revised again [10].

Hence, we now want to give at first, a clear and well-defined definition for all basic block types, in the way they are most commonly described in literature. Those more or less likely block patterns are discussed in the section of the *Classical AV Block Type Definitions*. For type I and type II block, the basic assumption is that there are two or more consecutive conducted PR intervals in which a single P wave fails to conduct to the ventricles. A third conduction type of an *advanced* second-degree block is also mentioned, as this pattern cannot be classified to the others according to the literature. [10]

Then, the idea of the MAVB is presented as a possible cause of complicated, irregular ventricular patterns in spite of regular atrial signals. The MAVB concept builds the centerpiece of our models and algorithms. With this new insights, however, some of the previous classifications appear in a different light. Based on this accumulated knowledge gained, we develop a completely new *combined multilevel* approach. This concept is able to explain most of the AV node characteristics easier, more precise and effective. To further explain the importance of the prevalent problem, we now start with examples and reasons for the many difficulties that arise in differentiating regular atrial tachycardias from AFib.

2.1 Differentiation of Regular Atrial Tachycardias from Atrial Fibrillation

With over 8% occurrence in hospitals, the most common abnormal ECG rhythms are represented by atrial fibrillation and atrial flutter [121]. The correct differentiation of regular atrial arrhythmias, including AFlut and focal atrial tachycardias, from AFib depicts a diagnostic challenge to both physicians as well as computerized algorithms. However, the correct diagnosis is essential as described in Section 1.6.6. The methods of treatment differ drastically implying an enormous improvement in the patients life quality as well as reduced mortality

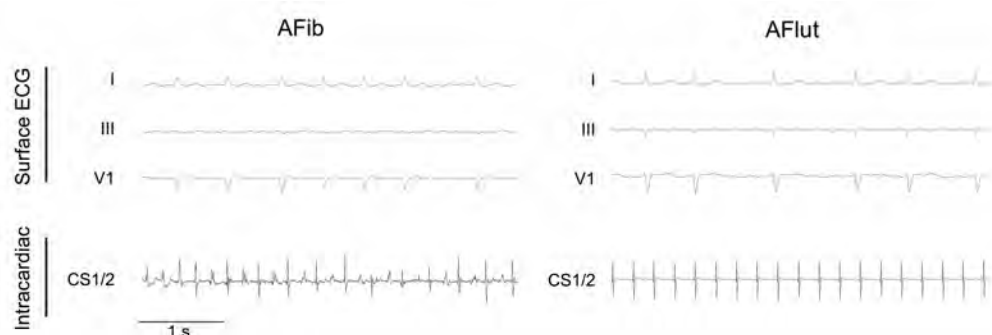


Figure 2.1: Exemplary ECGs of AFib and AFlut, which indicate the difficulty of discriminating the two Arrhythmias. The surface ECGs (leads I, III, and V1) on the upper panel and simultaneously obtained intracardiac tracings on the lower panel, recorded in the CS¹. On the left hand side, a Patient suffering from AFib is described. The surface ECG exhibits high-frequency, variable atrial activation in combination with an irregular ventricular response. Atrial electrograms reveal high-frequency signals (CL < 200 ms) with marked irregularity. On the right hand side, a Patient with atypical (non-isthmus dependent) atrial flutter is shown. The ECG shows merely discernible flutter waves in combination with an irregular ventricular response due to a MAVB, see Section 2.3. Simultaneously obtained intracardiac recordings (CS) show a totally regular atrial activation.

rate and severe side effects. There are numerous reports in literature, which describe the difficulties and the high misinterpretation rate on this topic by physicians and algorithms. We are now going to illustrate several arguments that can be considered as causes for this major problem. Then we present examples from literature as a further verification therefor.

2.1.1 Reasons for the Misinterpretation of AFib and AFlut

The discrimination between AFib and AFlut with the help of a surface ECG can be essentially complicated by several factors. Commonly, in series of AFib the ECG shows so-called *irregularly irregular* RR intervals with no distinct P waves. In case of typical AFlut, electrical activation produces a characteristic sawtooth pattern in the surface ECG. In Figure 2.1, we show that those main rules do not always apply. In some cases actually, it is incredibly difficult to reliably discriminate between those arrhythmias based on the surface ECG.

First of all, the disorganized RR intervals are often used as a main indicator in diagnosing AFib, especially when the ECG is lacking of a distinct sawtooth pattern. This only works poorly due to different reasons, as for example multilevel AV blocks, which lead to an irregular ventricular response even in regular atrial activity. The irregularly irregular RR intervals are not exclusive for AFib, but also very common in AFlut [78]. This is probably one of the

¹Electrograms obtained between the distal pair of electrodes of the coronary sinus catheter (CS1/2).

main reasons for missed AFlut cases. Secondly, AFib may come along with *coarse fibrillatory waves*, which are reminiscent of AFlut [75, 57]. Additionally to those causes, the presence of an artifact or premature atrial complexes may also result in overdiagnosing AFib [14]. Once again, most of those cases could be cured via ablation technique with a high-success rate, instead of a life-long treatment with anticoagulants.

On the other hand, AFlut may present atypical characteristics in the surface ECG leading to a missed AFib diagnosis. This includes hardly discernible low-voltage flutter waves, as can be seen in Figure 2.1. Furthermore, a common phenomenon in AFib is the so-called pseudo-regularization. Here, the RR variability decreases with an increase in heart rate, which leads to an *almost* regular rhythm [46].

2.1.2 Misinterpretation Examples Documented in Literature

Although, Bogun et al. [14] did not consider AFlut in their analysis, they presented interesting facts in their paper about misdiagnosis of AFib and its clinical consequence. They showed amongst others that cardiologists who reviewed ECGs, often accepted the computer generated misinterpretations. Furthermore, they stated that “overreliance on computerized algorithms and physician time constraints are the most likely factors resulting in the failure to correct an inaccurate computerized interpretation”. Those and other algorithmic approaches, and their pros and cons, are further discussed in Section 4.1.2. The following papers show the diagnostic accuracy on this topic in different studies with physicians. As far as the test data was accessible, we used it to compare the following example studies to our approaches in Section 5.4.1.

Knight et al. - Electrocardiographic Differentiation of AFlut from AFib by Physicians [75]

226 physicians responded out of a test group of 689 of medical house officers, internists, as well as cardiologist, or cardiology fellows (33% response rate). The test included 3 ECGs, which should be evaluated whether to be AFlut or AFib. The first ECG was AFib with prominent fibrillatory waves in only one lead. The second ECG showed AFib with prominent fibrillatory waves in several leads, and the third indicated AFlut with variable ventricular responses. The average misdiagnosis for the first ECG was 21%, 69% for the second ECG, and 13% misdiagnosed for the third. Especially the major misdiagnosis of AFib with prominent fibrillatory waves in both leads stands out, which was even worse diagnosed by cardiologists (79% wrong). The ECG of atrial flutter was frequently diagnosed correctly despite an irregular ventricular response. However, the limitation here could also be that only three ECGs were viewed and it would have been very unlikely that non of them was AFlut.

Shiyovich et al. - Accuracy of Diagnosing AFlut and AFib From a Surface ECG by Hospital Physicians: Analysis of Data From Internal Medicine Departments [131]

Shiyovich et al. did a reevaluation of 268 ECGs of patients, who had been discharged from hospital with AFlut or AFib. The gold standard² were two external cardiologists (one elec-

²See section 5.1.

trophysiologist), who analyzed the ECGs after certain criteria for AFlut and AFib. As a result, 16% (44 ECGs) were misinterpreted overall. 68% of the atrial flutter patients (25 ECGs) were incorrectly diagnosed. A detailed view on the AFlut ECGs show that 53% of typical and 80% of the atypical AFlut ECGs were incorrectly diagnosed.

They especially highlighted the significant number of misdiagnosed AFlut examples with irregular ventricular rhythm. On this, the frequently wrong assumption is probably that irregularly irregular RR intervals are by implication considered as AFib. Furthermore, they mentioned that reduced ECG quality often lead to a wrong diagnosis, because of artifacts created by electrode motion or else. Here, P waves are often misinterpreted in one or the other way. This problem occurs on a day to day basis in clinical practice, while it is overseen in scientific analysis with *clean* ECGs. In an analysis with only RR intervals used as input data, as we do, this problem can be avoided.

2.2 Classical AV Block Type Definitions

Before we start, we define the following notations for the different kinds of AV conduction times and intervals, which are also used in the upcoming model description.

Block Cycle $m : n$

For every m input signals in one AV block cycle, n beats are conducted.

Atrial Input := $A_i, i \in [1, m]$

Time point of the i th atrial excitation.

Atrial Cycle Length := AA

Time interval between two consecutive excitations in case of a regular atrial rhythm.

Ventricular Beat := $V_j, j \in [1, n]$

Time point of the j th ventricular conduction.

Conduction Constant := α

Regular signal conduction time which is present in normal sinus rhythm as well as in all various block types. In *sinus rhythm*, $\alpha = V_j - A_j$ solely represents the conduction time through the AV node.

Conduction Increment := $\Delta_j, j \in [1, n]$

Varying increment to the basic conduction time in type I blocks. The increment length depends on the number of conducted beats in the current block cycle. The first actual increment is present at the second conducted beat, which means $\Delta_1 = 0$.

AV Conduction Time := $AV_j, j \in [1, n]$

Entire conduction time interval from the atria to the ventricles at the j th conducted beat within a block cycle. This conduction time equals the PR interval in the ECG and can be described by: $AV_j = V_j - (A_j + \alpha + \sum \Delta_j)$.

Ventricular Interval := $VV_j, j \in [1, n]$

The j th ventricular interval within one block cycle of a type I, respectively type II block.

Block Pause := VV_n

Pause produced by the nonconducted signal at the end of every block cycle of a type I, respectively type II block.

2.2.1 Type I Block

We start with a closer look at the different kinds of type I blocks. Mobitz defined the *Type I Block* as “a progressive lengthening of AV conduction interval until an intermittent failure of one signal, followed by a shortening of the AV signal”, see [105]. In 1927, Wenckebach and Winterberg published a further characterization of the phenomenon [157], which is also known as *typical Wenckebach periodicity* (or phenomenon) and explicitly defined in the following section.

In 1978, the World Health Organization (WHO) [25] and the American College of Cardiology (ACC) [140] enhanced the original definition. They characterized this type by **the occurrence of a single nonconducted P wave associated with inconstant PR intervals before and after the blocked impulse**. This definition provides that there are at least two consecutive conducted P waves (i.e. 3:2 AV block) on which to determine the behavior of the PR interval. There are several other works showing that the first definition by Mobitz was not sufficient, because there is at least one differing kind of Wenckebach phenomenon. In consequence, El-Sherif [37] and others described the type I block in two categories, the “original”, former one as *typical* and all others as *atypical*.

Typical Type I Block or The Wenckebach Phenomenon

A *typical* type I block according to Wenckebach [157] has to fulfill the following four characteristics.³ However, the first two characteristics are actually sufficient for a unique definition, whereas the last two are logical consequences thereof. An example of a typical type I block with a 5:4 block pattern is shown in Figure 2.2.

1. A progressive lengthening of the PR interval:

$$\alpha + \Delta_1 < \alpha + \Delta_1 + \Delta_2 < \dots < \alpha + \sum_{j=1}^n \Delta_j, \quad \Delta_j > 0 \text{ for } j \geq 2.$$

2. A progressive decrease in the RR intervals:

$$VV_1 > VV_2 > \dots > VV_{n-1}$$

3. The increment between the first and the second conducted beats being the largest (combined with the previous definition follows):

$$\Delta_{max} = \Delta_2 > \Delta_3 > \dots > \Delta_n$$

³Sometimes represented by five or six characteristics, which just describe the same points, but split up.

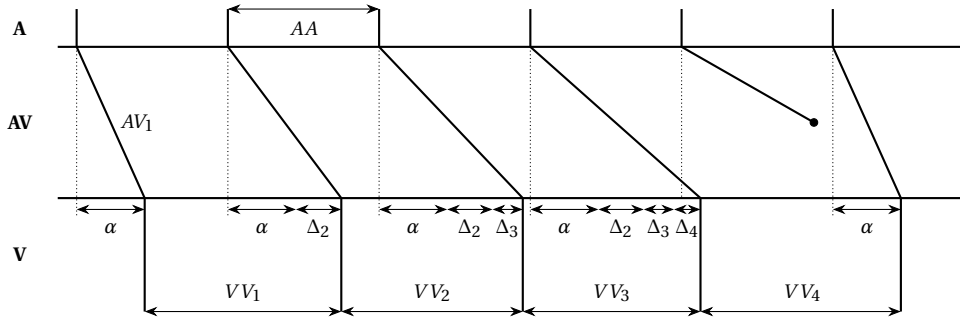


Figure 2.2: Conduction graph of a *typical* type I block with a 5:4 block pattern.

4. A pause produced by the nonconducted P wave equal to the difference between the last PR before and the first PR after the pause, subtracted from twice the PP interval:

$$VV_n = 2 \cdot AA - (AV_n - AV_1) = 2 \cdot AA - \sum_{j=2}^n \Delta_j$$

Although, the Wenckebach phenomenon is defined as *typical* type I block, mainly for historical reasons, it has turned out that other types are rather common. Denes et al. examined at 69 patients spontaneous or pacing-induced Wenckebach periods and discovered that 66% of the pacing-induced and 84% of the spontaneous type I blocks were *atypical* [26]. Furthermore, Friedman et al. showed similar numbers in the analysis of Wenckebach periodicity [42], whereas both found the characteristic that the typical Wenckebach conduction only occurred until a conduction ratio of 6 : 5 and is most likely in 4 : 3 pattern, see also Spodick [138]. Another interesting fact was that in 98% of all type I blocks (typical or atypical), the first PR interval was the shortest, on which the assumption $\Delta_1 = 0$ can be traced back.

The probably most common type I block pattern 3 : 2 obviously cannot be classified as typical or atypical, under the specified definitions, as there is only one increment present. Thus, $n \geq 3$ has to apply for a typical type I block classification to verify those definitions. Based on the literature results, we can conclude the following specifications for a *typical* type I block cycle of $(n + 1) : n$.

- The valid number of conducted signals per block cycle:

$$3 \leq n \leq 5$$

- Frequency of occurrence of the block type pattern:

$$\#(4 : 3) > \#(5 : 4) > \#(6 : 5)$$

- The increment at the first conducted beat can be neglected, and while being the small-

est counted as conduction constant:

$$\Delta_1 := 0$$

Atypical Type I Block

The *atypical* form of type I block combines all the conduction patterns based on the Wenckebach phenomenon “that are not typical”. In consequence, this means they do not fulfill every criteria presented in the typical section, but are still based on the underlying type I definition. There are several specifications though, which has been provided by literature [26, 42], and are described in the following in their frequency of occurrence.

1. The last increment increased from the previous one:

$$\Delta_n > \Delta_{n-1}$$

2. The last increment being the largest increment overall:

$$\Delta_n = \max_{j=1\dots n} \Delta_j$$

3. First (actual) increment is not the largest:

$$\exists j > 2, j \leq n: \Delta_2 < \Delta_j$$

4. PR interval repeated at least once during a block cycle:

$$\exists j > 1, j \leq n: AV_{j-1} = AV_j \Leftrightarrow \Delta_j = 0$$

5. PR interval decreasing at least once during a block cycle:

$$\exists j > 1, j \leq n: AV_{j-1} > AV_j \Leftrightarrow \Delta_j < 0$$

The most frequent atypical form reported is the increase of the PR increment of the last beat prior to the dropped P wave, or the last increment even being the largest. According to Denes, those two atypical forms of category 1 and 2, represent over two-thirds of all atypical block kinds [26]. Based on the literature results, we can conclude the following statements for an atypical type I block cycle of $(n + 1) : n$.

- Less than 5% of the Wenckebach periods in [26] have been above a ratio of 10 : 9. Additionally, longer periods can also be seen as periods of 1 : 1 conduction followed by a type II block. Hence, we fix the valid number of conducted signals per block cycle:

$$3 \leq n \leq 9$$

- Frequency of occurrence of the block type pattern:

$$\#(4:3) > \#(5:4) > \dots > \#(10:9)$$

- The increment at the first conducted beat can be neglected, and while being the smallest counted as conduction constant:

$$\Delta_1 := 0$$

3:2 Type I Block

As mentioned in this sections, a 3 : 2 block pattern, which satisfies the type I block definition, cannot be classified to typical or atypical. However, it is probably the most common kind thereof. Thus, we assign it in this separate section of 3 : 2 type I block.

2.2.2 Type II Block

In 1906, John Hay has actually been the first one to describe a varying form of the previously discovered Wenckebach phenomenon [52, 11]. As stated by Barold in [10], there are many differing definitions for second-degree atrioventricular blocks, especially for a type II block. Originally, Mobitz defined a type II block in 1924 as an "occasional block of one or more P waves with no change in the PR interval before and after the nonconducted P waves" [105]. There were several other definitions, by Katz and Pick in [71] for example, which contributed to the confusion about this type. They allowed a slight shortening of the PR interval after a dropped beat in Mobitz type block, however without defining "slight" at all. In 1978, the WHO [25] and the ACC [140] made clearer and currently the most accepted definitions for a type II block.

1. Type II AV block is characterized by **the occurrence of a single nonconducted P wave associated with constant PR intervals before and after the blocked impulse**. This definition provides, similar to type I that there are at least two consecutive conducted atrial signals. Additionally, the sinus rate or the AA interval has to be constant.
2. The pause encompassing the blocked P wave must be equal to two PP cycles:

$$VV_n = 2 \cdot AA$$

After these definitions, it becomes apparent that one type II block cycle also has the pattern of $(n + 1) : n$, where n beats are conducted. Figure 2.3 shows such a type II block cycle. As before, it obviously has to count $n \geq 3$, because otherwise the specified definitions cannot be applied. A maximum number of conducted beats within one block cycle of a type II block is hard to find in literature. Most of the time only relatively short conduction patterns are described in type II. We found one report however, about a 7 : 6 type II block in [29], but no higher conduction pattern anywhere else. Due to this, we conclude the following specification for a type II block.

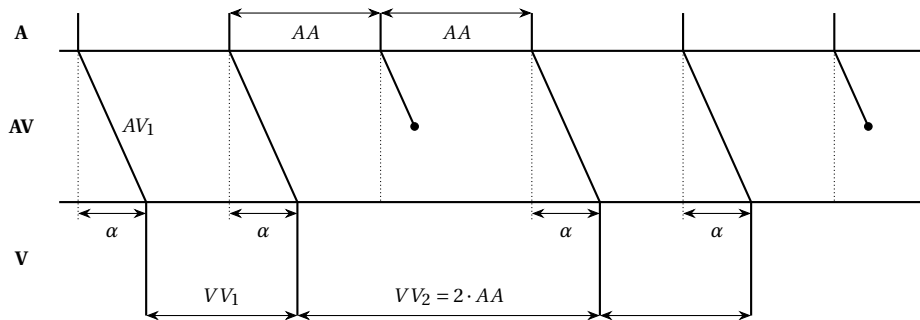


Figure 2.3: Conduction graph of a type II block with a 3:2 block pattern.

- The valid number of conducted atrial signals per block cycle:

$$3 \leq n \leq 6$$

2.2.3 Advanced Second-Degree AV Block

According to the guidelines of the ACC and the American Heart Association (AHA), an *advanced* second-degree AV block⁴ is characterized by **a block of two or more consecutive P waves, but an complete AV block is not present** [164, 165]. We previously mentioned that the most common 2 : 1 AV block, which is characterized by one conducted P wave for each P wave blocked, can progress from type I into a type II block and the other way around. In addition, the stated guidelines clearly say that a 2 : 1 block cannot be classified as either type I or type II. However, they miss to clarify the classification for this type.

Hence, the most logical prevalent definition is stated by Barold in [8]. He mentioned that a “two to one AV block is best considered as advanced second-degree AV block for the purpose of classification as are 3 : 1, 4 : 1, and so on, AV blocks according to the 1978 recommendations of the WHO and the ACC” [25, 140]. This leads us to the following definition, for an advanced second-degree AV block with a $m : 1$ conduction pattern. Here, for a block cycle of m atrial signals, just one is conducted, while $(m - 1)$ signals are blocked. An exemplary advanced second-degree AV block is described in Figure 2.4.

1. Advanced second-degree AV block is characterized by **one conducted P wave for each P wave blocked, or a block of two or more consecutive P waves, but an complete AV block is not present.**

Donoso et al. [29] presented 8 different clinical cases of advanced second-degree block, with conduction pattern from 2 : 1 to 5 : 1. Furthermore, Castellanos et al. described cases of advanced second-degree block in [22], where episodes of high stable patterns, e.g., 8 : 1 develop to lower grades of AV block even down 2 : 1 in several steps. They call this phenomenon *reverse alternating Wenckebach*. Castellanos constitute the reason for this kind of

⁴This kind of block is also referred to as *high degree* or *high grade* AV block.

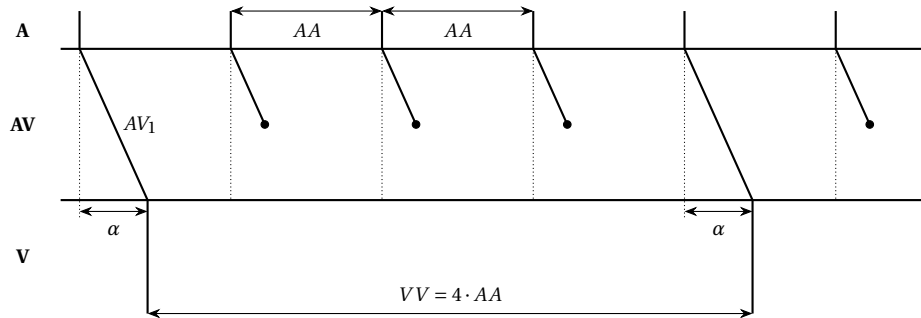


Figure 2.4: Conduction graph of an advanced second-degree block with a 4:1 block pattern.

AV blocks also in the MAVB concept, see the following Section. Furthermore, is to mention that they only described blocks with even numbers, like 8 : 1, 6 : 1, 4 : 1 or 2 : 1. They also found episodes higher than 8 : 1, however they have never been stable. Hence, we conclude the following specifications.

- The valid number of atrial signals per block cycle, where $(m - 1)$ signals are blocked:

$$2 \leq m \leq 8$$

- The frequency of occurrence of the block pattern is not completely clear. Most of the time it is described that the even-numbered block pattern are more likely than the odd-numbered. A 7 : 1 block is never described in adults to our knowledge, see also Section 2.4:

$$\#(2 : 1) > \#(4 : 1) > (\#(6 : 1), \#(8 : 1)) > (\#(3 : 1), \#(5 : 1))$$

2.3 Multilevel AV Block (MAVB)

The phenomenon of two consecutive block levels in the AV node was first mentioned, to our knowledge, by Langendorf and Katz in 1942. They found “evidence of two regions in the A-V junction and common bundle in which impulses are prevented from passing either all the time or on occasion” [82]. Before that, only alternate PR intervals with predominant 2 : 1 AV block conduction in atrial flutter were described by Lewis in 1912 [89], or Kaufman in 1927 [72].

In 1948, Langendorf introduced a certain AV conduction phenomenon as *concealed conduction* [81]. It was defined as any phenomenon which could not be observed directly on the ECG but influenced the subsequent ventricular conduction, hence the name concealed. Besoain-Santander, Pick and Langendorf also explained alternating type I blocks in AFlut, with a block in the higher level of the AV junction that halved the atrial rate (2 : 1 block), as well as a type I block below [13]. Langendorf, Pick [83] and Katz [71] continued this work and described multiple blockage and concealed conduction could both be present separately or

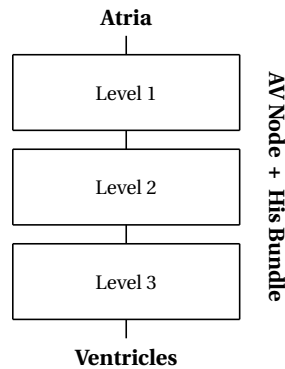


Figure 2.5: Visual description of a multilevel AV block.

in combination. However, due to intracardiac recordings, these conductions are not really *concealed* anymore. As stated by Josephson [67], it should be better called *specific consequences of incomplete penetration of impulses*. Newer definitions include, e.g., unexpected prolongation or failure of conduction, which may result from a nonconducted premature impulse in the AV conduction system. A further example would be the irregular ventricular response that arises in episodes of AFib due to the chaotic penetration entering the AV node.

In 1967, Watanabe and Dreifus were the first ones to actually measure two block levels in rabbit hearts via intracardiac recordings [153]. They found type II block mainly located in or below His bundle, whereas type I was mostly found in the upper AV junction. An advanced second-degree block of 3 : 1 was also be measured with the first blocked signal being commonly in higher AV regions than the second blocked signal. This detection would indicate a 3 : 2 block followed by a 2 : 1 block. These findings were inconsistent to the concealed conduction of Langendorf, but could actually be used as a first evidence that the MAVB is the underlying reason for similar observations and behaviors of the AV node, which has been “concealed” so far. For a basic visual description of the MAVB see Figure 2.5.

Leon et al. [86] investigated *alternating Wenckebach* episodes in 16 pacing induced patients. Those sequences were defined as “2 : 1 AV block in which conducted PR intervals progressively prolong, terminating in two or three blocked P waves”. They also confirmed in their conclusion that alternating Wenckebach episodes are best described by two block levels and not as Langendorf and Pick thought, as concealed conduction. In fact, they found three different groups, one with a type I block in AV node and 2 : 1 conduction in His, and moreover both types being located within the AV node. They concluded that alternating Wenckebach arise with an increase of the heart rate at a tiring AV node. More precisely, it starts at a slower heart rate with a 1 : 1 conduction on both levels. The faster the atrial rate gets, the block changes to a type I, followed by a 2 : 1 block on one of the levels, and finally to an additional type I conduction the other level. These findings were verified by His bundle recordings.

In 1976, Kosowsky et al. [77] showed in a study of 36 patients that MAVB is a rather common phenomenon. Two level AV blocks of different kinds are demonstrated in all patients

and even a third level is assumed in one patient. They especially indicated that in series of AFlut, lots of so far putative, complex AV block pattern, are more likely to be just simple multilevel blocks. For example, a stable 4 : 1 block might arise, in fact, due to two sequential 2 : 1 blocks. Several interesting examples of Kosowsky et al. are shown later on in Section 5.4.1 in an analysis with our models and algorithms.

A further enhancement on this topic was published by Slama et al. in 1979 [134], investigating 100 patients with atrial tachycardia or AFlut with an “absolutely regular PP interval”. They presented a model with three block levels, located within different regions of the AV node (atrionodal (AN), nodal (N), and nodal-His (NH)), but with a fixed block pattern on each according level. They proposed that a 2 : 1 conduction can occur on the first and third level, and a Type I block on the second. However, most of the times not all block levels are *active*, leaving the other(s) with a 1 : 1 conduction. Basically, two different types were common. Type A alternating Wenckebach phenomenon occurred in 75% of their patients and had 2 : 1 conduction on one level and a changing type I block on the other. The Type B alternating Wenckebach pattern was a type I block followed by a 2 : 1 block. Three active block levels were less common but also possible. And finally, 4 : 1 conduction can be explained by two 2 : 1 blocks on first and third level, passing through the middle level without being blocked. They expanded this approach in a case study a little later [135], proposing a further block level can appear in the bundle of His. These assumptions were confirmed by His bundle recordings. In this case, the patient had a 3 : 2 type I block, followed by a 2 : 1 block in the AV node and a 3 : 2 or 2 : 1 conduction in His, depending on the atrial rhythm.⁵ In addition, Littmann et al. [94] made similar findings in a case study with three pacing induced patients including His bundle recording. Castellano et al. did numerous works on this topic and also confirmed the previously described MAVB with up to three possible block levels [19, 20, 21, 23].

In conclusion, the concept of the multilevel atrioventricular block has been sufficiently demonstrated. As a matter of fact, it is even much more common than widely supposed, especially in fast and regular atrial rhythm as in supraventricular tachycardias (SVTs). It appears to be a problem of, at first, unclear and, later on, imprecise declarations for this phenomenon, which led to the confusion about the various specifications and descriptions of these types of second-degree AV block.

2.4 Combined Multilevel Concept for Second-Degree AV Block

So far in this chapter, we gave an extensive and detailed overview to the atrioventricular conduction behavior. The existing concepts do work quite well to explain some of the conduction mechanisms and patterns. However, as could be seen, it is still difficult to describe this process completely. Hence, we now want to combine the different insights gained of the AV node and develop a new concept of the various conduction types. Furthermore, the idea of the MAVB has proven to be relevant, especially in arrhythmias with fast atrial rates. To our expectation, these two concepts combined may be able to describe the whole process of a second-degree AV block both, more complete on the whole, and better in detail.

⁵The rhythm was regular and only changed after atrial overdrive pacing.

We would like to point out that we don't want to renew the definition of a type I or type II block, as they can be clinically useful. Our main focus, however, is to better understand the conduction mechanisms and suggest that type I and type II "represent different degrees of the same disorder rather than two distinct electrophysiologic processes", as stated by El-Sherif et al. in 1975 [36]. They presented a unified hypothesis of the second-degree AV block and according evidence, which would make the previous, separate classification of the AV block types redundant. Their observation showed that either no increment (or an increment of just a few milliseconds) can occur, but in the same time, it can also increase up to 180 ms. The same suggestion is made by Barold in [9] and [10] that "all type II blocks are really type I blocks, with increments in AV conduction so minuscule that they cannot be recorded or measured with standard equipment".

If we take a look at the previous definitions, the AV conduction in a type I or type II block can easily be explained by the same equation. For a block cycle of typical and atypical type I, there is just one variable Δ_j necessary, which is most likely somehow patient dependent but fixed at one individual. In case of type II, the increment can just assumed to be zero. Hence, all various types of signal conduction can be calculated with the following equation:

$$V_j = A_j + \alpha + \sum \Delta_j \quad (2.1)$$

In the second part of our concept, the multilevel idea comes into account. The following statements are based on medical and scientific knowledge presented in detail in the previous section. It was demonstrated in many publications that there are different anatomical areas from the AV node to the His bundle (or even the bundle branches), where conduction blocks are possible. Additionally, those regions were shown to block simultaneously up to 3 levels. Especially in very fast atrial rhythms, more levels are likely to become "active". In slower rhythms, it can be assumed that these levels remain in a 1 : 1 conduction. With this concept, all relevant advanced second-degree AV block types can be explained by two or three consecutive block levels (except a 7 : 1 block). As a reminder, the block cycles are specified up to 8 : 1 and more likely to be even-numbered. Furthermore, we only found one example in literature with a 7 : 1 advanced second-degree AV block in children, at an atrial rate of $500 \frac{\text{beats}}{\text{min}}$. Here, one can conclude that at such a high atrial pace there could be even a fourth active block level:

$$\begin{aligned} (3 : 1) &\equiv (3 : 2) \wedge (2 : 1), \\ (4 : 1) &\equiv (2 : 1) \wedge (2 : 1), \\ (5 : 1) &\equiv (5 : 4) \wedge (2 : 1) \wedge (2 : 1), \\ (6 : 1) &\equiv (3 : 2) \wedge (2 : 1) \wedge (2 : 1) \\ &\equiv (2 : 1) \wedge (3 : 2) \wedge (2 : 1), \\ (7 : 1) &\equiv (7 : 6) \wedge (3 : 2) \wedge (2 : 1) \wedge (2 : 1) \\ &\equiv (7 : 6) \wedge (2 : 1) \wedge (3 : 2) \wedge (2 : 1), \\ (8 : 1) &\equiv (2 : 1) \wedge (2 : 1) \wedge (2 : 1). \end{aligned}$$

These specific equations reveal, how all possible advanced second-degree AV block pat-

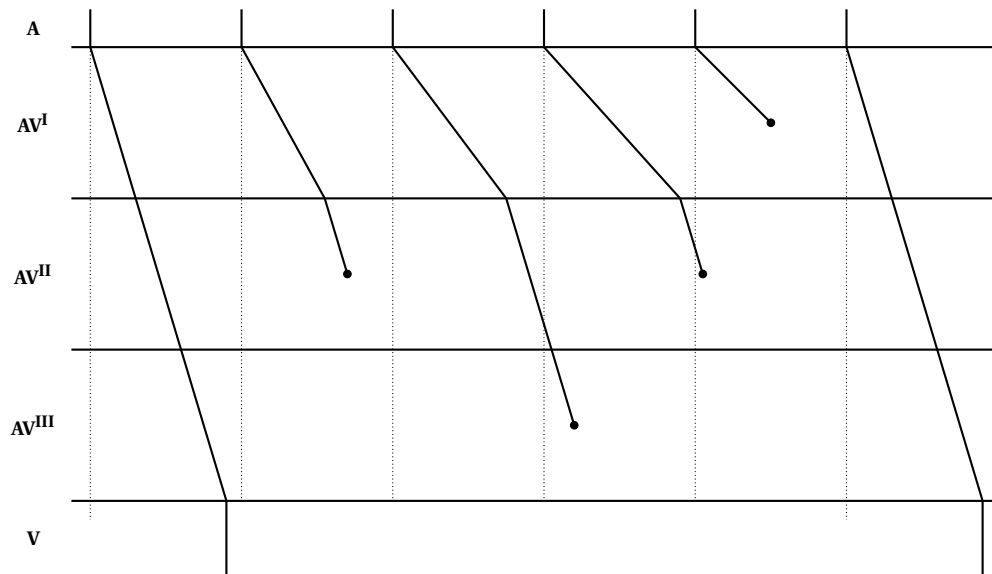


Figure 2.6: 5 : 1 second-degree AV block described by a MAVB of three consecutive block levels. In an upper region of the AV node, on the *first level*, a 5 : 4 type I block is prevalent. On the second and third level 2 : 1 blocks occur, which could happen in lower AV node regions or in the His bundle. This way, five atrial excitations, or input signals to the AV node, can conduct to just one ventricular output signal.

terns can be explained by anatomically successive, classical AV block types. They represent one and perhaps the most likely alternative for various advanced second-degree AV blocks. The composition of block levels is not necessarily unique, but this is also not required here. One can imagine, however, that by a different composition of blocks and levels many other block combinations $m : n$ from the atria to the ventricles may appear. In our view, this is exactly one of the underlying reasons why the discrimination of AFlut from AFib is often very complex. In Figure 2.6, this is exemplary shown for a 5 : 1 block, which is not supposed to appear on one level but explained by a MAVB.

To summarize, our approach is based on two steps. On the one hand, we describe all different classical block types in one simple combined conduction concept. On the other hand, we extend this idea on multiple possible levels, by which we are able to specify all possible types of *advanced* second-degree AV blocks. Altogether, this *combined multilevel concept* covers not only the advanced but all kinds of second-degree AV blocks that are described in literature, in a simpler and more logical way. Beyond that, we presented plenty of physiological evidence for both steps. In the following chapters, we take these insights to create new mathematical models of the AV node dynamics and further verify the underlying concept at many real life cases.

Chapter 3

Modeling Atrioventricular Dynamics

In the previous chapters, we gave an overview of the functionality and cardiac dynamics in healthy and diseased human hearts, as well as a detailed look on the conduction characteristics between atria and ventricles. Based on this knowledge, we intend to create mathematical models to describe these atrioventricular dynamics in a realistic manner. However, as common in applied areas such as biology, the electrical conduction in the heart is a nonlinear system with sometimes chaotic and unpredictable behavior. In this context, several modeling approaches are considered to test and compare the various possibilities. Our final objective is to be able to predict specific supraventricular tachycardias under certain surrounding constraints and also to better understand the mechanisms of the AV node. Therefore, we start with a short introduction in mathematical modeling and its importance to find the appropriate degree of abstraction. Then, various modeling approaches are analyzed to give a better understanding about the topic and to find the best one to achieve our objectives in the end.

It is possible to use statistical approaches on ECG basis, like pattern recognition via intensity or sequence in the ECG, which are presented at different examples in Section 3.1. While these are successfully used in some areas of ECG analysis, they do have negative aspects. Those are for example the long recording times, which are usually necessary for a significant diagnosis. Secondly, we have a closer look at first principle approaches in Section 3.2. Basic cellular models including ion channel dynamics are specified, from the first description of cellular membrane potential by Hodgkin and Huxley, over Noble's cardiac cell action potential, up to most recent AV node models. The advantages and disadvantages of both approaches are discussed at the end of each section.

Then, we analyze phenomenological models of the AV junction in Section 3.3 and begin with a formulation of the concrete mathematical problem. We show the classical AV block type conduction described by two different mathematical models. The recovery curve models are explained at specific examples from literature, before a completely new combined approach is developed, based on the findings of Chapter 2. With this *combined multilevel model*, we intend to describe the electrical conduction in the AV node better than the existing models and especially in the most complicated case of irregular ventricular pattern during regular atrial signals.

Mathematical Modeling

Mathematical models can be used to develop a scientific understanding for a certain problem, as a systems test environment, or a support or training in decision making. They are used to give a mathematical representation of the behavior of real objects and procedures,

which *always* illustrate a simplification of the real life example. Hence, the key point in modeling is to break up the complexity of a system and use simplified descriptions it. In that case, however, a simplification does not have to be a disadvantage, but actually has benefits. One can focus on the important behavior of a system, and sometimes a simplified model can even be used for various biological systems. In conclusion, the objective of good modeling is to find the simplest model that helps understand a system, by focusing on the relevant parts, and thus support a certain problem solving process. [136, 149]

Different Levels of Abstraction

The appropriate degree of detail is immensely important in developing a mathematical model. For the dynamics in the heart this could mean, e.g., to make a model as accurate as possible on cellular basis including action potentials, time-depending, and energy-depending membrane charge. Otherwise, one may apply a more general view on the electrophysiological dynamics, by modeling the conduction mechanisms in the AV node on the whole. As described above, simple mathematical models can be able to give a better understanding of certain naturally occurring procedures than high complex models. Our aim is to take a more detailed look at various kinds and to use the best possible modeling approach for our purpose. Hence, we first consider statistical approaches, which try to fit the measured ECG data as good as possible. This is followed by a section of first principle models based on cellular dynamics, or on micro-level scale. Finally, we focus on a larger scale, explaining the conduction processes in the AV junction by phenomenological models.

3.1 Statistical Approaches

In this section, we present several statistical methods for ECG analysis. Those are based on the hypothesis that two ECGs which have a similar signal structure in according leads, should probably have the same or at least a similar cardiological diagnosis. Generally, in statistical approaches applies, the more input data exists the better. On the other hand, there has to be at least a specific number of input data, in our case RR intervals that a certain method works at all. In the following, we describe two different approaches of the statistical kind, which are tested and compared to our methods in Section 5.2 later on.

3.1.1 RR Interval Periodicity

This method has been presented by Krummen et al. [78], because the periodicity in RR intervals is often used for the AFlut versus AFib differentiation. They intended to check, if this assumption is valid or as they assumed, the method just poorly identifies the correct arrhythmia. The test specifics were based on the *analysis of RR interval periodicity*, which should be an indicator for the regularity of AFlut. Here, a periodic RR interval was defined as a multiple of the shortest RR interval within the considered ECG period (± 25 ms). This procedure should simulate variable AV blocks. For example, a 5 : 4 block cycle is prevalent, if the current RR interval is 1.25 times the shortest RR interval (1.33-fold for a 4 : 3 block, 1.5-fold for 3 : 2,

and so on). Finally, the overall percentage of the periodic to the non-periodic RR intervals is calculated.

The test group included 66 patients in total, 21 patients with each atypical and typical AFlut, and 24 patients with AFib. Typical AFlut was defined as counterclockwise activation, while atypical AFlut was diagnosed by activation distinct thereof. AFib was diagnosed if the atrial electrograms lacked 1:1 conduction to all atrial regions. Therefore, as gold standard, only intracardiac methods were used to diagnose the rhythm. The results were illustrated as receiver operating characteristic (ROC)¹, which displayed that RR periodicity poorly separates AFlut from AFib. In typical AFlut, the RR intervals showed at least an average periodicity of 60%. This differentiation of typical AFlut to AFib had a specificity of 86% and a sensitivity of 66%. In the case of atypical AFlut on the other hand, RR periodicity did not separate from AFib at all. Krummen et al. came to the conclusion that irregularly irregular RR intervals are not specific for AFib and are especially common in atypical AFlut.

In Section 5.2.1, we show this method applied to our own test data and verify the results of Krummen et al. On the one hand, this indicates that this statistical approach is not applicable at all. On the other hand, and more important, the result supports the hypothesis that a diagnosis only based on irregular irregularity is highly misleading.

3.1.2 Heart Rate Variability and Poincaré Plots

A *Poincaré plot* is a method to analyze complex systems, while including a data set into a higher dimensional space. In medicine it is often used to analyze the heart rate variability (HRV), in the manner that the interval RR_i is plotted against the previous interval RR_{i-1} . This visualization technique can be used to recognize certain shape pattern with the human eye, and hence identify beat-to-beat cycles.

Esperer et al. [39] used this method to analyze long-term ECGs, recorded for 24 hours in portable *Holter* devices². They discriminated between sinus rhythm, atrial fibrillation, atrial tachycardias, atrial premature beat, and ventricular premature beat, based on the Poincaré³ block pattern. These patterns were, for example, *fan*, *island*, or *lobe* shaped. They presented quite impressive results with a sensitivity and specificity of 100% for AFlut ($n = 157$ Holter recordings) and 100% sensitivity and 97% specificity for AFib ($n = 1255$).

In conclusion, to analyze the HRV in Poincaré plots works really good in long-term ECGs of 24 hours of recording. One limitation might be that there is no comment about the types of the atrial flutter used in the test data set, whether to be any atypical kinds or simply typical flutter examples. Furthermore, and unfortunately, the long recording time is exactly the main issue here. This is caused by the fact, that in the clinical workaday life, usually fast feedback and decisions are desired or even crucial. In common clinical resting ECGs, there is usually a sequence of only 10-20 RR intervals used, instead of a 24 hour recording with about 100000 RR intervals. We reveal the problem of this method applied to short recording times clearly at our examples in Section 5.2.2.

¹Described in detail in Section 5.1.3.

²Named after its inventor Norman J. Holter (1914–1983), an American biophysicist.

³They used the term Lorenz plot, which is also common in literature.

3.2 First Principle Models

In 1952, Alan Hodgkin and Andrew Huxley achieved a real breakthrough in modeling cellular dynamics of a giant squid axon, which they gained the Nobel Prize for in 1963 [147]. Based on these discoveries of the Hodgkin-Huxley equations for ion channels, the first mathematical model for cardiac action potentials and pacemaker rhythm was built by Denis Noble in 1962 [109]. This was the groundwork for all the following cardiac cell models, to which Denis Noble also contributed a lot. However, according to a review about cardiac cell models by Noble in 2012 [112], in about 100 significant contributions, there is just one cellular based model about the atrioventricular node so far. This model was presented by Inada et al. in 2009 [60], where they developed an action potential model for cells of a rabbit AV node. We now show the basic structure of a cardiac cell model with the help of the most important discoveries on this topic, up to the AV nodal cell model of Inada et al. Furthermore, other approaches of simplified cardiac models are mentioned and finally some of the downsides of first principle models in clinical practice are discussed.

3.2.1 Hodgkin-Huxley Model

Since the first one, many different cardiac cell models have been developed, varying in complexity and states, from atrial or ventricular cells to specialized pacemaker cells. At first, we want to give an impression how to simulate neurons and action potentials, by describing the improvements of Hodgkin and Huxley, which also lead to the first cardiac cell model of Purkinje fibers by Denis Noble.

Equation 3.1 shows the basic model of cellular membrane potential by Hodgkin and Huxley of 1952 [147]. The total membrane current, between the inside and the outside of a nerve cell, is divided into membrane capacity and ionic current. This combination of charge reactions and electric current flow was one of the main factors for the success of the Hodgkin-Huxley model to simulate neurons [112].

$$I_m(t) = C_m \frac{dV(t)}{dt} + I_{ion}(t), \quad (3.1)$$

where

- $I_m(t)$ is the total membrane current per unit area, measured in $\frac{\mu A}{cm^2}$,
- C_m is the membrane capacity in $\frac{\mu F}{cm^2}$,
- $V(t) = V_{inside} - V_{outside}$ is the difference of the membrane potential from the inside to the outside of the cell, measured in mV,
- $I_{ion}(t)$ is the current density carried by ions,
- t is time, usually specified in ms.

Note that without any externally applied current, the total membrane current of a cell is zero, hence with $I_m = 0$ follows:

$$\frac{dV(t)}{dt} = \frac{-I_{\text{ion}}(t)}{C_m} \quad (3.2)$$

The ionic current can be further split up into several components $I_{\text{ion}} = I_{Na} + I_K + I_l$. Hodgkin and Huxley discovered that these components mainly consist of sodium ions I_{Na} , and potassium ions I_K . In addition, there is a so-called leakage current I_l , which combines all other ions. The ionic current flow, in turn, obeys Ohm's law $I = \frac{U}{R} \iff I = g \cdot U$, with voltage U , and the electrical resistance $R = \frac{1}{g}$, where g is the electrical conductance. Using Nernst's formula (see Equation 1.1), the ionic currents can now be expressed by the ionic conductances where V can be directly measured as displacement from the resting potential:

$$\begin{aligned} I_{Na}(V, t) &= g_{Na}(V, t) \cdot (V(t) - E_{Na}), \\ I_K(V, t) &= g_K(V, t) \cdot (V(t) - E_K), \\ I_l(t) &= g_l \cdot (V(t) - E_l), \end{aligned} \quad (3.3)$$

where

- I_{Na} , I_K , I_l are the ionic currents of sodium, potassium, and leakage current,
- E_{Na} , E_K , E_l are the equilibrium potentials of sodium, potassium, and of the leakage ions, which are assumed to be constant (measured in mV),
- g_{Na} , g_K is the sodium, respectively potassium conductance through the cell membrane, which is dependent to time and membrane potential (measured in $\frac{\text{mS}}{\text{cm}^2}$),
- g_l is the leakage conductance through the cell membrane, assumed to be constant.

In the second, experimental part, Hodgkin and Huxley tried to simulate the potassium and sodium conductances by other equations (3.4) to simplify the system for calculation. For this purpose, they introduced a so-called *gating variable* of potassium conductance n , as well as the gating variables of sodium conductance m and h . In the dynamic Equations 3.5, these describe the actual flow rates through the membrane, with a maximum conductance \hat{g} of the according ion.

$$\begin{aligned} I_K(t) &= \hat{g}_K \cdot n(t)^4 \cdot (V(t) - E_k) \\ I_{Na}(t) &= \hat{g}_{Na} \cdot m(t)^3 \cdot h(t) \cdot (V(t) - E_{Na}) \end{aligned} \quad (3.4)$$

To summarize, the Hodgkin-Huxley model was developed to predict the conditions that describe how action potentials are initiated, including threshold and refractory periods. It is able to reproduce the experimentally measured action potentials in a very precise way. The model is a dynamic system of nonlinear differential equations with four time-dependent state variables, described in the set of 3.5 and 3.6. The parameters of $\alpha_{n,m,h}$ and $\beta_{n,m,h}$ have been experimentally determined by Hodgkin and Huxley under specific conditions,

to fit the data of the giant axon of the squid, depending on voltage V . For the practical experiment, they used the voltage-clamp technique⁴ to measure the current through cellular membranes. This technique uses two electrodes, which are intubated into a cell. One electrode inserts sufficient current to the cell, so that the membrane potential is kept constant. The other electrode serves to measure the ionic current through the membrane in relation to an extracellular, indifferent electrode.

$$\begin{aligned}\frac{dn(t)}{dt} &= \alpha_n(V) \cdot (1 - n(t)) - \beta_n(V) \cdot n(t), \\ \frac{dm(t)}{dt} &= \alpha_m(V) \cdot (1 - m(t)) - \beta_m(V) \cdot m(t), \\ \frac{dh(t)}{dt} &= \alpha_h(V) \cdot (1 - h(t)) - \beta_h(V) \cdot h(t),\end{aligned}\tag{3.5}$$

$$\begin{aligned}C_m \frac{dV(t)}{dt} &= \hat{g}_K \cdot n(t)^4 \cdot (E_K - V(t)) + \\ &\hat{g}_{Na} \cdot m(t)^3 \cdot h(t) \cdot (E_{Na} - V(t)) + g_l \cdot (E_l - V(t)) - I_m(t),\end{aligned}\tag{3.6}$$

where

- $n(t)$ is the potassium conductance gating variable, which is dimensionless and between 0 and 1,
- $m(t)$, $h(t)$ are sodium conductance gating variables, which are dimensionless and between 0 and 1,
- $\alpha_{n,m,h}$, $\beta_{n,m,h}$ are rate constants for each specific ion channel, depending on voltage but not on time, with the dimension $\frac{1}{\text{ms}}$
- \hat{g}_K , \hat{g}_{Na} is the maximum conductance of the according ion, measured in $\frac{\text{mS}}{\text{cm}^2}$.

This continuous time model was solved by Hodgkin and Huxley numerically. Because of its complexity, there are many approaches to simplify the system, while trying to keep the most important properties. One kind hereof, is the FitzHugh-Nagumo model, which is the basis for one of the subsequently presented AV node models in Section 3.2.4.

3.2.2 Noble Model

Denis Noble further developed this model, also in an iterative, experimental modeling process, from the action potential of a squid giant axon to a cardiac action potential and pacemaker rhythm. The first fundamental difference of those two cell types is that the action potential of a cardiac cell is considerably longer than the one of a nerve cell. Furthermore, there are *pacemaker* regions with unstable resting potential, see Section 1.3. A further description of the ion movements and cardiac action potentials was also given in Section 1.4.

⁴The voltage-clamp technique was developed by Kenneth Cole in 1947.

In the following, equations and certain parameters are stated, specified by Noble in [109]. The major difference lies in the potassium channels of cardiac cells, consisting of more than one channel, which Noble demonstrated. He described a new *inward* rectifier I_{K1} and a *delayed* rectifier I_{K2} .⁵ Hence, the potassium current equations are different compared to the Hodgkin-Huxley model, given by the sum of those two channels. With a fixed equilibrium potential $E_K = -100$ mV follows:

$$I_K(V, t) = (g_{K1}(V) + g_{K2}(t)) \cdot (V + 100), \quad (3.7)$$

$$g_{K1}(V) = 1.2 \cdot \exp\left(\frac{-V - 90}{50}\right) + 0.015 \cdot \exp\left(\frac{V + 90}{60}\right), \quad g_{K2}(t) = 1.2 \cdot n(t)^4, \quad (3.8)$$

$$\alpha_n(V) = \frac{0.0001 \cdot (-V - 50)}{\exp\left(\frac{-V - 50}{10}\right) - 1}, \quad \beta_n(V) = 0.002 \cdot \exp\left(\frac{-V - 90}{80}\right). \quad (3.9)$$

The ionic current equations for sodium, however, are similar to the Equations 3.4 and 3.5. Here, the equilibrium potential is set to $E_{Na} = 40$ mV, while the maximum conductance is determined by $\hat{g}_{Na} = 400 \frac{\text{mS}}{\text{cm}^2}$. Additionally, a small component of $g_{Na} = 0.14 \frac{\text{mS}}{\text{cm}^2}$ was assumed to be independent of V and t . For further information on this, see Noble's publication of 1962 [109]:

$$I_{Na}(V, t) = (400 \cdot m(t)^3 \cdot h(t) + 0.14) \cdot (V - 40), \quad (3.10)$$

$$\alpha_m(V) = \frac{0.1 \cdot (-V - 48)}{\exp\left(\frac{-V - 48}{15}\right) - 1}, \quad \beta_m(V) = \frac{0.12 \cdot (V + 8)}{\exp\left(\frac{V + 8}{5}\right) - 1}, \quad (3.11)$$

$$\alpha_h(V) = 0.17 \cdot \exp\left(\frac{-V - 90}{20}\right), \quad \beta_h(V) = \frac{1}{\exp\left(\frac{-V - 42}{10}\right) + 1}. \quad (3.12)$$

Finally, also the leakage current equation remains the same. At this, the variable of the leakage conductance is specified by $g_l = 0.075 \frac{\text{mS}}{\text{cm}^2}$, and the equilibrium potential is set to $E_l = -60$ mV:

$$I_l(t) = 0.075 \cdot (V + 60). \quad (3.13)$$

This enhanced model of Noble [109], correctly represented the role of the potassium channels for cardiac cells. It furthermore could predict several new phenomena, like the pacemaker rhythm at about the right frequency. Nevertheless, the model missed the crucial calcium channels, which weren't demonstrated until 1967 by Harald Reuter [123]. We implemented this specific equations of Denis Noble, including the four differential states and all described parameters and variables. The solution is presented in Figure 3.2 in the discussion of this section, when we also take a closer look at some of the negative aspects of these models. But first, we continue with further improvements in cardiac cell modeling.

⁵The delayed rectifier actually consists of several components, which was discovered later.

3.2.3 Ion Pumps, Exchangers, and Calcium Dynamics

We want to depict two further publications, because of their very important improvements in cardiac cell modeling. Compared to the first Noble or the Hodgkin-Huxley model, the membrane current of later models often includes a more detailed ionic current flow. The main difference lies in the additional calcium ion ingredient and the according interactions of sodium-calcium $\text{Na}^+/\text{Ca}^{2+}$ exchanger, sodium-potassium Na^+/K^+ pump, as well as the description of intracellular calcium signaling. The first model that took the importance of all those dynamics into account, was given by DiFrancesco and Noble in 1985 [28]. Hilgemann and Noble further developed the calcium dynamics two years later in [55]. This model includes ten different ion currents rather than three as the Hodgkin-Huxley model, and 16 first-order differential equations in total.

$$I_{ion} = I_f + I_K + I_{K1} + I_{to} + I_{b, Na} + I_{b, Ca} + I_p + I_{NaCa} + I_{Na} + I_{si}, \quad (3.14)$$

where

- I_f is a hyperpolarizing-activated current based on K^+ and Na^+ ions,
- I_K is a time-dependent delayed rectifier of a K^+ current,
- I_{K1} is a time-independent background K^+ current,
- I_{to} is a transient outward current, activated by Ca^{2+} ions and dependent on the extracellular K^+ concentration,
- $I_{b, Na}$ is a background sodium current,
- $I_{b, Ca}$ is a voltage-dependent calcium current,
- I_p is the Na^+/K^+ exchange pump current, sometimes also referred to as I_{NaK} ,
- I_{NaCa} is the $\text{Na}^+/\text{Ca}^{2+}$ exchange current,
- I_{Na} is the fast inward sodium current with the according gating variables m , h ,
- I_{si} is the second inward current and its components that depend on Ca^{2+} , K^+ , and Na^+ ions. It is controlled by two gating variables d , f , similar to the previous gating formulations of Equation 3.5.

Furthermore, there is the intracellular concentration of sodium, potassium, and calcium included in the model. An extensive description of all parameters and the according equations is given in [28]. We just want to mention the most important improvements, like the sodium-potassium pump for example. This *active* pumping process uses the energy of adenosine triphosphate (ATP), hence it acts against the prevalent electrochemical gradients, to move three Na^+ ions out of and two K^+ ions into the cell. Additionally, the sodium-calcium exchanger plays an important role in signal processing of cardiac cells. Here, the potential

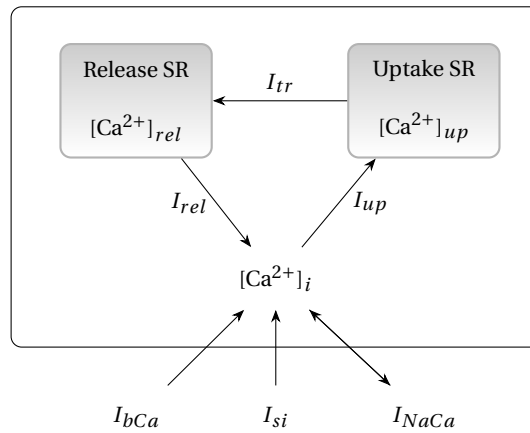


Figure 3.1: Mechanisms of the intracellular calcium ion movements from the DiFrancesco-Noble model. They split the cell into components of uptake and release sarcoplasmic reticulum (SR), as well as cytosol. Calcium is transported by an energy consuming pump into an uptake store. Some of these ions are then transferred into the release SR, respectively a release state. During an action potential, the actual calcium release happens in turn due to an intracellular increase of calcium.

energy of the sodium gradient, due to the Na^+/K^+ pumping, is used for the calcium transport against its gradient.⁶ It exchanges three Na^+ ions for every Ca^{2+} ion, which results in an inward current.

In consequence, this exchange process has in turn a big influence on the intracellular calcium concentration. DiFrancesco and Noble also included those intracellular dynamics in their model as well as the according concept that the *sarcoplasmic reticulum* (SR) is able to store most of the calcium ions. They assumed that there are three intracellular components of *uptake* SR, *release* SR, and cytosol⁷. A description of these components and the intracellular dynamics is given in Figure 3.1. As mentioned earlier, there are loads of other types of cardiac cell models. For more insight about the various types and the cardiac model development, see Noble's publications [110, 111, 112].

3.2.4 AV Node Models

In 2009, Inada et al. presented the first and so far only cellular model which includes the ion channel movements of the AV node. It is a one-dimensional multicellular model of a rabbit heart, with the regions of the SA node, the right atrium as well as the AV node. Here, the AV node is further split up into three regions of AN, N, and NH cells, for which the action potentials were calculated. The basic composition of the model includes a fast and slow pathway physiology for the AV node. It is built upon the structure and dynamics for cardiac cell mod-

⁶This process is called a *secondary active transport* as a result of the *first active transport* using ATP.

⁷Intracellular liquid.

eling that have been presented in this chapter. The detailed equations can be explored in the data supplements of their publication [60]. Interestingly, they were able to simulate AVNRT behavior, as well as the according treatment procedures via ablation, and by the application of antiarrhythmic agents. They were also capable of reproducing the effects of AFib on the AV node tissue, via randomly applied stimulations on the atrial cells for which AV node filtering could be observed. However, they described that the simulated tachycardias are very sensitive against variations in refractory period or conduction velocity, which additionally contributes to our conclusion in the discussion, later on. Besides, the full complexity of the AV node structure could not be specified in the model. Nevertheless, this publication is clearly an important improvement to build a complete cellular based model of the heart.

Simplified Approaches Derived From Cellular Models

There is a different strategy to model electrophysiological behavior. With fewer degrees of freedom it is possible reduce the complexity of the cellular based models. First of all, the FitzHugh-Nagumo model reduces the four-dimensional Hodgkin-Huxley model into a two-dimensional system. Here, the idea was to separate excitation and propagation from the electrochemical properties of sodium and potassium ion flow. The basic finding of FitzHugh was that the gating variables have very different kinetics. On the one hand, the sodium gating variable m , which converges very fast, is kept instantaneously in a steady-state. On the other hand, the slow dynamics (h, n) are symmetric in their process, what can be used to eliminate one variable. In the simplified system of the FitzHugh-Nagumo model, the fast dynamics are described by a voltage-like variable v , representing excitability, and the slow variables that correspond to a recovery variable w , representing refractoriness.

Podziemski et al. presented a simplified approach of the SA node, the right atrium, and the AV node in 2013 [117]. Their aim was to develop a model that is able to simulate long RR sequences of arrhythmias, like AVNRT, in real-time, including a slow and a fast anatomical pathway. Thus, they were able to reproduce the behavior of this tachycardia, and others, which were obtained in the electrophysiology lab for comparison. The model is described on a two-dimensional anatomical geometry, where only the required structures are simulated in detail. The tissue areas were modeled with two geometries, a two-dimensional plane and a cylindrical surface, composed of a 100 x 100 matrix of computational cells. The simplifications imply a representation in form of the FitzHugh-Nagumo model, see Equation 3.15, which they used to describe the electrical activity in the atrial muscle tissue. For the SA and AV node, Podziemski et al. used van der Pol-Duffing equations, which are given in Equation 3.16. In 2014, a similar model was formulated by Li in a three-dimensional, anatomically-detailed model of the rabbit right atrium that contained the sinoatrial and atrioventricular nodes [91].

$$\begin{aligned}\frac{dv(t)}{dt} &= \alpha \left(v - \frac{1}{3}v^3 - w \right) + \nabla(D\nabla v), \\ \frac{dw(t)}{dt} &= \mu(v + \beta - \gamma w),\end{aligned}\tag{3.15}$$

$$\begin{aligned}\frac{dv(t)}{dt} &= \frac{\alpha}{\mu} \left(v - \frac{1}{3}v^3 - w \right) + \nabla(D\nabla v), \\ \frac{dw(t)}{dt} &= \frac{f}{\alpha} v(v+d)(v+e),\end{aligned}\tag{3.16}$$

where

- $v = v(x, y)$ is the activation variable corresponding to the action potential of the tissue element located at (x, y) ,
- $w = w(x, y)$ is the control variable in the tissue element at (x, y) ,
- α is the damping constant,
- μ determines the amplitude of oscillations,
- f enables to rescale the frequency without changing the structure of the phase of the system,
- d, e are parameters,
- $\nabla(D\nabla v)$ is the diffusion coupling term with $D = D(x, y)$, which was inserted into the van der Pol-Duffing model, so that the differential equation for v matches the corresponding equation in the FitzHugh-Nagumo model.

So far, we considered the electrical excitation propagation through individual cells, or on a micro-level scale. However, it is also possible to examine the conduction mechanisms on a larger scale, but still derived from cellular models. This could mean, for example, that parts of the heart tissue are averaged to cell compounds. An even larger scale is described in the following section of the phenomenological models 3.3. One example is based on *cellular automata* and presented by Small in [136]. This approach is a simplification of cardiac dynamics applied on cell compounds, which are used to represent the propagation of excitation of cardiac tissue. It can be implemented in a setting of two-dimensional, homogeneous cells. Here, wave propagation patterns depend on probabilities of excitation by neighboring cells. This cellular automaton describes various simulations of regular cardiac dynamics, in regular tachycardia, and in atrial fibrillation.

Another category, based on a simplified description of the cellular processes, are *bidomain* models. These are models, for which at every point in the two domains of intracellular and extracellular space, electrical potentials are defined separately. The intracellular and extracellular space have unequal anisotropy ratios, which means “they have a different electrical conductivity in the direction parallel to the myocardial fibers than in the direction perpendicular to them”⁸. Bidomain models are able to accurately model extracellular stimulation, even though they are a huge simplification, compared to the complex micro scale models. Nevertheless, these models are still computationally expensive. Potse et al. described in their publication, that it took two days on 32 processors to simulate one complete cardiac cycle in

⁸From “Scholarpedia”, by Bradley J. Roth, 2008 [124]. Licensed under *Creative Commons Attribution NonCommercial ShareAlike 3.0 Unported License*.

sinus rhythm [118]. For a more detailed view on bidomain models see [150]. There is a further simplification in so-called *monodomain* models, to gain higher computational speed. Here, equal anisotropy ratios for the intra- and extracellular domains are assumed, although that removes the physiological foundation. It can be seen as a heuristic approximation of the bidomain model to get a faster solution. It is also used to improve numerical efficiency for the bidomain model [45].

3.2.5 Discussion

At first sight, it is probably the most intuitive way in modeling of aiming for the best possible accuracy, to receive the desired result in return. As discussed in the beginning of this chapter, however, this statement is not always true. In the end, the question is whether it is reasonable to use one of the presented methods to describe the AV node characteristics, and especially to solve the problem of discriminating AFlut from AFib. Actually, there are also some downsides in the first principle approaches. According to Noble's review [112], there is still only one detailed cellular model of the atrioventricular node, which is not human but of rabbit cells. Despite the high accuracy of this approach of Inada et al., the AV node characteristics are not entirely investigated so far. Moreover, the complexity of ion channel dynamics is extraordinary high and can often only be applied under specific simulation and computation environments. In consequence, these models are very sensitive against parameter variations.

In order to take a closer look at the first principle approaches, we implemented the first Noble model of 1962, to illustrate the action potential of a basic cardiac cell. In Figure 3.2, the four time time-dependent state variables of these equations are described. The figures contain the differential state functions with the original parameters as well as the same functions with one modified parameter. This model is much less complex than the later developed ones including the complete calcium dynamics. But even with a slight variation of only a single parameter, the solution drastically changes. Building on this, the many different components of the cardiac conduction system, even down to the level of ion channels and dynamics, vary from patient to patient [50, 141]. Because of the high degree of detail of first principle models and in consequence a necessary patient specific modeling, in clinical day-to-day practice this approach would be very impractical or even impossible to use at present.

Another way of realization could be better, namely to use simplified models. However, similar problems appear in bidomain models, even though they are less complex than cellular based models. In other approaches like Podziemski or Li, there is still some work to do, to proof that those models are able to reproduce most of the dynamics of the human atrioventricular node. Especially to simulate the various kinds of electrical activity during arrhythmias is still highly difficult. Again, the patient specific parameters cause trouble in the fast clinical workday. Despite the obvious complexity of the first principle systems, however, one can see that the time shift is very regular in all states of Figure 3.2. Additionally applies that the interest in an particular action potential, a gating variable, or the very details of the membrane potential, is not a crucial factor in our specific application. Now, if only the basic conduction behavior in the AV node is of interest, we can probably simplify

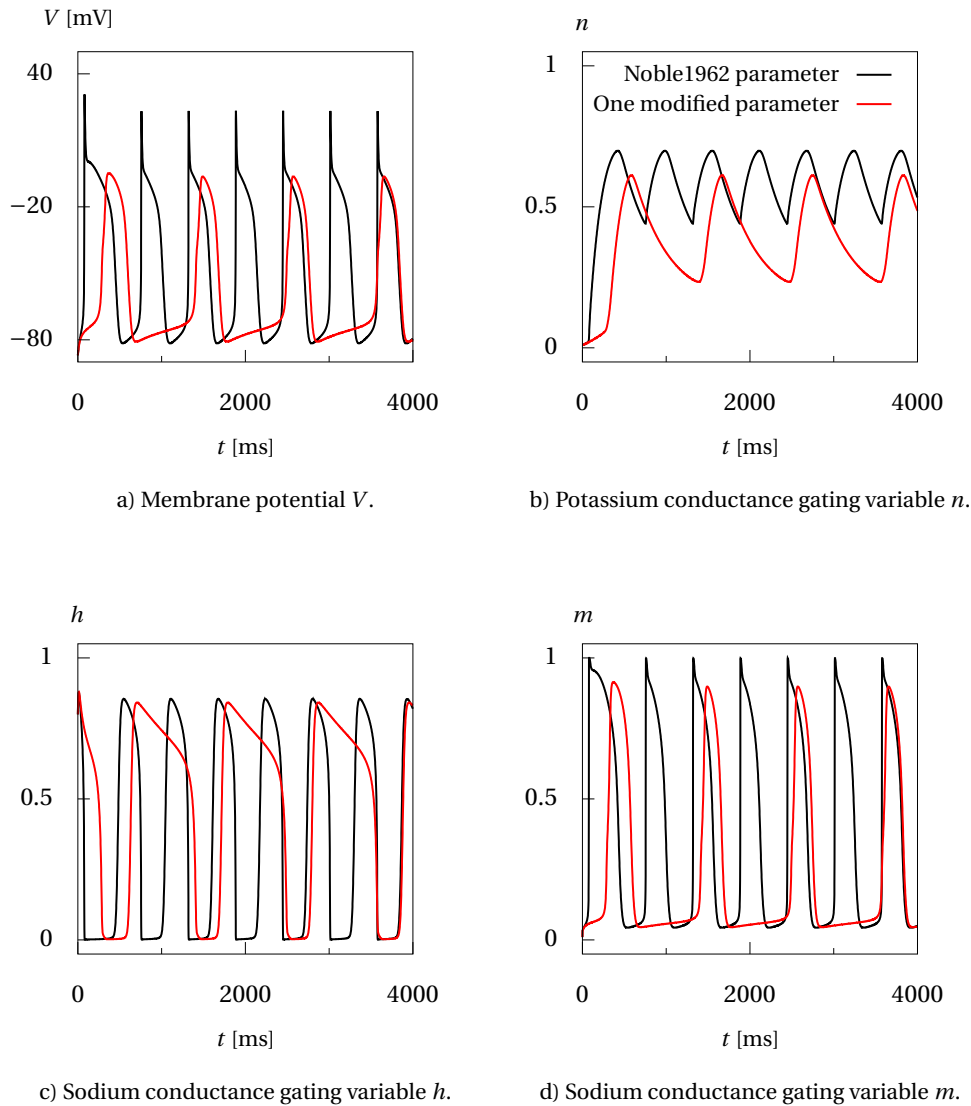


Figure 3.2: Impact of parameter \hat{g}_{Na} on the solution of Noble Equation 3.5 and 3.6. In each plot, the cellular dynamics are described, time-dependent on membrane potential or the specific gating variable. Compare also the similarities of these simulated action potentials to the action potential described in Figure 1.6 in Chapter 1.

some things drastically. In conclusion, there is the possibility to focus on a different kind of modeling approach, or more precisely, to take a look at phenomenological models of the AV junction.

3.3 Phenomenological Models of the AV Junction

So far, we overviewed several methods of modeling in this chapter. For the prevalent problem, however, they all have some weaknesses. Statistical methods have limitations especially when there is not sufficient data available to compare, or the data is not accurate enough. If there is too little known about the underlying processes, or it gets too complex to create a first principle model, it is probably not the best approach as well. Another method from a different point of view is to create a model based on the phenomenological observations. Such a *phenomenological model* might be a better way to solve this challenge. Thus, we now present different mathematical models based on the insights we gained about the human heart in Chapter 1, and above all, based on the AV node characteristics presented in detail in Chapter 2.

We start with a specifically designed model for the *classical AV block* of type I and type II, including the advanced second-degree AV block. This is followed by various approaches from literature to predict the electrical conduction phenomena by an *AV nodal recovery curve*. Finally, the *combined multilevel model* is defined based on the newly developed concept of Section 2.4. Of course, those approaches are also considered in an application later on and validated in Section 5.3 of the numerical results. But first of all, we specify the problem formulation of a general phenomenological model in Definition 3.1. In the following sections, the exact conduction process is then mathematically specified in detail, for each approach accordingly.

Definition 3.1 (Phenomenological AV Block Model)

Let $\mathcal{T} := [t_0, t_f] \cap \mathbb{N}$ be the time horizon of the analyzed ECG sector, a finite subset of all atrial excitations $\mathcal{A} = \{A_i \in \mathcal{T} \mid 1 \leq i \leq m\}$ with m elements, and $\mathcal{V} = \{V_j \in \mathcal{T} \mid 1 \leq j \leq n\}$ a finite subset of ventricular excitations with n elements. Then, a basic phenomenological model of the AV node is defined by the mapping of function

$$f : \mathcal{A} \rightarrow \mathcal{V}, \quad A_i \mapsto V_j, \quad A_i < V_j. \quad (3.17)$$

Furthermore, there is a subset $\mathcal{B} \subset \mathcal{A}$ defined, including all non-conducted or blocked atrial elements with $|\mathcal{B}| = n - m$. △

For the sets of atrial and ventricular excitations \mathcal{A} , \mathcal{V} obviously applies that the number of elements is $n \leq m$. In the case of $m = n$, all atrial signals are conducted to the ventricles and no AV block is prevalent at all. Additionally, f is injective but not surjective in general, only in the case of $m = n$. All time points measured in the ECG or applied in the AV conduction models are defined to be integers in a degree of accuracy in milliseconds. Due to this reason, all time points or intervals are subsets of \mathbb{N} .

3.3.1 Classical AV Block Type Models

In this section, we create two different models which are both able to describe the AV signal conduction in a type II block, an advanced second-degree AV block, as well as a 3 : 2 type I block. Furthermore, the *square root model* is capable of reproducing a *typical* type I block, while the *linear model*, on the other hand, can additionally display an *atypical* type I block. In conclusion, this section is completely build upon the classical AV block type definitions made in Chapter 2.2 and the two models are able to describe all possible kinds hereof. An overview about the used variables and the according specifications is given in Table 3.1. The following Definition 3.2 further specifies the basic conduction concept of the two types of classical AV Block models.

Definition 3.2 (Classical AV Block Model)

Let $\bar{C} \subset \mathbb{N}$ be the set of all signal conduction time intervals and f a phenomenological model function. The conduction for all kinds of classical AV block models can be described by

$$f(A_i) = A_i + \alpha + \Delta_k \quad (3.18)$$

with a fixed, patient specific conduction constant $\alpha \in \bar{C}$ and the conduction increment $\Delta_k \in \bar{C}$ that depends on the number of conducted signals $k = 1, 2, 3, \dots$ within one block cycle. For an atrial signal to conduct shall further apply

$$A_i > V_{j-1}, \quad i, j > 1, \quad (3.19)$$

where the last conducted signal is assumed to be $V_{j-1} = f(A_{i-1})$. This is equivalent to the codomain definition of

$$\mathcal{V} = \{V_j \in \mathcal{T} \mid V_j = A_i + \alpha + \Delta_k, i \geq j, A_i > V_{j-1} \text{ or } i = 1\}. \quad \Delta$$

In Equation 3.18, α is the regular signal conduction interval in sinus rhythm, which is always prevalent. Δ_k can be seen as the additional part that arises only for the varying conduction interval during fast atrial rhythm and leads to AV blocks. Both parameters can be regarded as patient specific constants. In addition to the signal conduction of Equation 3.18, the inequality 3.19 determines whether a signal is being conducted or blocked. As one can see, this depends on the previously conducted signal, which in turn is dependent on the atrial input interval and the conduction parameters. A signal is conducted, as long as the inequality 3.19 is true. Otherwise the incoming signal is blocked and in consequence k is reset. The first incoming signal A_1 , is defined to be conducted under any given conditions. As this basic principle is very important, we want to explain it more precisely.

One can imagine, if an atrial signal reaches the AV cell or cell compound while the previous signal is still being processed, the cell is definitely in a refractory state. Of course, the refractory time doesn't have to be exactly defined by the constraint of 3.19 and most likely will vary from patient to patient. But, with this constraint we are able to realistically describe the electrophysiological process of refractoriness in a cell, without introducing an additional parameter for this phenomenon. Besides, all classical block type patterns that are found in literature, including advanced second-degree AV block with more than one blocked signals,

Variable	Specification	Description
Sets		
\mathcal{T}	$\mathcal{T} := [t_0, t_f] \subset \mathbb{N}$	Time horizon of the analyzed ECG sector
\mathcal{A}	$\mathcal{A} \subset \mathcal{T}$	Time points of all atrial excitations
\mathcal{B}	$\mathcal{B} \subset \mathcal{A}$	Time points of all blocked atrial excitations
$\bar{\mathcal{C}}$	$c \in \bar{\mathcal{C}} \subset \mathbb{N}$	All possible AV conduction time intervals ⁹
\mathcal{V}	$\mathcal{V} \subset \mathcal{T}$	Time points of all ventricular excitations
Indices		
i	$1 \leq i \leq m$	Index counter per incoming signal
j	$1 \leq j \leq n$	Index counter per conducted signal
k	$k = 1, 2, 3, \dots$	Conducted signal counter within one block cycle
Input Data		
m	$m \in \mathbb{N}$	Number of incoming signals
A_i	$A_i \in \mathcal{A}$	Time point of the i th atrial input signal
α	$\alpha \in \bar{\mathcal{C}}$	Regular signal conduction time interval
Δ_k	$\Delta_k \in \bar{\mathcal{C}}$	Varying conduction increment depending on k
Output Data		
n	$n \in \mathbb{N}$	Number of conducted signals
V_j	$V_j \in \mathcal{V}$	Time point of the j th conducted ventricular signal

Table 3.1: Basic variables and descriptions for a classical AV block type model of the signal conduction between atria and ventricles for one AV block level.

can be displayed by it.

This can be demonstrated at a quick example of an atrial flutter patient with very fast and regular atrial excitations. For this purpose, let's assume that the fast atrial rhythm leads to a basic type II block, which means no varying conduction increment. In this case, the conduction constant α is able to solely represent the signal conduction time through the AV node, while the corresponding increment can be set to zero $\Delta_k = 0 \forall k$. Now, if the atrial excitation rate is faster (hence smaller) than the signal conduction interval $A_i - A_{i-1} < \alpha$, which is equivalent to $A_i < V_{j-1} = A_{i-1} + \alpha$, the cells are obviously not ready to get excited again and the signal is blocked. If the atrial excitation interval is at least twice as fast as the input interval, two signals get blocked, and so on. This process accordingly works for the other block types, taking Δ_k into account.

Square Root Model

The characteristics for the typical type I block, defined by Wenckebach, were specified in Section 2.2.1. As conditions, it is sufficient to use the first two of the four characteristics, because the other two are logically redundant. These are a progressive lengthening of the PR

⁹Unless stated otherwise, we use the term *interval* as time interval or duration throughout the whole dissertation and not in the context of a mathematical interval.

For both classical AV block models, the decision whether a signal is being conducted or blocked is defined by the constraint of Equation 3.19, even though it implies a different signal conduction type. On the one hand, the classical AV block model is able to depict all basic kinds of second-degree AV blocks with just two similar approaches that were describe in Section 2.2. Furthermore, this model is quite simple, which could also be a big advantage in implementation or computing time. On the downside, the model is inflexible to changes from one to another block cycle within one ECG sector \mathcal{T} . For example, the transition from a 4 : 3 to a 3 : 2 block, without changing the atrial input rate or the patient specific parameters α or Δ_k . Besides, the model only describes one AV block level so far. A closer examination about the behavior of the classical model in application, is given in Section 5.3.

3.3.2 AV Nodal Recovery Curve Models

Another way to predict the complex behavior of the AV node, was presented by Shrier et al. in 1987 [132]. They tried to reproduce clinically measured conduction phenomena in the heart with an *atrioventricular nodal recovery curve*. This idea goes way back to 1926, when Lewis and Master demonstrated that the Q-P interval could be used as an indicator for the recover phenomenon of the AV nodal tissue [88]. Besides, Talajic et al. presented a *unified model of atrioventricular nodal conduction that predicts dynamic changes in Wenckebach periodicity* in 1991 [143], based on the Shrier model. Recently, further recovery curve models have been published, which are also briefly outlined in this section. Now at first, the recovery time interval is defined as follows:

Definition 3.3 (Recovery Time Interval)

Let $\overline{\mathcal{R}} \subset \overline{\mathcal{T}}$ be set of all AV nodal recovery intervals. Then $VA_{j-1} \in \overline{\mathcal{R}}$ is the recovery interval from the preceding conducted beat with

$$VA_{j-1} := \sum_{l=1}^p AA_{l_{j-1}} - AV_{j-1}, \quad j \in [2, m], \quad (3.22)$$

where $AV_{j-1} \in \overline{\mathcal{C}}$ is the conduction interval of the previously conducted beat and the atrial intervals $AA_{l_{j-1}} \in \overline{\mathcal{A}}$ are summed up from this last conducted beat. Furthermore applies that $p \in \mathbb{N}$ is the first signal

$$VA_{j-1} > \theta, \quad (3.23)$$

for which the recovery interval exceeds the refractory period $\theta \in \overline{\mathcal{C}}$. △

In other words, $(p - 1)$ represents the number of blocked atrial beats and θ determines the minimum recovery interval VA that allows a signal conduction. Using these specifications, we can now describe the recovery curve model in Definition 3.4. This problem formulation shows that an increase of the recovery time VA_{j-1} comes along with an exponential decrease of the conduction time AV_j .

Variable	Specification	Description
Sets		
$\overline{\mathcal{T}}$	$t \in \overline{\mathcal{T}} \subset \mathbb{N}$	Set of all possible time intervals
$\overline{\mathcal{A}}$	$AA \in \overline{\mathcal{A}} \subset \overline{\mathcal{T}}$	Set of all atrial cycle length time intervals
$\overline{\mathcal{R}}$	$r \in \overline{\mathcal{R}} \subset \overline{\mathcal{T}}$	Set of all AV nodal recovery time intervals
Indices		
l	$1 \leq l \leq p$	Index counter from the last conducted beat
$p-1$	$p \in \mathbb{N}$	Number of blocked beats during recovery
Input Data		
$AA_{l_{j-1}}$	$AA_{l_{j-1}} \in \overline{\mathcal{A}}$	Atrial time intervals from the last conducted beat
VA_{j-1}	$VA_{j-1} \in \overline{\mathcal{R}}$	Recovery interval from preceding conducted beat
θ	$\theta \in \overline{\mathcal{C}}$	Absolute refractory period
α	$\alpha \in \overline{\mathcal{C}}$	Min. AV conduction interval after full recovery
Δ	$\Delta \in \mathbb{N}$	Conduction increment or fatigue parameter
$\beta, \hat{\beta}, \delta$	$\beta, \hat{\beta}, \delta \in \mathbb{N}$	Facilitation parameters ¹⁰
$\tau_{rec}, \tau_{fat}, \tau_{fac}$	$\tau_{rec}, \tau_{fat}, \tau_{fac} \in \mathbb{N}$	Recovery, fatigue, and facilitation time constant
Output Data		
AV_j	$AV_j \in \overline{\mathcal{C}}$	AV conduction interval at the j th conducted beat

Table 3.2: Additional variables and descriptions for a recovery curve model of the signal conduction time in the AV node.

Definition 3.4 (Recovery Curve Model)

The AV nodal recovery curve $g: \overline{\mathcal{R}} \rightarrow \overline{\mathcal{C}}$ is described by an exponential function of the preceding recovery interval

$$g(VA_{j-1}) = AV_j = \alpha + \hat{\beta} \cdot \exp\left(\frac{-VA_{j-1}}{\tau_{rec}}\right), \quad (3.24)$$

with the patient dependent constants of a fixed regular conduction interval $\alpha \in \overline{\mathcal{C}}$, a recovery parameter $\hat{\beta} \in \mathbb{N}$, and a specific recovery time constant $\tau_{rec} \in \mathbb{N}$. \triangle

The problem specification of the recovery curve model is, at first sight, build up on a different idea compared to the classical model. The function describes the AV nodal conduction time directly dependent on the preceding recovery interval, rather than the ventricular signal time dependent on the atrial input. Furthermore can be noted, that here the blocked beats are counted in contrast to the conducted beats as in the classical approach. Both models, however, use a similar approach of the refractory period described by an inequality constraint. In the recovery curve model, the refractory period $\theta \in \overline{\mathcal{C}}$ is directly defined and determines whether a signal is conducted or blocked. In the classical model, this decision is indirectly specified and depends on the following atrial input signal.

¹⁰In case of both Shrier models, $\hat{\beta}$ can be seen as patient specific recovery parameter.

Shrier Model

In particular, Shrier et al. built an iterative setting where they intracardially measured His (H) bundle deflections of periodic atrial pacing stimulation (S) and this way determined the AV conduction time (SH) as well as the recovery time (HS). For the sake of continuity and simplification, we restate some of the variables used by Shrier et al. Additionally applies in our case that the atrial signal A is not necessarily regular, because we do not only consider pacing induced examples. Furthermore, the ventricular symbol V stands for the His deflection, respectively the output signal of the AV node. Accordingly, AV is the conduction time while VA denotes the recovery time. All new variables that are used in this section, or previously defined variables, which imply a similar specification as before, are listed in Table 3.2. For example, the minimum AV conduction time after full recovery of the according cells can be described by the conduction constant α . This also equals the basic conduction time of a signal at all block types or in sinus rhythm, as defined in Section 2.2.

In their specific description of the AV nodal recovery curve model, they used two different exponential functions to fit the obtained data for various patients. The first model function is exactly given by the basic recovery curve model of Equation 3.24, the second one is illustrated in Equation 3.25. As mentioned earlier, we modified the parameter notation of the original model to adjust them to the previous definitions as well as to the Talajic model.

$$AV_j = \alpha + \hat{\beta} \cdot \exp\left(\frac{-VA_{j-1}}{\tau_{\text{rec}}}\right) + \Delta \cdot \exp\left(\frac{-VA_{j-1}}{\tau_{\text{fat}}}\right) \quad (3.25)$$

The additional exponential term, which was added in this equation, can be seen as responsible for the fatigue of the AV node, as Talajic et al. described in their publication.¹¹ Also, the corresponding constant given by Δ , can be seen as a part of the conduction increment, see the following section for further information.

Talajic Model

Talajic et al. mentioned, that they presented the first AV model where time-dependent processes other than recovery came into account. They included more stimulation history to the recovery curve model based on three concrete assumptions that are described as follows:

$$AV_j = \alpha + \beta \cdot \exp\left(\frac{-VA_{j-1}}{\tau_{\text{rec}}}\right) + \Delta_j, \quad (3.26)$$

$$\Delta_j = \Delta_{j-1} \cdot \exp\left(\frac{-AA_{j-1}}{\tau_{\text{fat}}}\right) + \Delta \cdot \exp\left(\frac{-VA_{j-1}}{\tau_{\text{fat}}}\right), \quad (3.27)$$

$$\beta = \hat{\beta} - \delta \cdot \exp\left(\frac{-AA_{j-2}}{\tau_{\text{fac}}}\right). \quad (3.28)$$

At first, there is the basic, time-dependent recovery, given in the first exponential term in Equation 3.26. Secondly, there is a fatigue of the AV node described in the second exponential term in combination with Δ_j . It is caused by a response of a continuous, high-frequency

¹¹ Shrier et al. missed a more detailed description of the purpose of some patient dependent constants.

activation leading to a slowing conduction and modeled by Equation 3.27. Thirdly, they showed an effect of short cycles to advance recovery, called *facilitation*, which is described by β in Equation 3.28.¹²

The amount of conduction slowing caused by fatigue is added at each AV nodal activation and can be seen as equivalent to the conduction increment of the classical model. However, this increment is not directly depending on a conducted signal counter k as before, but on the previous atrial as well as the recovery interval. Additionally, every atrial signal, not only the conducted ones, counts as contribution to the fatigue increment Δ_j . The facilitation parameter β , on the other hand, supports the recovery process. While in the Shrier model this parameter is just predefined as a constant, here comes an equation into account. The longer the incoming intervals from the second last to the last conducted beat is, the more it approaches the maximum facilitation constant $\hat{\beta}$. For this equation needs to be noted, that Talajic et al. only considered conducted signals as *incoming* intervals, which is in fact a misleading description for this variable. We defined this parameter as $AA_{I_{j-2}}$ according to Definition 3.3. The variables of τ_{rec} , τ_{fat} , and τ_{fac} denote the patient specific recovery time constant, the fatigue time constant, and the facilitation time constant, respectively.

Discussion

The groundwork for most recovery curve approaches was provided by the publication of Shrier et al., who presented interesting results at various patients. They computed the according pacing frequency using the AV nodal recovery curve and only some measurable patient specific constants. They also showed the conduction pattern migrates from 6 : 5 type I to a 2 : 1 block in one patient, depending on the atrial cycle length. The complete recovery curve model in the simplest version of Shrier et al. is described in Algorithm 3.2. To get a comparable model, we modified the image function to a phenomenological AV block model $f : \mathcal{A} \rightarrow \mathcal{V}$, as in Definition 3.1. Again, this model can be transferred to the second Shrier version including two exponential parts, which is also displayed in Appendix A.

Basically, the recovery curve models are able to describe several phenomena of the AV node conduction. However, Shrier only analyzed the block pattern of type I to a 2 : 1 block pattern and is missing other conduction phenomena, as Castellanos et al. remarked [18]. A few years later, Talajic et al. illustrated some other weaknesses of this model in terms of the strong dependency of the recovery curve due to the pacing rate. Furthermore, Talajic noted the missing explanation for a varying block pattern during constant rate atrial pacing [143]. The extension of Talajic thus added detailed behavior of the AV conduction that can be observed. In 2002, Jorgensen et al. used statistical methods to receive more accurate parameters for the recovery curve model Equation 3.24, but in atrial fibrillation and atrial flutter [65]. Their work was based on ventricular as well as intracardially measured atrial activity. In a retrospective study, they analyzed AV dynamics like nodal recovery or dual pathway phenomenon in AFib and AFlut, at various atrial cycle lengths. A further and very interesting discovery of this publication was the instability of AV conduction pattern at high atrial rates and accordingly at multiple block levels. This instability or changes in block pattern can be seen in most of the AFlut examples where no typical sawtooth pattern is prevalent. These

¹²Again, it should be noted that the used variables and equations are adapted from the original model.

findings are confirmed by our data set of regular atrial tachycardias and the according solutions in Chapter 5.

It seems, that compared to the classical models, more conduction phenomena might be reproduced by the recovery curve approach. Nevertheless, it still needs to be determined more precisely which kinds of second-degree AV blocks can be described in practice by the AV nodal recovery curve models. Hence, we implemented both Shrier models in our software package and tested it at various ECG examples from our data set. The results are shown and further analyzed in Section 5.3.2. The Talajic model was not implemented, because the findings of Masè et al. showed that “the impact of fatigue and facilitation decreases at increasing levels of block” and that especially in atrial flutter this effect should be limited [98]. Finally is to mention, that this approach is kind of an alternative concept to the multilevel idea. Here, *advanced second-degree AV blocks* are described as several blocked beats on one level rather than one blocked beat on multiple levels. However, it should be noted that neither in the primary versions of Shrier and Talajic, nor in the dual pathway approach of Masè et al., are able to describe all complex ventricular excitation pattern without changing the atrial cycle length [18, 98].

Algorithm 3.2:

Input: m incoming signals A_i , conduction constant α , refractory time θ , patient dependent constants $\hat{\beta}$, τ_{rec} , AV conduction interval at the first beat AV_1

Output: n conducted signal time points V_j

begin

```

   $V_1 = A_1 + AV_1$ 
   $VA_1 = -AV_1$ 
   $j = 2$ 
   $AA_l = 0$ 
  for  $i = 2$  to  $m$  do
     $AA_l = AA_l + AA_{j-1}$ 
    if  $AA_l + VA_{j-1} > \theta$  then                                     /* Signal can be processed */
       $AV_j = \alpha + \hat{\beta} \cdot \exp\left(\frac{-VA_{j-1}}{\tau_{\text{rec}}}\right)$ 
       $V_j = A_i + AV_j$ 
       $VA_j = -AV_j$ 
       $j = j + 1$ 
       $AA_l = 0$ 
    else                                                             /* Signal can not be processed */
       $VA_{j-1} = VA_{j-1} + (A_i - A_{i-1})$ 
       $n = j - 1$ 

```

3.3.3 Combined Multilevel Model

The main idea of the combined multilevel approach is to use the advantages of the models that have been discussed so far, and extend it to multiple block levels. So first of all, we

Variable	Specification	Description
Sets		
\mathcal{AV}^I	$AV_j^I \in \mathcal{AV}^I \subset \mathcal{T}$	Set of conducted signals on 1st AV block level
\mathcal{AV}^{II}	$AV_j^{II} \in \mathcal{AV}^{II} \subset \mathcal{T}$	Set of conducted signals on 2nd AV block level
Input Data		
m^{II}	$m^{II} = n^I$	Number of input signals on 2nd block level equals number of output signals on 1st level
AV_i^{II}	$AV_i^{II} = AV_j^I$	Time point of i th input signal on 2nd block level equals j th output signal on 1st level
Output Data		
n^{II}	$n^{II} = m^{III}$	Number of conducted signals on 2nd block level equals number of output signals on 3rd level
AV_j^{II}	$AV_j^{II} = AV_i^{III}$	Time point of j th conducted signal on 2nd level equals i th input signal on 3rd block level

Table 3.3: Basic variables and definitions for the combined multilevel model, describing the signal conduction between atria and ventricles for multiple AV block levels. Here, the input and output variables for the second block level are given. A further explanation of the various block level symbols is given in the text.

expand the basic phenomenological model to several block levels with the following Definition 3.5.

Definition 3.5 (Multilevel Model)

Let f , g , h be phenomenological model functions, where every function describes a different AV block level with $AV_j^I \in \mathcal{AV}^I \subset \mathcal{T}$, $AV_j^{II} \in \mathcal{AV}^{II} \subset \mathcal{T}$, and the mapping functions:

$$h: \mathcal{A} \rightarrow \mathcal{AV}^I, g: \mathcal{AV}^I \rightarrow \mathcal{AV}^{II}, \text{ and } f: \mathcal{AV}^{II} \rightarrow \mathcal{V}. \quad (3.29)$$

The composition of $f \circ g \circ h$ then defines a multilevel model of successively combined AV block levels. △

Including the physiological background described in Section 2.3, we define three possible block levels that can be active at the same time. In Table 3.3, the input and output variables for such a multilevel model and in specific for the second block level are given. All variables and specifications for the other levels follow with the according level symbol I, II, or III. In general applies, that the input for the first block level is still given by the set of all atrial excitations \mathcal{A} , which in conclusion means that $A_i \equiv AV_i^I$. On the other hand, the output on the last active block level can assumed to be equivalent to the ventricular excitations. For the sake of simplicity, these are described by the according symbol $V_j \in \mathcal{V}$ instead of an AV block level sign. Furthermore applies, that a level is usually neglected if the block level is inactive, respectively if there is a 1 : 1 conduction on the total time horizon \mathcal{T} .

So far, this was the definition of the multiple levels, now we have a closer look at the concrete conduction mechanism on each block level. As seen in Chapter 2, a unified hypothesis for the conduction of the second-degree AV block makes probably more sense physiologically than two completely distinct blocking type mechanisms. Furthermore, conduction pattern sometimes occur with little changes in the conduction ratio from one block cycle to the next one, but within one block level. This was also described in the publications, presented in Section 2.3, especially in the considered cases of very fast atrial intervals. A further proof of this alternating phenomenon is viewed at several real life ECG examples of patients with cardiac arrhythmia in Section 5.4. These changes in the conduction pattern are not completely regular but can develop from 6 : 5 to 3 : 2 over several steps for example. The effects sometimes appear slightly random considering only a short window of a couple of block cycles, which is existent in a common ECG strip. In fact however, they do follow certain rules of AV block characteristics. The medical reasons for these effects can be manifold which we already discussed previously. This would be for example fatigue or recovery of the AV node, just like causes by medicinal treatment. On the other hand, there might come some further patient dependent factors into play.

The concepts of the classical or the recovery curve approach are able to describe some of the conduction types for individual patients. However, to cover all these effects in a way similar to the so far presented phenomenological models can cause problems, as can be seen in the validation of these approaches in Section 5.3. This becomes particularly obvious in the considered cases including a short time window of about 15 to 30 RR intervals. Taken together, for a patient independent model that can describe all possible kinds of AV blocks, it is perhaps just not the best idea, or could be in fact impossible, to create a model in the kind of the other phenomenological ones. But including the illustrated medical knowledge it is probably a better approach to create an algorithmic solution for this problem. Hence, we decided to use the mechanisms of the phenomenological models for the AV block conduction, but extend these by algorithmic tools to get a complete and especially patient independent mathematical model for second-degree AV blocks. The concrete model is illustrated in the following Chapter Algorithms & Implementation in Section 4.2.4.

Chapter 4

Algorithms & Implementation

Many of the modern ECG devices provide algorithms to support physicians in finding the correct diagnosis for a certain disease. For some heart diseases this works pretty well, but as previously described, the differentiation of AFlut from AFib is in many cases hindered by several factors. Bogun et al. report a misdiagnosis of AFlut as AFib in 35% (382 of 1085 patients) of clinically applied algorithms [14]. Our claim is however, to implement an algorithm that is not only able to identify the underlying AV block type but also to compute the actual cycle length activation in cases of a regular atrial rate. For this purpose, we use the phenomenological models of the AV node, described in Section 3.3, in combination with a newly developed algorithm. This combination of mathematical and algorithmic approach also considers the electrophysiological mechanism of the MAVB phenomenon. It is implemented in the *HEAT* software package, which is able find the correct diagnosis, solely based on a few RR intervals and within real-time. The complete software as well as the individual components are explained in detail in the second part of this chapter.

From the raw ECG signal to the correct diagnosis, however, several steps are necessary at first. Hence, we start with a glance at some signal processing methods that can be used for example to filter the ECG signal and detect R waves. Three of the most established ECG interpretation algorithms are also analyzed which all base on signal processing methods. Then, two specific publication examples are further examined that describe this kind of approach for the discrimination of AFlut from AFib. Finally, the advantages and drawbacks of these methods are discussed, while we also compare the various algorithmic approaches against each other, as regards diagnostic skills and necessary input data.

4.1 Signal Processing Methods for ECG Analysis

The basic idea of signal processing, to transform time dependent signals into a frequency domain, is a common approach in the ECG analysis. There are different time points in this analysis procedure, where signal processing is used within ECG devices. The first step is usually a preprocessing to filter the signals against noise. Then, there are various kinds of approaches to detect specific parts of the ECG signal which were shown in detail in Figure 1.9. These could be for example, QRS complex or P waves detection. Besides, there is wave form analysis or measurement of distances between these parts for a further interpretation.

In the following sections can be seen that signal processing methods work quite well, or are even necessary, for some parts of the ECG analysis process while in other parts these methods are more error-prone. One of the biggest problems is their vulnerability for so-called ECG artifacts. These are electrocardiographic measurements that do not arise in the heart, but are generated through internal or external influence. These artifacts could be caused by

poor electrode contact, electrical noise due to patients movement, or else. Unfortunately, artifacts are a rather common phenomenon especially in patients having cardiac arrhythmia. This fact could explain the trouble to use these methods to discriminate regular supraventricular tachycardias like AFlut from AFib. We now give a short introduction in ECG filtering methods as well as R wave detection that we also implemented in our software package.

4.1.1 Filtering ECG Signals and R Wave Detection

There are many different signal processing methods used in the field of ECG processing. In our software package this is used solely as a data acquisition method but not for the specific discrimination algorithm like in other algorithms, see Section 4.1.2. Hence, we just want to give a short overview about the topic. As mentioned above, there can be unwanted objects in the ECG signal like artifacts. In any case, even if there are no larger artifacts, there is always some kind of noise in the signal due to the nature of the recording method. Therefore, the ECG signal processing usually starts with some kind of filtering. The tricky thing about filtering is, however, that it probably not only removes e.g. muscle noise but also attenuates the actual signal we want to analyze due to the same frequencies. Thus, there are different kinds of filters used to get the desired signal as good as possible.

The *low pass filter* removes the higher frequencies from the signal which can arise from external sources for example. This filter also affects the profile of the QRS complex as a higher frequency signal. To block the lower frequencies on the other hand, a so-called *high pass filter* is used. Here, mainly common muscle generated waveforms are removed or the direct current offset caused by the electrode contact on the skin. In this context, problems can occur because the P wave is often in the range of these lower frequencies. This is especially the case in supraventricular tachycardias as described in Section 2.1. Furthermore, another common technique is the *notch filter*. This is a kind of mixture between the two others where a specific range of frequency can be adjusted. This technique is used in the Glasgow Algorithm for example, described in the following section. [38, 162]

After filtering the ECG signals, the first thing to do is always to find the QRS complex which is the most prominent and readable part of the ECG curve. There are several techniques to get this specific sector of the recording. Either of these methods is based on one of the various signal processing tools like short-time Fourier transform (STFT) or wavelets. There is much literature on this topic therefore we only want to refer to it at this point [1, 69, 90].

Another approach which we like to have a closer look at, is the template matching technique of the sliding window. Here, at first a template of the QRS complex is constructed. The basic idea is then to compare this template as a “sliding window” successively to the ECG signal and seek for matches. Therefore, one can use a function to find the difference or correlation between the template and ECG signal with a certain minimum threshold [136]. In the GE Marquette 12SL Algorithm illustrated in the following section, this method is implemented with the additional adjustment of the template at every recognized QRS complex. On the other hand, one can also use the first and second derivative of the ECG signal, instead of a template, because of the large slope at the beginning of the QRS signal. This method is used in the R wave detection of our algorithm as presented in Section 4.2.2, as well as applied in existing medical devices [122].

4.1.2 Established ECG Interpretation Algorithms

There are various interpretation algorithms implemented in ECG devices, which are generally based on signal processing methods. In this section, we present three different of these ECG algorithms that belong to the most popular ones. We have a closer look at their specific methods and skills, which are in total more extensive than the discrimination of AFlut and AFib. In the end of this section, we are then able to compare these various skills, in other words we are able to analyze the essential differences between our algorithm and the existing ones.

GE Marquette 12SL Algorithm

The Marquette 12SL algorithm was according to their physicians guide “the first commercially available ECG program to analyze all 12 leads” and embedded into a computerized electrocardiograph in the early 1980s [53]. The following algorithm details are mainly received out of this documentation. The ECG data is simultaneously acquired by a 12-lead ECG with a sampling rate of 500 Hz, which equates a value at every 0.05 mm on an ECG with a paper speed of $25 \frac{\text{mm}}{\text{s}}$. At first, probable pacemaker artifacts are removed, because these could be mistaken for a QRS complex due to a large amplitude. Secondly, it measures specific ECG data like QRS detection, ventricular rate calculation, P wave detection, and else. Here, we focus on the QRS detection, because all other measurements and diagnosis steps are based on it.

A filter attenuates high and low frequencies to get a better look at the QRS complexes, which are usually displayed in the mid-band frequencies. The output of this filter of all 12 leads is summed up. If a certain threshold is crossed in this final signal, a QRS complex is considered to be detected. After a QRS complex is found the detection is blocked for 200 ms to avoid the misdetection of a T wave. Additionally, the GE Marquette uses a template matching detector. With the first QRS complex detected by the threshold algorithm, a template is made for each lead. This template is slid along the signal to recognize similar wave forms. If the threshold algorithm detects something, but the template does not match, a different beat type is assumed and a new template is stored for further beat analysis.

The diagnosis of the GE Marquette 12SL includes gender and age specific criteria applied on 10 s of ECG recording. The suggested diagnosis is identified via decision tree of the following major categories. The algorithm looks successively after electronic artificial pacing, atrial flutter, ectopic atrial rhythm, sinus rhythm, junctional rhythm, and atrial fibrillation. Obviously, we focus on AFlut and AFib detection here, which is based in the following criteria:

Atrial flutter The program must detect an atrial rate from 200 to $350 \frac{\text{beats}}{\text{min}}$, which is found by the P wave detection.¹ The P wave detection is also based on a threshold, build upon the QRS detection algorithm.

Atrial fibrillation If none other category or rhythm has been detected, the program looks for atrial fibrillation, which means more precisely that one of the two following tests has

¹Values denoted for adults.

to be true. Test 1 requires an irregularly irregular rhythm that means a deviation of more than 15% of the average RR interval and no regular atrial rhythm detected. The second test requires an atrial rate over 400 ms.

Glasgow Algorithm

The Glasgow Algorithm was developed by Peter Macfarlane and his team at the University of Glasgow. This 12 lead ECG analysis algorithm is also one of the first developed ones and was approved by the U.S. Food and Drug Association (FDA) in the early 1990s [116]. The main area of application of the Glasgow algorithm is in heart monitors and especially defibrillators. The ECG data is also recorded for 10 s with a sampling rate of 500 Hz and afterwards filtered for noise reduction. Then, the *spatial velocity (SV)* is calculated given by the following equation:

$$SV = \frac{\sqrt{a^2 + b^2 + c^2}}{T} \quad (4.1)$$

where T is the sampling interval, a the change of amplitude in the first, b in the second, and c in the third input lead. The maximum values of this function are used as reference points, which occur in each QRS complex. From this point, beginning and end of the QRS complex are determined for which the spatial velocity falls under a critical value. P as well as T wave are located accordingly [95]. For the QRS type detection, they use an interactive process to compare the first complex with the second within one lead. This works like a kind of sliding window procedure, where always the next beat is compared to the current one. When the difference between the two is less than a threshold value, they are supposed to belong to the same class and so on. Otherwise, if the difference exceeds the threshold value, a new class is created.

The Glasgow algorithm takes gender as well as the age of a patient into account for diagnosing. The detailed algorithm with its decision tree can be seen in [108]. Unfortunately, we could not find a detailed description for the AFib detection published. The check for AFlut starts directly after the basic P wave search algorithm by means of two stages. First, a series of PP intervals has to be in the range of 150 to 300 ms². Secondly, there is a search for sawtooth pattern in a single lead, for which each RR interval has to cross a threshold given by 95% of the maximum gradient. If there is at least one RR interval with more than one threshold crossing than AFlut is assumed to be present. If not, the threshold is set to 90% and the test is repeated. Again if not, a last attempt is made in case of a heart rate $> 100 \frac{\text{beats}}{\text{min}}$ on the complete RR segment.³

HES Algorithm

The Hannover ECG System (HES) is a diagnostic ECG program for the analysis and interpretation of ECG data, first developed at the University of Hannover and refined for more than

²They note that the specified range for AFlut is intentionally wider than the usual textbook limits for AFlut, due to better results.

³In the first search the RR interval was cut at beginning and end to avoid misdetection of QRS complexes.

35 years. It is implemented in various ECG devices and also belongs to the most widespread and established ECG interpretation algorithms. The program also starts with 10 s of ECG recording with a sampling rate of 500 Hz. There is a QRS detection implemented with a kind of spatial velocity, which is similar to the one of the Glasgow Algorithm. In particular, it is defined as the rate of change in an input signal with respect to time. The exact specification of the onset of the QRS complex is finalized with a certain threshold and further patient dependent parameters. [74]

Just as the others, the HES Algorithm has also various diagnostic skills implemented. A method for the discrimination between AFlut and AFib, by computing a flutter index, was presented by Fischer et al. in [40]. This approach differs from the other two algorithms which were presented so far. Before the real analysis starts, a preprocessing via decision tree is done. If a specific flag is set, the program undertakes several steps to filter unnecessary noise, or signals like the QRS complex, which is not needed for the following P wave analysis. The processed signals of lead II and V1 are separated into ten intervals of 1 s. For each interval and lead a discrete Fourier analysis is applied and a fundamental atrial frequency is determined. A linear discriminant analysis is then used to get a probability for atrial flutter. If the probability within one interval is over 50%, AFlut is supposed. Finally, this resulting flutter index classifies the complete ECG in AFlut, mixed AFlut/AFib, or AFib.

4.1.3 Signal Processing Methods for Discriminating AFlut from AFib

Taha et al. analyzed an automated discrimination between AFib and AFlut in 12-lead resting ECGs [142]. Therefore, they used a group of over 4000 ECGs and presented spectral methods in comparison to the GE Marquette 12SL, which was describe in detail in Section 4.1.2. The test included spectral entropy to measure the stochastic complexity of a signal. In other words, they try to find some kind of regularity or irregularity in the atrial activity. Here, the hypothesis is that atrial fibrillation would generate higher and much more spectral entropy waves. They found that spectra for AFib are, in fact, characterized by large spectral entropy values in combination with multiple spectral peaks. This is most likely caused by multiple circularity waves. On the other hand, the spectra for atrial flutter have smaller values and narrow single peaks. This comes from the singular origin of AFlut. In a second step, spectral peak detection was used for the final discrimination. Taken together, they found that selectively applied spectral methods, only provide a poor result in diagnosing AFlut from AFib. As a post-analysis algorithm, however, the spectral measures could significantly improve the discrimination rate. Here, Taha et al. were able to reduce the cross-classification error between AFib and AFlut of the GE algorithm from 5.6% to 2.5%. A further interpretation is given in the discussion about these methods in the following section.

Hoppe et al. tried to distinguish AFlut from AFib with apparent electrocardiographic organization using dominant and narrow F-wave spectra in [57]. Their test group of 39 patients consisted of 21 flutter and 18 fibrillation cases. They found that in contrast to AFib, AFlut is associated with dominant and narrow peaks reflecting single macroreentrant wave fronts. On the basis of the spectra of F waves which were obtained from atrial ECGs, they developed a diagnostic algorithm that is able to discriminate between both arrhythmias. According to their specifications, they achieved a high accuracy with that method.

4.1.4 Discussion

At first glance, the signal processing methods of the previous section show some good results. Nevertheless, there are some major issues with the presented methods, as we mentioned in a previous publication of Scholz et al. [129]. Unfortunately, the available AFlut cases of Taha et al. were not specified more precisely, whether to be typical or atypical. A further reduction of significance is that they did not have intracardiac electrograms available to validate the suggested diagnosis, which can be a huge problem as these experts often disagree [125]. Furthermore, all ECGs of Hoppe et al. were recorded under artificial conditions, namely, in the sedated state and using a high-quality physiological recorder. Additionally, regions of extreme noise were excluded from the analysis, while the study is based on a relatively small number of individuals. As expected, when applying this algorithm to a real-world population, discrimination was considerably lower, even though 11% of the ECGs had been excluded from the analysis owing to poor quality, see Krummen et al. [79].

Regarding the established ECG recording algorithms, they are definitely able to get decent results in the recognition of the typical AFlut cases with a prominent sawtooth-like pattern. Nevertheless, there is a high misdiagnosis of clinically applied algorithms reported for the discrimination of AFlut as AFib [14]. One of the reasons might be that the used signal processing methods exhibit a high degree of susceptibility to artifacts, because they are applied on the more vulnerable P waves. These results also underline the clinical observation that a discrimination based on atrial activation is often impossible due to the absence of unambiguously identifiable flutter waves [125]. In Table 4.1 and 4.2, the established software is compared to our software package HEAT with respect to diagnosis variety and necessary input data. Here, one of the major advantages of our approach is illustrated, without considering the diagnostic performance which we take into account later on. To be specific, we only need the RR intervals as input data for the desired arrhythmia discrimination. Besides the robustness, this can have important benefits as the area of application is strongly extended. More on that topic in the final Chapter 6.

Name	R Wave Detection	Heart Rate Calc.	Heart Rhythm	Premature Contraction	AFlut/AFib Discr.	Other
GE Marquette	x	x	x	x	x	x
Glasgow	x	x	x	x	x	x
HES	x	x	x	x	x	x
HEAT	x	x	x	x	x	-

Table 4.1: Comparison of the diagnosis variety of the different algorithms. The detection of premature atrial, or ventricular contractions can directly be displayed in HEAT. Most of the other algorithms automatically recognize and exclude these extrasystoles for rhythm analysis.

Algorithm	10 s 12-Lead ECG	Long-Term Holter Rec.	Short RR Interval Series
RR Interval Periodicity	-	-	(x)
HRV and Poincaré Plots	-	x	(x)
GE Marquette	x	x	-
Glasgow	x	x	-
HES	x	x	-
HEAT	x	x	x

Table 4.2: Possible input data for different approaches of discrimination between AFlut and AFib. For the statistical methods, short series of RR intervals are practically possible to use, but not meaningful. Therefore, see also the validation of the statistical approaches in Section 5.2.

4.2 HEAT Software Package

First of all, the **Heidelberg Electrocardiogram Analysis Tool (HEAT)** has been developed to discriminate between regular atrial tachycardias and AFib. However, the project started only with some testing algorithms to approach this problem, in the meantime a complete software package with various abilities has been developed. There is the possibility for data acquisition via mobile app directly at the patients bedside as well as other diagnostic skills. We start this section with an overview about the complete HEAT software and its workflow, before we go further into detail.

Compared to the previously presented algorithms, the input data is completely based on R waves or in particular on the RR intervals. This can be a major advantage when the P waves cannot be detected properly due to artifacts, which is a very common case in supraventricular tachycardias. It also means and more important, that the HEAT Algorithm needs less input data than other programs, which can be a particular benefit in some areas of application. These medical application areas include single lead devices, like most of the implantable ones, or devices which are only able to detect the ventricular signal of the R wave. Further examples on this topic are presented in the final Chapter 6.

4.2.1 Overview

The intention of the current algorithm is not to diagnose all kinds of cardiac arrhythmia, but to be specialized for some diseases. Thus, HEAT can for example be seen as an addition to the algorithms presented in Section 4.1.2. In this case, it could be implemented as an specific upgrade to these programs or as additional validation guarantee for example. Nevertheless, the current software package is also able to support a physician in the daily hospital routine as an easy, fast, and reliable diagnostic assistance, as can be seen in this section. A further possibility for the future is that HEAT could easily be extended to more diagnosis options, if desired. Figure 4.1 gives an overview of the complete workflow of the HEAT software and its intended use. There are basically two different usage possibilities, because HEAT is implemented as an application for mobile devices as well as a desktop PC software. So the intended use for a physician in a clinical daily routine can be for example, to use the software in his office when looking at a difficult patient case. With the *HEAT Mobile App* it is additionally possible to use it immediately at a patients bedside, or wherever the question for discrimination of AFlut and AFib appears. The actual centerpiece of the software including all described models and the MAVB algorithm is implemented in the *HEAT solver*.

The first part takes the data acquisition into account, which is described in the upper section of Figure 4.1. For the desktop version, the RR intervals can either be manually entered if at hand, or the R wave detection algorithm can be used. Therefore, an image or scan of the ECG can be opened in the program.⁴ With this software the user has the possibility via user interface to test various algorithms, models, objective functions, and else, basically everything described and tested in this dissertation. The mobile app version has two input options. On the one hand, the user can take a picture of an ECG printout and again the R wave detection algorithm is started. On the other hand, it is possible to record the beeping

⁴For the desktop version the automatic RR detection mode is currently still in a testing phase.

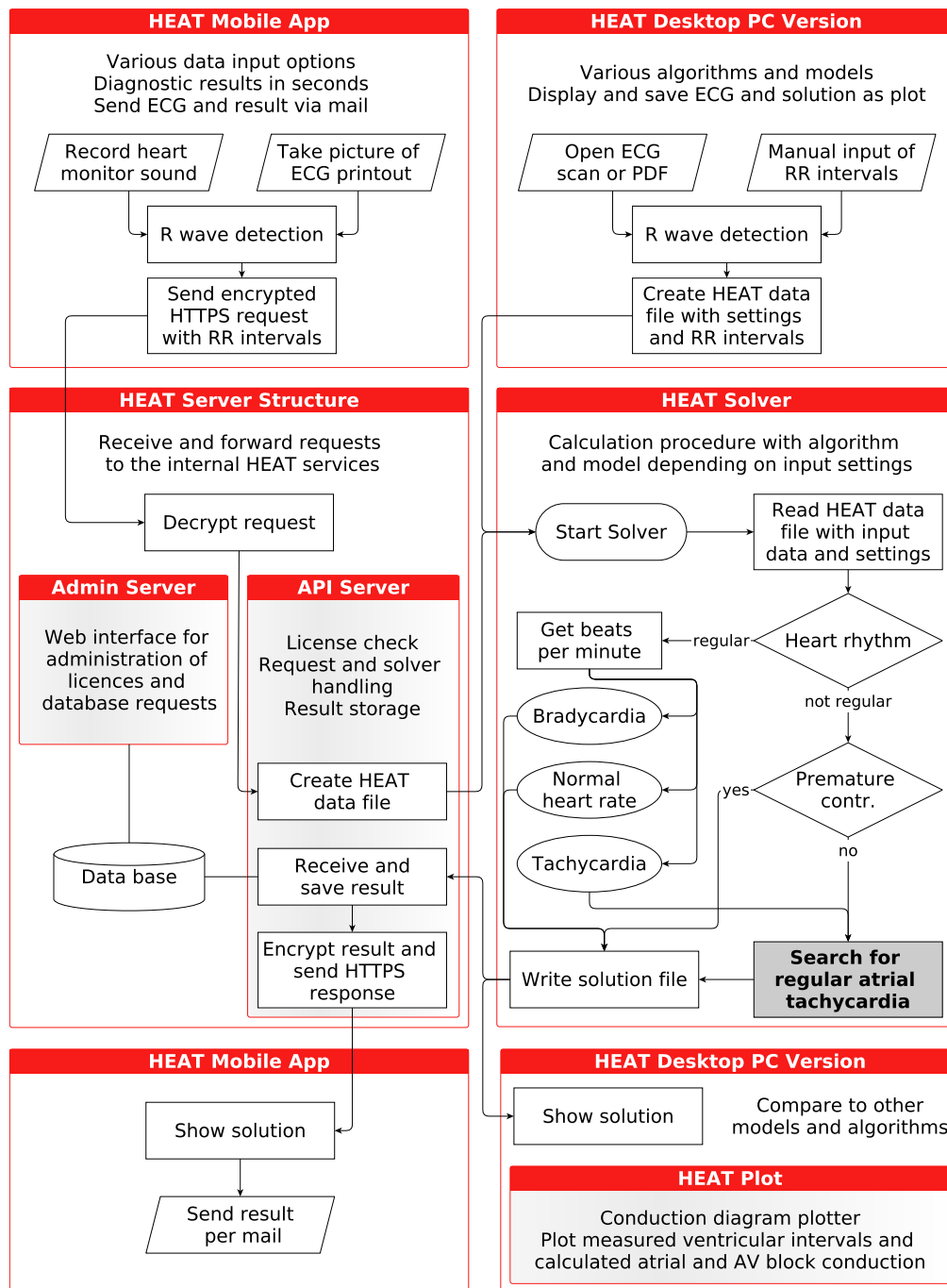


Figure 4.1: Overview of the HEAT software package, for a detailed description see text.

sound of a heart monitor, which is translated into RR intervals. Both of these mobile data acquisition approaches are described in the following section 4.2.2.

Now, a HEAT data file is created including the patient input of the RR intervals, as well as the desired settings. For the mobile app the solver module runs on a state-of-the-art secure server for a faster computation. Thus, the input data is sent encrypted via HTTPS connection to the server. This structure also includes an API server which is responsible for user license check, HEAT data file generation, and result handling. The licenses can be managed via web interface only by the administrator. From there, it is also possible to take a look at anonymized requests and computation results. Once the solver calculations are finished, the result is sent back to the user via HTTPS encryption.

So let's have a closer look at the solver module where the actual calculation is done, described on the center right hand side of Figure 4.1. Depending on the input settings, first of all the solver checks for a regular heart rhythm. The non-pathological heart rate variability in percentage can also be defined here. In case of a regular rhythm, the heart rate is determined and depending on that, the rhythm is categorized as bradycardia, normal heart rate, or tachycardia. When a tachycardia is existent, the algorithm search for regular atrial tachycardia is started to compute the regular atrial cycle length. If the heart rhythm is not regular, a check for premature contraction is done. In case of a non regular heart rhythm where no premature contraction could be found, the same algorithm is started. This *search for regular atrial tachycardia* is particularly marked in Figure 4.1 because it includes the most important feature of the whole software package. It includes the combined multilevel algorithm that is able to find all possible kinds of second-degree AV blocks, which is explained in detail in Section 4.2.4. All solution variables are written to a solution file which is further processed on the HEAT server or directly handled by the desktop software.

In the final step, the result is presented in the app with the possibility to send the result and ECG via mail for patient data management or later examination. The desktop version has the additional option to plot the measured RR intervals as well as the computed solution in a conduction diagram. Here, the solution can easily be analyzed, compared to other models and algorithms, or saved as PDF file for further processing. Obviously, all of these tools are used for the analysis in this dissertation which can be seen in Chapter 5 of the Numerical Results.

4.2.2 Data Acquisition

Before we can start with any kind of algorithmic calculations, we need to determine the necessary input data. In our particular case, this data is given by the RR intervals or in other words by the duration between a few ventricular signals. The HEAT software package has various options to gain this input data. On the one hand, a physician can use the HEAT Desktop PC Version. Of course, it is possible to measure the RR time intervals manually and directly from a surface ECG. Hence, there is an option to simply enter this data in the desktop version and create a new test case. While HEAT manages the automatic data processing, the user is able to choose between the various options of diagnostic algorithms, different mathematical models, as well as other settings. As described in Section 4.1.3, there are also methods for an automatic acquisition of QRS complexes respectively the R waves from an

ECG signal. The image and signal processing methods for both kinds of user applications are similar. For the desktop version however, this option is still in testing phase so far, thus we skip a closer look at this in here.

Nevertheless, there is the HEAT Mobile App which is already able to automatically process the input of the ECG data. Besides, the mobile app can handle the interactions with the physician right at the patients bedside if necessary. At first, there is the possibility to record the beeping sound signal of a heart monitor. This beeping sound reflects the pulse signal received from a patient. The HEAT Mobile App can measure and transform this signal into the necessary input data for the HEAT Algorithm for further processing.⁵ Secondly, it is possible to make a photograph of the ECG via camera of the mobile device and decode the signal via image recognition. For this, we developed an algorithm that executes several steps to gain the desired RR interval time duration. As this is “just” an addition to our main algorithm and is not in the main focus of this dissertation, we will only briefly explain the several algorithmic steps in the following.

In general, a physician has an ECG printout available to analyze. Using the HEAT Mobile App, it is now possible to simply take a photograph of this printout which acts as input data. Hence, we need to start with image processing methods to extract and recognize the actual printout within the picture, even before we can come to the ECG signal processing. At first, a perspective distortion needs to be applied using the four corners, to receive an undistorted image. Therefore, we use amongst else the Canny Edge Algorithm [113]. Now, the extraction of the desired ECG signal can start using several noise filter techniques. To receive the actual R wave, we then use a specifically developed method based on the first and second derivative as mentioned in Section 4.1.1. Finally, the actual RR time duration needs to be calculated using the correct ECG paper speed, which can be adjusted in the app.

4.2.3 Solution Space

In this section, we determine the feasible regions for the present discrimination problem based on a medical background. In particular, we want to identify these regions for the following combined multilevel algorithm, which is described in Section 4.2.4. The main reason for this purpose is to constrain the complexity of the involved enumeration problem to get a faster and more reasonable computation process.

As seen in Chapter 2, even the state-of-the-art medical knowledge is not always conform to each other or the clinical definitions are not entirely clear. Hence, in some of the following assumptions hard decisions need to be made to get a reasonable or solvable problem description. Those constraints may in some cases exclude an unusual solution, nevertheless, we try to cover all solution possibilities in the feasible set definition. In the following, the underlying medical assumptions are clarified before we determine the according parameters mathematically. A summary of all parameters and the definition of the according feasible set is listed in Table 4.3.

⁵Within this dissertation, it has not been investigated whether the pulse signal is completely accurate to the corresponding ventricular signal. There are various publications on this topic, but to our knowledge, this task has not been completely cleared yet.

ECG Sector Length The considered ECG sector \mathcal{T} is constrained by a certain number n of R waves $R_j \in \mathcal{T}$, with $j \leq n$ and $j, n \in \mathbb{N}$. Obviously, if the ECG sector is too short, there is not enough input information to gain a solid result. Hence, we define a lower bound of 6 R waves. On the other hand, our approach has also an upper constraint which is caused by a logic medical point. In fact, the longer the watched ECG sector is, the more likely there can occur slight variations in the patients atrial cycle length. The accumulation of these variations would make our assumptions in case of a regular atria and the involved calculations invalid. In conclusion, the upper bound for an ECG sector is set to 25 R waves.⁶

$$6 \leq \#R \leq 25 \quad (4.2)$$

It should be noted, that these bounds are just used to find the optimal ECG length for the discrimination of AFlut and AFib at our validation data set, which is described in Section 5.4. This optimal number of R waves or respectively RR intervals $\#RR_{\text{opt}}$ is then used, whenever enough ECG data is available. On the other hand, the lower bound is also adapted to a minimum number of intervals $\#RR_{\text{min}}$, where a significant discrimination result can be reached.

Basic Atrial Cycle Length Usually, atrial tachycardias are defined with a regular atrial rhythm at a constant rate above $100 \frac{\text{beats}}{\text{min}}$. Here, atrial flutter lies between 220 to $320 \frac{\text{beats}}{\text{min}}$, which corresponds to a possible atrial range of 273 to 188 ms. Other atrial tachycardias that lead to a second-degree AV block are most likely to be within the atrial rates of 150 to $220 \frac{\text{beats}}{\text{min}}$, which are intervals from 400 to 273 ms [67]. In general, second-degree AV blocks do not occur in atrial tachycardias between 100 to $150 \frac{\text{beats}}{\text{min}}$ and are thus, easier recognized as described by Josephson [67]. Therefore, we excluded these slower rhythms in this feasible set of the regular atrial cycle length to determine supraventricular tachycardias.

$$188 \text{ms} \leq AA \leq 400 \text{ms} \quad (4.3)$$

The enumeration step size of the atrial cycle length is set to the smallest feasible value of 1 ms. We also use this variable for parallelization in the software implementation because it is independent of the conduction in the AV node, easy to split up, and appears in all various model cases. Hence, for the available number of cores, a cycle length sector is calculated and searched for the best solution. The best solutions of each sector are compared to each other in the end, which leads to the optimal solution.

Basic Number of AV Block Levels Based on the discoveries of Section 2.3, the maximum possible number of simultaneously active AV block levels is 3.

$$1 \leq \# \text{Level} \leq 3 \quad (4.4)$$

⁶It should be noted that for a better differentiation between measured and simulated signals we use different symbols. The measured signals are inspired by the ECG notation of R wave, or P wave respectively. The simulated notation was given in the previous chapter with V for ventricular signals for example.

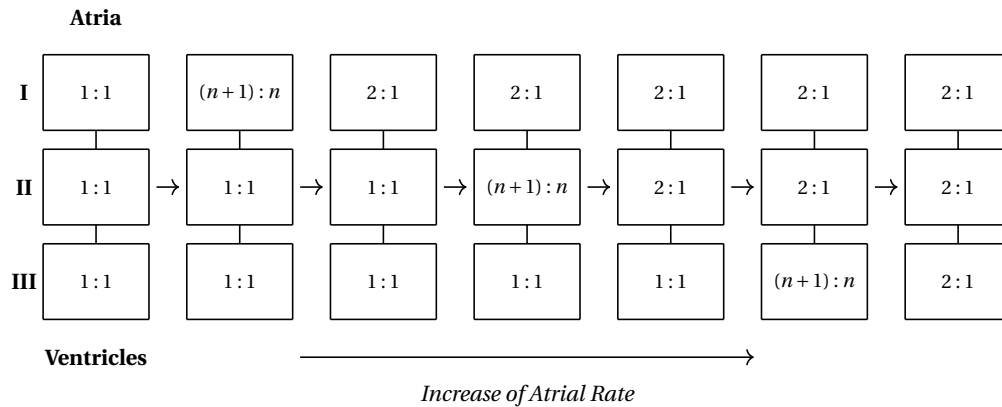


Figure 4.2: Visual description of the AV block process with MAVB at increased atrial rate, adapted from [86]. The conduction ratio of $(n + 1) : n$ in this figure includes possible changes in the conduction ratio or a ratio which is not constant at $2 : 1$. The order of the specific blocking is an exemplary representation. Hence, it is not necessarily the first block level which becomes active at first. Further details are explained in the text.

Another basic condition is that the faster the atrial rate gets the more incoming signals get blocked. If the maximum possible block per level of $2 : 1$ is reached, another level “becomes active”. As already described in the MAVB Section 2.3, this theory was illustrated for a two level block by Leon in [86] and further confirmed of various sources by intracardiac electrograms. This kind of MAVB is exemplified for three block levels in Figure 4.2. Here, the order of the block levels is not necessarily as in the illustrated way. Hence, the first block level doesn’t have to become active first. However, it is described in literature that the occurrence of the first level to block $2 : 1$ is more likely than the other way around [94]. Furthermore applies, that the specific atrial cycle lengths for changes or additional block levels are patient dependent. On the other hand, these changes can also appear in a limited form at a fixed atrial cycle length, see also the next paragraph.

Conduction Ratio Considered the other way around, at a fixed atrial cycle length applies for more than one active block level that the other levels have to block in a maximum possible way. This means for two active block levels that one of them has to have a $2 : 1$ conduction. The same applies for three active levels accordingly. This fact is very important to reduce the computation time and is further explained in the following Section 4.2.4. Additionally, we assume that all advanced second-degree AV blocks are in fact type I or type II conduction mechanisms on multiple block levels, also as demonstrated in Section 2.3. In conclusion, this means that *it is not possible that two incoming signals are blocked in a row within the same cell compound*, because in this case the MAVB would come into account. In combination with the possible number

of AV block levels, the overall maximum conduction ratio in the AV node is 8 : 1. This equals three active block levels each with a 2 : 1 conduction ratio. Besides, it follows that all block pattern on one level are based on $(n+1) : n$ conduction. We define a minimum conduction ratio per level for $n = 6$ or a 7 : 6 block, which is also based on the medical findings of Section 2.2.1. Therefore, for the conduction ratio per level follows:

$$(n+1) : n \quad \forall n \in [1, 6] \quad (4.5)$$

Furthermore, we act on the assumption that on one level there are changes in the block pattern possible, however, based on certain rules. These rules include that from one block to the following one, the block pattern can only change with $n \pm 3$. This would be for example from 3 : 2 to 5 : 4, or similar, but *not* from 2 : 1 to 6 : 5. Also keep in mind, that changes in the conduction ratio could also appear from $(n+1) : n$ to 1 : 1 which would make one block level “inactive”. However, these changes between active and inactive levels also rely on certain rules, which are described more closely in the next section.

Further Constraint of Atrial Cycle Length - Upper Bound Using the assumptions of the previous paragraphs, the possible atrial cycle length can be further constrained in many cases. In fact, we can use the additional input information of the maximum \widehat{RR} interval length to limit the upper bound. At first however, we have to find the lowest output that can possibly appear with a second-degree AV block with a specific incoming atrial cycle length of AA . For the first block level this value is $AA + 1$ as the basic duration for a signal to conduct from one level to the next is at least 1. Additionally applies that if more than one block level is active the atrial cycle length has to be doubled on each other level. This is based on the assumption that there has to be a 2 : 1 conduction on at least $(n-1)$ active levels. Hence, it is possible to calculate the “lowest possible”, maximum \widehat{RR} interval for a specific number of levels and a given atrial cycle length.

$$2^{\#Level-1} \cdot (AA + 1) \leq \widehat{RR} \quad \Rightarrow \quad AA \leq \frac{\widehat{RR}}{2^{\#Level-1}} - 1 \quad (4.6)$$

On the other hand, the maximum possible atrial cycle length $\widehat{AA}_{\#Level}$ can be determined with the input information of the measured \widehat{RR} interval by the following equation. The total number of specific AV block levels is given by the value of $\#Level$. For one level this is defined by \widehat{AA}_I , for two block levels by \widehat{AA}_{II} , and for three block levels in total by \widehat{AA}_{III} accordingly.

$$\widehat{AA}_{\#Level} = \frac{\widehat{RR}}{2^{\#Level-1}} - 1 \quad (4.7)$$

Additionally, the minimum ventricular interval length \widetilde{RR} can be used to further restrict the upper bound in a few cases. Obviously, the atrial input interval cannot be bigger than the smallest ventricular output. In consequence, we can determine the upper bound on one level in this way. With the MAVB in mind, however, we need to

Feasible Set	Description
$\overline{AA} = \{AA \in \overline{AA} \subset \overline{T} \mid 188 \leq AA \leq 400$ $\wedge \frac{\widehat{RR}}{2^{\#Level}} \leq AA \leq \frac{\widehat{RR}}{2^{\#Level-1}} - 1\}$	Feasible atrial cycle lengths overall and possibly further constrained
$\# \overline{R} = \{n \in \mathbb{N} \mid 6 \leq n \leq 25\}$	Number of feasible R waves for test set
$\# \overline{RR} = \{n \in \mathbb{N} \mid \#RR_{\min} \leq n \leq \#RR_{\text{opt}}\}$	Number of feasible RR intervals
$\overline{C} = \{\alpha \in \mathbb{N} \mid \alpha_{\#Level} \leq AA \cdot 2^{\#Level-1}\}$	Feasible conduction constant per level
$(n+1) : n \quad \forall n \in [1, 6]$	Feasible conduction ratio on one level
$1 \leq \#Level \leq 3$	Number of possible AV block level

Table 4.3: Feasible sets of the combined multilevel model and algorithm. The set of feasible R waves are used to find the optimal number of R waves, respectively RR intervals. The same applies for the minimum acceptable number of ventricular intervals to find a sufficient solution.

have a look at the doubled minimum atrial cycle length. Because in case of a two level block, the overall maximum atrial cycle length ($AA_{\max} = 400$ ms) is bigger than twice the overall minimum atrial cycle length ($AA_{\min} = 188$ ms). Hence, AA_{\max} can be constrained in the following case for a one level block with the necessary condition:

$$\widetilde{RR} \leq 2 \cdot AA_{\min} \quad \Rightarrow \quad \widehat{AA}_I = \widetilde{RR} \quad (4.8)$$

Further Constraint of Atrial Cycle Length - Lower Bound On the other hand, the lower bound for the atrial cycle length can also be determined using \widehat{RR} . Here, the question is how it is possible to describe the maximum ventricular interval using the lowest possible atrial input. The answer is, obviously, to use the maximum block of 2 : 1 on each level. Hence, the lower atrial bound for each level $\widetilde{AA}_{\#Level}$ respectively, can be calculated in the following way:⁷

$$AA \cdot 2^{\#Level} \geq \widehat{RR} \quad \Rightarrow \quad \widetilde{AA}_{\#Level} = \frac{\widehat{RR}}{2^{\#Level}} \quad (4.9)$$

Further Constraint of Number of AV Block Levels In consequence of the previous two paragraphs, this also means that the possible number of block levels can be constrained by an upper bound for a certain range of atrial cycle lengths. In fact, if $\widetilde{AA}_{\#Level}$ for a certain number of levels is smaller than the overall possible atrial cycle length AA_{\min} follows logically that this level has to be inactive. Contrariwise, if the lower bound for a level $\widetilde{AA}_{\#Level}$ is bigger than the actual overall possible atrial input AA_{\max} , there has to be at least one more block level.

⁷Due to a normal medical conditioned variability or to put it in mathematical terms *inaccuracy*, we relax the lower bound by an inaccuracy variable of 25 ms.

Conduction Constant For the actual signal computation process from one to the next level between atria and ventricles, we use the classical linear model of Equation 3.21. Further reasons for this purpose and explanations on the model are illustrated in the following section. For now, it is enough to know that the conduction constant α can be constrained as well based on the previous medical findings. The maximum value $\hat{\alpha}_{\#Level}$ on each level is given by the maximum possible incoming value on the according level. Naturally, this is caused by the condition that not more than one signal can be blocked in a row on a level. The largest potential output interval for one level is, hence, produced by a 2 : 1 block in doubling the incoming interval size. In consequence, we can follow:

$$\alpha_{\#Level} \leq AA \cdot 2^{\#Level-1} \quad \Rightarrow \quad \hat{\alpha}_{\#Level} = AA \cdot 2^{\#Level-1} \quad (4.10)$$

4.2.4 Combined Multilevel Algorithm

In this section, we present our novel concept of the *combined multilevel algorithm* that is able to describe the electrophysiological processes in the human heart in a realistic way. More precisely, this algorithm is intended to diagnose regular atrial tachycardias including atrial flutter solely based on the input values of a few RR intervals. It is implemented with an algorithmic approach based on the medical facts of Chapter 2. The signal conduction between atria and ventricles can be represented by all possible kinds of second-degree AV blocks, like 2 : 1, type I or type II. However, as described earlier we assume that the various block types are rather based on the same mechanism thus *combined*. Furthermore, we take the *multilevel* concept of Section 2.3 into account. Now, the underlying idea is to find a regular atrial rate in combination with a particular MAVB that is able to simulate the measured pattern of the RR intervals on the ventricular level as good as possible. This diagnostic workflow is further analyzed in Section 5.1.2 in terms of the objective functions applied and also illustrated at this point in Figure 5.1. Secondly, we want to receive these good results within a short computation time or at best in real-time. The groundwork for this part was explained in the previous Section 4.2.3 Solution Space, where we constrained the feasible set of some variables. In the end, the number of calculations depends on the complexity of the underlying RR interval sequence on the one hand. But even more important is a good algorithmic structure based on the medical facts and mathematical conclusions that guarantees a constant and fast computing time. The entire combined multilevel algorithm is now explicitly illustrated and finalized. From here on, this algorithm in combination with the implemented, preceding detection possibilities is referred to as *HEAT Algorithm*.

Brute-Force Approach

First of all, we would like to point out the complexity of this problem. Our newly developed algorithm is basically build as an enumeration of all possible solutions. The challenges with enumeration arise in general with the enormous amount of calculations. So, the main problem of this brute-force approach comes with the computational costs caused by the number of free parameters. As mentioned above, we use a phenomenological model as basis for the

algorithm. In particular, the classical linear model f^{lin} of Equation 3.21 is utilized. However, the feasible set of the classical linear model by itself is not particularly small. But the problem gains further complexity with the fact that the conduction ratio can vary in its pattern from one block cycle to the other and is *not* constant as in the classical models. Obviously, the multiple number of block levels increase the difficulty of the problem in addition.

To be more specific on the significant parameters, there is at first the recording length of the analyzed ECG given by the number of RR intervals. To even reach a valid solution, a very fine enumeration grid of the unknown atrial cycle length AA is crucial. Additionally, the free parameters of the AV conduction model come into play. This is on the one hand the conduction constant α as well as the conduction increment Δ . In this case however, the conduction increment is able to vary in order to be able to display the changing “type I” conduction ratio. Hence, at every ventricular signal the conduction ratio could possibly take another value. Furthermore, there is also the unknown starting point of the measured ECG. This means that the used recording could start within one block cycle at the i th signal and does not have to start necessarily with the first one. Finally, taking also the MAVB on up to three levels into account, this already enormous number of possible solutions are raised to a higher power with every additional block level.

In conclusion, it is obvious that without logical improvements and algorithmic optimization, the calculation time of this approach would explode or would not be solvable at all within reasonable time. However, a reduction of the problem with a clever branch and bound strategy can help to find a solution within real-time. Therefore, it is important to define some particular “rules” on which the concept is build upon. These are then used to develop an algorithm that is able to depict most of the possible AV conduction mechanisms.

Branch & Bound Steps of the HEAT Algorithm

In this section we describe the actual workflow of the algorithm with all its branch and bound steps that are necessary to reduce the complexity of the present problem. The specific values for some of the used parameters, their notation and the corresponding medical knowledge were already illustrated in the Solution Space Section 4.2.3. Hence, we use this previous section as foundation for the following and more detailed explanation of the procedure of the HEAT Algorithm.

In the first part, we begin with the preparation steps for the enumeration to keep the task as small as possible. For this purpose, the feasible sets of various parameters are constrained, only based on the input values of the RR intervals as well as logical conclusions. We demonstrate a short algorithmic overview for every specific parameter and how the problem is solved in the implementation. Additionally, an explanation is given to clarify the corresponding matter in detail. The second part includes further preparations for the signal conduction of the used phenomenological model. We show how various conduction ratios for specific incoming signals are calculated and illustrate further constraints for the parameters of the model. The actual calculation process of the conducted and blocked signals is then illustrated in the final part of this section. This implementation is realized in a specific multilevel AV block class build upon the previous assumptions. These combined algorithmic procedures reflect the search for regular atrial tachycardias within the HEAT software package.

Part I - Constraining the Enumeration Parameters

1. Get Optimal ECG Length

At the beginning, the ECG is just shortened to the optimal number of RR intervals, if necessary, which gives the best decision result to the according problem based on our research. We already defined a reasonable minimum and maximum ECG length which is used in Chapter 5 to compute the optimal ECG length $\#RR_{opt}$. This ECG length provides the best discrimination result between regular atrial tachycardias and AFib based on our test data. Additionally, there is a minimum number of ventricular intervals $\#RR_{min}$. If there are less RR intervals than the optimal ECG length, this lower bound guarantees that it is still a significant result calculated.

Algorithm 4.1:

Input: Number of n RR time intervals $\#RR_n$ measured from an ECG

Output: Optimal number of intervals $\#RR_{opt}$

begin

```

  if  $\#RR_n > \#RR_{opt}$  then
    |  $\#RR_n = \#RR_{opt}$ 
  else if  $\#RR_n < \#RR_{min}$  then
    | break

```

2. Compute Feasible Atrial Range per Level

The minimum and especially the maximum measured RR time interval can be used to calculate the atrial cycle length that is mathematically feasible for a specific number of AV block levels, based on the medical rules. This means in consequence that the number of possibilities for the atrial rate can be reduced within the enumeration process. Based on this, we could also constrain the number of AV block levels that can occur, which is explained in the next paragraph.

a) Lower Bound

Algorithm 4.2: computeAtrialMinPerLevel

Input: Maximum \widehat{RR} interval, minimum overall atrial cycle length AA_{min}

Output: Vector of minimum atrial cycle length per level $\widetilde{AA}[i]$ for $i \in \{1, 2, 3\}$

begin

```

   $\widetilde{AA}_I = \frac{\widehat{RR}}{2}$ ,  $\widetilde{AA}_{II} = \frac{\widehat{RR}}{4}$ ,  $\widetilde{AA}_{III} = \frac{\widehat{RR}}{8}$ 
  if  $\widetilde{AA}_I > AA_{min}$  then
    |  $\widetilde{AA}.push\_back(\widetilde{AA}_I)$ 
  else
    |  $\widetilde{AA}.push\_back(AA_{min})$ 

```

At first, we calculate the minimum atrial cycle length for one \widetilde{AA}_I , two \widetilde{AA}_{II} , and three \widetilde{AA}_{III} possible levels using Equation 4.9. With this value, we are then able to determine the potential atrial cycle length for the total number of block levels which are used in the enumeration procedure. In Algorithm 4.2, we noted the if-then-else statement only for the first parameter, the other two parameters of \widetilde{AA}_{II} and \widetilde{AA}_{III} follow accordingly.

b) Upper Bound

Algorithm 4.3: computeAtrialMaxPerLevel

Input: Min. \widetilde{RR} and max. \widehat{RR} interval, max. overall atrial cycle length AA_{\max}

Output: Vector of maximum atrial cycle length per level $\widehat{AA}[i]$ for $i \in \{1, 2, 3\}$

begin

```

 $\widehat{AA}_I = \widehat{RR} - 1$ 
if  $\widehat{AA}_I < AA_{\max}$  then
  |  $\widehat{AA}.push\_back(\widehat{AA}_I)$ 
else if  $\widetilde{RR} < 2 \cdot AA_{\min}$  then
  |  $\widehat{AA}.push\_back(\widetilde{RR})$ 
else
  |  $\widehat{AA}.push\_back(AA_{\max})$ 

 $\widehat{AA}_{II} = \frac{\widehat{RR}}{2} - 1, \quad \widehat{AA}_{III} = \frac{\widehat{RR}}{4} - 1$ 
if  $\widehat{AA}_{II} < AA_{\max}$  then
  |  $\widehat{AA}.push\_back(\widehat{AA}_{II})$ 
else
  |  $\widehat{AA}.push\_back(AA_{\max})$ 

```

On the other hand, the maximum atrial cycle length per level $\widehat{AA}_{\#Level}$ can be computed using Equation 4.7. Additionally, a second condition of Equation 4.8 is able to limit the atrial upper bound for one level. The other parameters \widehat{AA}_{II} and \widehat{AA}_{III} can be determined similar to the lower bound. In consequence, the atrial cycle length can be restricted in between these minimum and maximum values for a specific number of AV block level.

3. Number of Level Determination

Additionally, we can also limit the possible active number of block levels in some cases. If the maximum possible atrial cycle length for a specific level is smaller than the lowest overall atrial cycle length AA_{\min} defined as 188 ms, then the level can obviously not be active. According to our assumptions, at least one block level has to be active, hence, we do not have to check on one level in Algorithm 4.4.

Algorithm 4.4: checkMaxAvLevel

Input: Vector of maximum atrial cycle length per level $\widehat{AA}[i]$ for $i \in \{1, 2, 3\}$,
minimum overall atrial cycle length AA_{\min}

Output: Maximum number of AV block levels

begin

```

  for  $i = 2$  to  $3$  do
    if  $\widehat{AA}[i] < AA_{\min}$  then
      maxAvLevel =  $i - 1$ 

```

Contrariwise, more levels have to be active if the minimum possible atrial cycle length for a specific level is bigger than the maximum overall atrial cycle length AA_{\max} of 400 ms. As before, there are three number of active levels at most, according to our assumptions. Hence, we do not have to check for more than three levels.

Algorithm 4.5: checkMinAvLevel

Input: Vector of minimum atrial cycle length per level $\widetilde{AA}[i]$ for $i \in \{1, 2, 3\}$,
maximum overall atrial cycle length AA_{\max}

Output: Minimum number of AV block levels

begin

```

  for  $i = 1$  to  $2$  do
    if  $\widetilde{AA}[i] > AA_{\max}$  then
      minAvLevel =  $i + 1$ 

```

By including both steps of the previous and this paragraph, we are actually able to reduce the complexity of the problem enormously. Even more important, this reduction is done before the real calculation procedure starts which results in a major speed-up for the entire HEAT Algorithm.

4. Possible AV Block Level Combinations

In the last step of the preparations for the enumeration procedure, we use the assumptions of Section 4.2.3 that not all level combinations are possible in a MAVB. For one block level we already discussed that there are various possibilities from the maximum block of a continuous 2 : 1 ratio, to a varying block type of $(n + 1) : n$. For a better differentiation of the types on each level, we denote a possible varying pattern with *type I* and in the other case just with 2 : 1 block. In general, we call an AV block that occurs only on one level as *MAVB I*. Based on the literature findings with intracardially measured signals, we determine that if one of the active block levels comes with a type I block, the others have to block in the maximum possible way or need to be inactive [20, 134]. Thus, we define two different types of two level blocks with a 2 : 1 block on the first and a type I on the second level called *MAVB 2a*, or the other way around

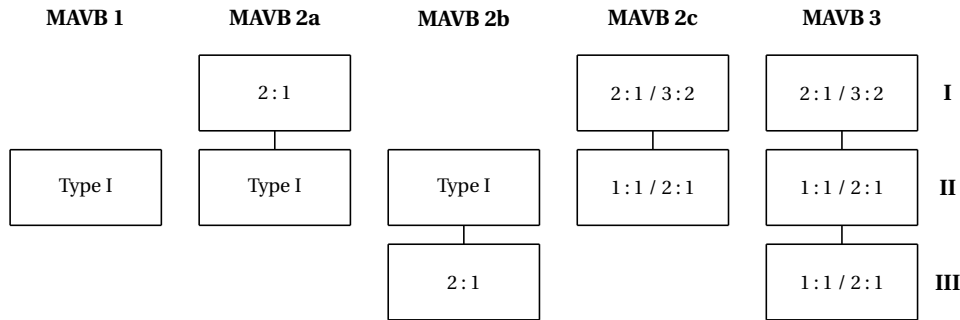


Figure 4.3: Various possible level combinations of a MAVB implemented in the HEAT Algorithm and based on medical facts. Here, type I conduction can be any $(n + 1) : n$ block including varying type pattern. Further explanation is given in the text.

which is called *MAVB 2b*. However, we investigated that there is a third possible two level conduction type. To be more specific, an additional block level can become suddenly active on the last level, usually depending on type pattern changes on one of the previously blocked levels. This is usually only the case, if a conduction changes from $2 : 1$ to $3 : 2$ on the first level, which means in the highest possible way. In consequence the second level becomes active from a $1 : 1$ to a $2 : 1$ conduction, because the incoming signal comes suddenly much earlier than before. An example with active and inactive changes on the last MAVB level is given in the chapter of the Numerical Results in Figure 5.12. For two block levels, we call this case *MAVB 2c*.

There are much less cases reported for three active block in total, but to our knowledge there is no example where a clear or continuous type I block is visible any level [77, 134, 20]. Further applies that three block levels, in general, only appear at the highest blocking rates as in the MAVB 2c type. Hence, the *MAVB 3* is specified similar to this type with a $2 : 1$ or $3 : 2$ block on the first level as well as a $1 : 1$ or $2 : 1$ conduction ratio on both, second and third level. All MAVB cases are visualized in Figure 4.3, where another fact becomes obvious on a more detailed examination. While the different MAVB types vary in their number of levels, or in other words to be active or inactive, the blocking types can actually be assigned to specific AV node regions. On the other hand, this point corresponds to many medical literature findings. As Slama et al. illustrated in [134], the type I block is usually located in the *N zone* of the AV node which is, in fact, the middle zone of the AV node between *A-N* and *N-H* zone. This hypothesis could be confirmed by other electrophysiological studies based on intracardiac measurements [102, 153]. Despite everything, we still consider the various AV block types to arise from the same physiological disorder as we mentioned earlier. Besides, we are aware that there could be other blocking pattern or MAVB possibilities in particular patients and that these constraints may exclude some MAVB cases. Nevertheless, we tried to base our assumptions on a profound medical background to build an algorithm that is able to solve the underlying discrimination problem in the best possible way.

Part II - Determination and Constraint of the Model Parameters

1. Compute Conduction Ratios

To actually compute the conduction of the signals from the atria to the ventricles, we use a modified linear model. This means that the basic functionality is similar to the linear model f^{lin} of Section 3.3.1, but the conduction ratio of $(n+1) : n$ can change from one block cycle to the other. Besides, the model is extended to multiple block levels. To be able to describe a varying type I block in the end, we actually need to calculate the parameters for the different ratios. Using f^{lin} , this is mainly done by a modification of the conduction increment Δ , but also the conduction constant α needs to be used.

a) 2 : 1 Conduction Ratio

First of all, we need the incoming interval times for the considered level to be able to calculate the conduction constant $\alpha_{2:1}$, for which a 2 : 1 block appears. On the first level with a given and regular atrial cycle length AA it can be computed as in Equation 4.11. Here, for a continuous 2 : 1 block applies $\Delta_k = 0 \forall k$. In combination with a constraint for a signal to be blocked or conducted of Equation 3.19 follows:

$$\begin{aligned} V_j &= f^{\text{lin}}(A_i) = A_i + \alpha + k \cdot \Delta \\ A_{i+1} \stackrel{!}{\leq} V_j &\Rightarrow \alpha_{2:1I} \geq A_{i+1} - A_i = AA \end{aligned} \quad (4.11)$$

In conclusion, we can just fix $\alpha_{2:1}$ at this point because we just want to create one kind of this conduction ratio so far. However, if a MAVB 2b is existent with the second level conducting in 2 : 1, the $\alpha_{2:1}$ needs to be calculated differently because of probably irregular output intervals from the first level. Hence, for a 2 : 1 conduction on whole block level, we need to find the maximum incoming interval. Again, the $\alpha_{2:1II}$ can be fixed for our purpose:

$$\alpha_{2:1II} = \max_{j=1 \dots m-1} AV_{j+1}^I - AV_j^I \quad (4.12)$$

To be even more specific, the described rule applies in the same way for a third level of MAVB 3. Hence, we can conclude that a 2 : 1 block can be created in any case by calculating $\alpha_{2:1}$ on the specific level with the maximum incoming signal:

$$\alpha_{2:1} = \max_{j=1 \dots m} AV_j^{I, II, III} \quad (4.13)$$

However, it needs to be proved that this interval cannot be larger or equal than twice the minimum incoming signal. This is based on the predefined condition that two successive signals cannot both get blocked.

Proof

$$\max_{j=1 \dots m-1} AV_{j+1}^I - AV_j^I < 2 \cdot \left(\min_{j=1 \dots m-1} AV_{j+1}^I - AV_j^I \right)$$

On level one, the maximum output interval appears in any case with a 2 : 1 block. For the minimum output interval using the linear model, Δ has to be minimal but at least with a 3 : 2 conduction ratio. That means in conclusion $\Delta = 1$ has to apply.

$$\begin{aligned} \max_{j=1\dots m-1} AV_{j+1}^I - AV_j^I &\leq 2 \cdot AA \\ \min_{j=1\dots m-1} AV_{j+1}^I - AV_j^I &\geq AA + 1 \end{aligned} \quad (4.14)$$

Using these conditions, we can conclude that the assumption is valid for any possible input values.

$$(4.14) \quad \Rightarrow \quad 2 \cdot AA < 2 \cdot AA + 2 \quad \square$$

b) Type I Level

Based on the same idea as in the previous paragraph, it is also possible to calculate any other $(n+1) : n$ conduction pattern. Here, the potential level combinations we defined earlier help that the problem gets not too complicated. Actually, we know that in any of the defined MAVB cases a specific type I level has to have a regular incoming signal. This is caused by the fact that the regular atrial rate of AFlut or an additional 2 : 1 block level which can appear prior to a type I level. This makes it possible to calculate any $(n+1) : n$ block cycle with a known regular incoming interval for a complete block level, only depending on the conduction constant α .⁸

Algorithm 4.6: Compute Conduction Increments

Input: Maximum incoming interval between two conducted signals of the previous level *getMaxInterval*, maximum number of conducted signals in a row n_{\max}

Output: Vector of increments $\Delta_{n+1:n}$ for various block types of conduction ratio

begin

```

maxIncrement = incoming → getMaxInterval() -  $\alpha$ 
for  $n = 2$  to  $n_{\max}$  do
  |  $\Delta$ .push_back( $\frac{\text{maxIncrement}}{n-1}$ )

```

Again, we use the linear model equation and calculate the vector of the conduction increment $\Delta_{n+1:n}$ for the specific block cycles. Equation 4.15 shows this calculation for the first level with the atrial interval AA , while the second block level follows accordingly with AV^I as incoming signals. Using the same assumptions as in Equation 4.11, we can conclude:

$$\Delta_{n+1:n} = \frac{AA - \alpha}{k} \quad n = k + 1, k > 0 \quad (4.15)$$

⁸Note that in case of a 2 : 1 conduction, the α is the only and essential parameter, because of $k = 0$ which erases Δ out of the equation. Then, we just proceed as in the previous paragraph.

Now, the conduction increment for any desired conduction ratio $(n + 1) : n$ can be calculated with a previously fixed conduction constant α . This is an important point, because this way we are able to vary the conduction increment to a corresponding block pattern on an entire level *only* by modifying α . In conclusion, this leaves just one free model parameter for the enumeration procedure, besides the varying conduction ratio.

2. Upper Bound of the Conduction Constant α

Based on the feasible set description of Section 4.2.3, we are also able to set an upper bound for the conduction constant α depending on the specific atrial rate. For each according level it can be constrained as described in Algorithm 4.7.

Algorithm 4.7: Get Max Conduction Constant

Input: Current atrial cycle length AA used for calculation of the AV block

Output: Vector of the maximum conduction constants $\hat{\alpha}$ for each level

begin

```

  for Level = 1 to 3 do
     $\hat{\alpha} = AA \cdot 2^{\text{Level}}$ 

```

Part III - Calculation of Various Multilevel AV Blocks

In this part of the HEAT Algorithm, we explain how the various kinds of MAVBs are calculated in specific. As follows from the previous paragraphs, the enumeration variables so far consist of the atrial cycle length AA as well as the conduction constant α . Furthermore, it should be noted that a parallelization is implemented in the algorithm for faster calculation. Therefore, we use the atrial cycle length to split up the problem to the maximum number of cores provided by the computer. The existing task to solve the different kinds of MAVBs is then processed one after the other. Constantly, the best solutions are compared to each other using a specific objective function that can also be adjusted as desired between three different kinds of mean absolute error (MAE), root mean squared error (RMSE), and normalized mean squared error (NMSE). A detailed explanation on the objective functions and how the objective function values are calculated, is given in Section 5.1.2.

1. Compute Varying Type I Block on Last Level - MAVB 1 & MAVB 2a

First of all, we need to come up with an idea how to compute a changing type I block level with the best possible conduction ratios for the given conduction constant and atrial cycle length. Before the start, the vector of the conduction increments Δ is calculated to get the desired conduction ratio, depending on the input intervals and the current α . This was previously illustrated in Part II of the algorithm description. In Algorithm 4.8, the basic approach is described which is similar to the classical linear model. However, to compute varying conduction ratios we need another function to get the best possible ones. The basic version hereof is implemented in Algorithm 4.9.

Algorithm 4.8: computeTypeIBlockLevel

Input: Vector of incoming signal times in , conduction constant α , vector of conduction increments $\Delta_{n+1:n}$

Output: Vector of conducted signal times

begin

```

ratio = getBestInitialConductionRatio()
k = 0
conductedSignal = in[0] +  $\alpha$  +  $k \cdot \Delta_{n+1:n}$ (ratio)
conducted.push_back (conductedSignal)
for  $i = 1$  to  $in \rightarrow getnSignals$  do
    if  $in[i] > conducted[getnSignals - 1]$  then
        conductedSignal =  $in[i] + \alpha + k \cdot \Delta_{n+1:n}$ (ratio)
        conducted.push_back (conductedSignal)
        k++
    else
        ratio = getBestConductionRatio()
        k = 0

```

Algorithm 4.9: getBestConductionRatio - Type I Last Level

Input: Previous conduction ratio, current incoming signal number, vector of incoming signal times in , vector of ventricular signals V , max. deviation

Output: Best conduction ratio

begin

```

minRatio = getMinConductionRatio (previousRatio)
maxRatio = getMaxConductionRatio (previousRatio)
for  $iRatio = minRatio$  to  $maxRatio$  do
    k = 0
    j = conducted  $\rightarrow$  getnSignals

    for  $i = iIncoming$  to  $iIncoming + iRatio$  do
        conductedSignal =  $in[i] + \alpha + k \cdot \Delta_{n+1:n}$ (ratio)
        k++
        deviation = abs (conductedSignal -  $V[j]$ )

        if  $deviation > MAX\_DEVIATION$  then
            | break;
        else if  $k == iRatio$  then
            | bestRatio = iRatio
        j++
return bestRatio

```

All possible combinations from the lowest to the highest possible conduction ratio are checked locally.⁹ Additionally, we define a certain accuracy to check if the simulated ventricular signal V fits to the corresponding measured R wave from the ECG. Missed solutions are eliminated at once to prevent the problem to gain further complexity. In consequence, Algorithm 4.9 finds the highest possible block cycle of $(n + 1) : n$ that is within a certain accuracy. Using the approach presented in this paragraph, we are able to calculate varying type I blocks as well as multilevel blocks in the kind of MAVB 2a. Here, the first level of a continuous 2 : 1 block can easily be calculated with the basic classical linear model. The regular conducted signals of the first level are then used for the second level using the type 1 block computation algorithm.

2. Compute Varying Type I Block on First Level - MAVB 2b

If a changing type I block is on the first level followed by a continuous 2 : 1 block as in the MAVB 2b, we can use a similar approach than the previous one, however, with some modifications. Our proceeding and the basic idea is basically the same as in Algorithm 4.8 to find the best fitting conduction ratio for the current block cycle. The difference is now that we skip every second signal in the comparison to the ventricular signals. Thus, for this type of MAVB we replace Algorithm 4.9 by the one described in Algorithm 4.10. This way, we are able to simulate the 2 : 1 block on the last level.

Therefore, it needs to be discovered whether the current incoming signal is a “skipped” one, hence blocked on the following level, or if it is completely conducted to the ventricles. Because we define the first signal of the ECG sequence overall as to be conducted, it follows logically that if there is an odd number of, so far, conducted signals on this level, the current signal needs to be blocked.¹⁰ In the other case of an even number of conducted signals, the previous signal must have been blocked on the second level and the current one is conducted. Besides, there is a second difference in contrast to the previous approach where the longest possible conduction ratio within a certain accuracy was taken as best conduction ratio. Now, we actually calculate the objective function values of the possible block cycles and compare it to each other. This works much better for this approach, because in case of a skipped signals logically no possibility of comparison to ventricular signal is. It should be noted that this approach could also be used for type I block on the last level. However, in this case it turned out that the comparison of the absolute deviation at a single signal works better than the calculation of the actual objective function value of a complete block cycle. This is caused by the fact that sometimes the correct solution is sorted out because of a similar but slightly worse objective function value at a longer block cycle. In this case of MAVB 1 and MAVB 2a, it was shown that the longer block cycle is more important than the slightly better objective function value.

⁹ In the conduction ratio paragraph of Section 4.2.3 we defined this ratio from one block cycle to the other with ± 3 . However, our results showed these variations of ± 3 rarely occur and that the range ± 2 includes the most cases. Hence, we constrained this variable due to a better discrimination result and less false positive recognized AFib ECGs.

¹⁰ It would not make any sense to simulate a blocked signal at the beginning on an ECG strip, hence, we can just define that the first atrial signal is conducted to the ventricles.

Algorithm 4.10: getBestConductionRatio - Type I First Level

Input: Previous conduction ratio, current incoming signal number, vector of incoming signal times in , vector of ventricular signals V

Output: Best conduction ratio

```

begin
  minRatio = getMinConductionRatio (previousRatio)
  maxRatio = getMaxConductionRatio (previousRatio)

  for  $iRatio = minRatio$  to  $maxRatio$  do
     $k = 0$ 
     $nConducted = conducted \rightarrow getnSignals$ 

    for  $i = iIncoming$  to  $iIncoming + iRatio$  do
      if  $isOdd(nConducted)$  then                                /* Skip signal */
         $nConducted++$ 
         $k++$ 
         $i++$ 
         $conductedSignal = in[i] + \alpha + k \cdot \Delta_{n+1:n}(ratio)$ 
         $blockCycle.add(conductedSignal)$ 

         $j = \frac{nConducted}{2}$ 
         $currentVentricular.add(V[j])$ 
         $nConducted++$ 
         $k++$ 

     $solution = getObjectiveFunctionValue(blockCycle, currentVentricular)$ 
    if  $solution \leq bestSolution$  then
       $bestSolution = solution$ 
       $bestRatio = iRatio$ 
  return  $bestRatio$ 

```

3. Compute Varying Type I Block Followed by a 2 : 1 / 1 : 1 Level - MAVB 2c

We defined earlier that in a MAVB 2c, there can either appear a 2 : 1 or a 3 : 2 block on the first level. Furthermore, the second level can be a continuous 2 : 1 block or only partially active with a changing 2 : 1 / 1 : 1 conduction. Although, we could use a variation of the Algorithm 4.10, it is possible to reduce the complexity of this algorithm. This is caused by the additional information about the conduction ratio on the first level. The main difference, however, is the possibility to skip either two *or just one* conducted signal in comparison to the ventricular signals. This way, we are able to simulate a 2 : 1 block as well as a the 1 : 1 conduction on the last level, without actually calculating the complete level at each conduction ratio.

In conclusion, we just look for the next conducted signal that is able to strike a ventricular signal within the defined range and count the skipped signals. If this number is even then only one or two 2 : 1 blocks can appear. If this number is odd, there has to be one 3 : 2 block. Additionally, there is the possibility that one complete block cycle is skipped if a complete 2 : 1 block occurs on the first and the second level. To be more specific, if three successive 2 : 1 block cycles on the first level conduct to two ventricular signals thus the middle cycle would be blocked on the second level. In this case, the number of skipped signals on the first level is 3, then we just add this specific conduction ratio and compare, once more, with a new incoming signal in the next step of the loop.

Algorithm 4.11: getBestConductionRatio - Type I First, 1 : 1 / 2 : 1 Second

Input: Current incoming signal number, vector of incoming signal times in , vector of ventricular signals V , number of so far compared ventricular signals $jVentricular$, maximum deviation constant

Output: Best conduction ratio

```

begin
  k = 0
  maxSkippedSignals = 3

  for  $i = iIncoming$  to  $iIncoming + maxSkippedSignals$  do
    conductedSignal =  $in[i] + \alpha + k \cdot \Delta_{n+1:n}(twoToOne)$ 
    k++
    deviation = abs (conductedSignal -  $V[jVentricular]$ )

    if  $deviation \leq MAX\_DEVIATION$  then
      nSkippedSignals =  $i - iIncoming$ 
      break

  if  $isEven(nSkippedSignals)$  then
    bestRatio = twoToOne
  else
    bestRatio = threeToTwo

  if  $nSkippedSignals < 2$  then
    jVentricular++;
  return bestRatio

```

For the 2 : 1 / 1 : 1 block level, we need to check again if the following conducted signal is within the defined accuracy of the according ventricular signal. But, we have the additional information that only 2 : 1 or 1 : 1 blocks are possible. Hence, we can just compare the next potentially conducted signal to the next ventricular one and if its

within this certain range there is a 1 : 1 conduction. If not, the next signal is definitely blocked and in consequence a 2 : 1 block on the current signal.

Algorithm 4.12: getBestConductionRatio - 2 : 1 / 1 : 1 Level

Input: Current incoming signal number, vector of incoming signal times *in*, vector of ventricular signals *V*, maximum deviation constant

Output: Vector of conducted signal times

begin

```

    j = conducted → getnSignals(); if j < ventricular → getnSignals - 1 then
        nextConductedSignal = in[i+1] + computeConduction (oneToOne)

        deviation = abs (nextConductedSignal - V[j + 1])
        if deviation < MAX_DEVIATION then
            | bestRatio = oneToOne
        else
            | bestRatio = twoToOne
    else
        | bestRatio = oneToOne
    return bestRatio

```

4. Compute Varying Type I Block Followed by two 2 : 1 / 1 : 1 Levels - MAVB 3

With the idea of Algorithm 4.11 presented in the previous paragraph, we basically build the foundation for the three level algorithm. Now, the only difference is that there can be a maximum number of 7 instead of 3 skipped signals on the first level. This case happens if only 2 : 1 blocks occur on every level. But also every other case of 2 : 1 / 3 : 2 variation in between is covered. Hence, for the first level we just need to adjust the number of *nSkippedSignals*. For the third level, the 4.12 can be used just in the same way. For the second level however, we need to adjust this algorithm slightly and not only compare the following incoming signal but also the one after that in case of a 2 : 1 block. Again, this is done to simulate a probable block on third level. With this last type of multilevel AV block we covered all specified case that we defined on the medical background. Now, it needs to be determined how the specified medical theory and our models and algorithms build upon it, works at real life examples. These Numerical Result are presented in the following Chapter 5.

HEAT Algorithm Summarized

With the presented algorithmic steps and optimization we are able to compute not only an extraordinary result in the discrimination between regular atrial tachycardias and atrial fibrillation, but also this complex problem is solved within real-time. The numerical results of this algorithm are presented in the following Chapter 5. Finally, the complete HEAT Algorithm is summarized in Algorithm 4.13.

Algorithm 4.13: HEAT Algorithm

Input: RR intervals

Output: AFlut / AFib discrimination

begin

Step I - Constraining the Enumeration Parameters
Algorithm 4.1, 4.2, 4.3, 4.4, 4.5

Step II - Determination and Constraint of the Model Parameters
Algorithm 4.6, 4.7

Step III - Calculation of Various Multilevel AV Blocks
Algorithm 4.8, 4.9, 4.10, 4.11, 4.12

Chapter 5

Numerical Results

After developing a mathematical model and algorithms based on a well investigated medicinal background, we would like to confirm the presented hypotheses of this dissertation. Therefore, we use existing and verified databases, as well as a very large and newly collected data set of regular atrial tachycardias and AFib, which satisfies the highest possible gold standard¹. Based on this huge data set, we compare the presented methods and approaches against each other, to see the advantages and disadvantage of one or the other. On the one hand, statistical approaches on this topic are tested, while we also demonstrate the performance of the phenomenological models at real life ECG examples. Finally, we test the HEAT software package in a detailed validation process and show the corresponding results. Thereby, we confirm some of our innovative medical insights of second-degree AV block conduction mechanisms and the newly developed mathematical methods at real life examples. As further validation, we compete with studies performed by physicians or other algorithms on data that could be extracted from literature.

Before we get to these results, we now illustrate the verification requirements which guarantee a high quality of the used data sets and in conclusion the whole validation process. The data sets are explained in detail in the first section. The basic method to discriminate between the two cardiac arrhythmia is given in the presentation of various objective functions. It is also described how the performance of different approaches and methods can be measured appropriately and compared to each other.

5.1 Verification Requirements

To validate a diagnostic method it is absolutely necessary to guarantee the quality of the used test data. In many cases of medical practice, an exact measurement of the required values or a specific diagnosis cannot be made without an autopsy. Hence, in order to keep the patient alive, a so-called gold standard test is required for this verification. It refers to the best possible decision criteria of a test set, against which the new tests or results are compared to.

In our case for example, the exact diagnosis for the prevalent supraventricular tachycardia cannot be made easily. A gold standard criteria would be, to show a surface ECG to as many specialists as possible and rely on their expertise. However, as seen in publications in Section 2.1, even experts have a high misdiagnosis rate on the difficult, prevalent topic. So another, probably more objective approach could be that the decision between regular atrial tachycardias and AFib is made by evaluating whether the atrial conduction is regular

¹Further explained in the following section.

or chaotic. The atrial conduction can reliably be measured by an intracardiac electrogram, which is unfortunately not available in general, but only the surface ECG. Therefore, we collected a huge amount of intracardiac electrograms, to create the best possible gold standard for differentiation between regular atrial tachycardias and AFib.

5.1.1 Heidelberg University Hospital Data Set

To test our algorithms and other approaches in a real world environment, we build up a huge data set of supraventricular tachycardia cases. These were randomly extracted and include simultaneously recorded surface ECG leads as well as intracardially measured electrograms. We collected altogether 380 examples of AFlut and AFib in 160 different patients. Thereof, in each case 190 ECG segments contain one of the two arrhythmias. Two or three varying time frames of one patient were analyzed at the most. On the one hand, we use multiple time frames to further confirm the computed AV block solution and a possibly correct detected atrial rate. On the other hand, we want to reduce the risk for problems with ECG abnormalities due to patients movement for example.

To discriminate between the different arrhythmias, the atrial signal from the intracardiac (IC) electrogram was analyzed whether to be regular or irregular. A regular rhythm was defined by a atrial variation of ≤ 5 ms in one ECG segment. Contrariwise, a chaotic rhythm could easily be recognized, because of its high and chaotic atrial variation. Hereby, the IC signals were only used for the verification process of the date set and *not* as a data input for the algorithm. For validation process on the other hand, only the RR intervals are used, which can be obtained from a common surface ECG. This way, we managed to build probably one of the largest test data sets for the discrimination of regular atrial tachycardias from AFib using the best possible gold standard. In the following it is called the *Heidelberg University Hospital Data Set*.²

5.1.2 Objective Functions

Having a verified data set, we now want to describe the method to discriminate between atrial tachycardias described by a regular atrial rhythm and atrial fibrillation coming with chaotic excitations within the atria. In this context, all objective functions are illustrated that are used to obtain the best result for this discrimination. The basic idea of our approach is, to find a realistic AV conduction to a regular atrial rhythm that leads as exact as possible to the ventricular activation measured in a surface ECG. If the the AV conduction depending on the underlying mathematical model is correct, which is equivalent to the statement that the simulated and the measured R waves are similar, it follows logically that the atrial rhythm is in fact regular. On the other hand, if we are not able to find regular atrial intervals in combination with such an AV block pattern, the atrial input is probably chaotic, hence AFib is present.

To get a mathematical indicator for this discrimination, we compare the time series calculated by means of the mathematical models, to the corresponding ventricular activation

²The study design was approved by the ethics committee of the University of Heidelberg and conforms to the standards defined in the Helsinki Declaration.

measured from surface ECG. In Figure 5.1, the diagnostic workflow of this approach is illustrated at an example. The objective is to minimize the difference between the series of simulated time points V_j and the measured R_j . The latter ones, in this case taken from lead aVR, can be extracted from any surface ECG. The exact atrial cycle length of lead $CS_{3/4}$ in this case, on the other hand, can only be obtained by an intracardiac electrogram, which was discussed in Section 1.5. This intracardiac data is usually not available for decision making and, in the entire dissertation, only used to verify the algorithm a posteriori. We implemented different types of objective functions, for which we aim to find a feasible set with the minimal solution, respectively the deviation of the simulated to the measured ECG data. In the second step, we compare this minimum to a certain cutoff value to decide whether the solution is good enough to be valid or not. More information on the optimal cutoff value is given in following Section 5.1.3.

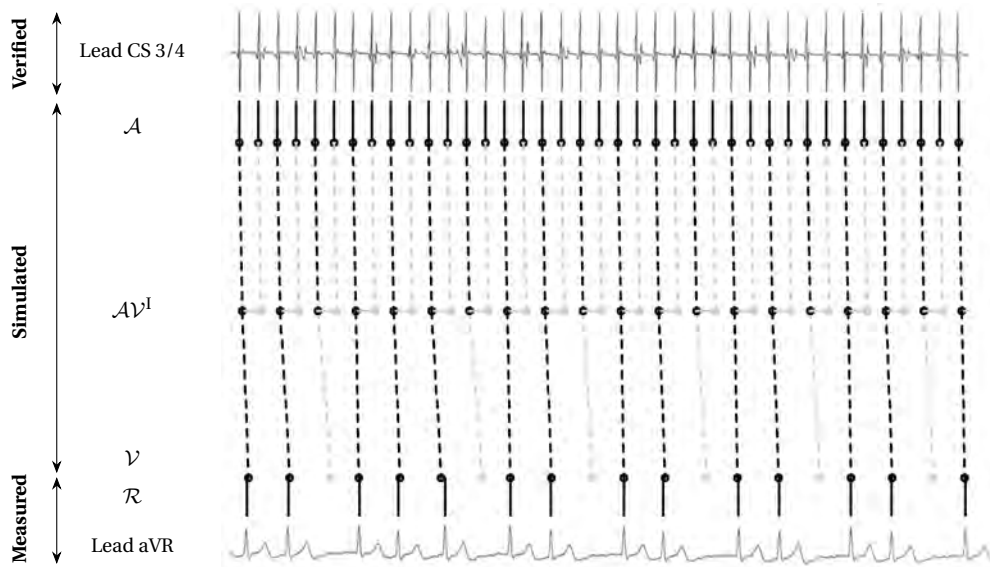


Figure 5.1: Diagnostic workflow of our approach. The algorithm simulates the atrial CL as well as a characterization of the AV block type, here a MAVB with a 2 : 1 AV block on the first followed by a type I block on the second level. The objective is to fit the simulated ventricular data as exact as possible to the ventricular data measured in the ECG. A further description of the workflow is given in the text.

As first optimality criterion, the L_1 norm is used in combination with the number of ventricular signals as scaling factor. This yields in fact to the mean absolute error (MAE) for the final objective function, as shown in Equation 5.1. Secondly, we use two different techniques based on the method of least squares (LSQ), or the L_2 norm, to determine the correlation between the two signals. On the one hand, there is the root mean squared error (RMSE) given in Equation 5.2, which is also commonly applied in statistics. Again, including the scaling factor of the number of ventricular signals and but in this case in combination with the L_2 norm.

Furthermore, there is the normalized mean squared error (NMSE) which additionally takes the ECG time length into account, as can be seen in Equation 5.3.

Definition 5.1 (Objective Functions)

Let $R_j \in \mathcal{R}$ be the exactly measured ventricular ECG signal at the j th position in the analyzed ECG sector \mathcal{T} , with $\mathcal{R} \subset \mathcal{T}$. The objective function of a phenomenological model f is then described as mean absolute error based on the L_1 norm condition

$$MAE := \frac{\|f(A) - R\|_1}{n} = \frac{1}{n} \cdot \sum_{j=1}^n |V_j - R_j|, \quad (5.1)$$

as root mean squared error based on the least squares condition

$$RMSE := \sqrt{\frac{\|f(A) - R\|_2^2}{n}} = \sqrt{\frac{1}{n} \cdot \sum_{j=1}^n (V_j - R_j)^2}, \quad (5.2)$$

or as normalized mean squared error also based on the least squares condition

$$NMSE := \frac{\|f(A) - R\|_2^2}{n \cdot (f(A_n) - f(V_1))} = \frac{\sum_{j=1}^n (V_j - R_j)^2}{n \cdot (V_n - V_1)}. \quad (5.3)$$

△

The main differences of the approaches based on L1 or L2 norm are that the least squares is described to be less robust, but stable, while the least absolute deviation is known to be more robust, but with an unstable solution. Robustness in this case means that the MAE is more robust to single outliers and the least squares give more weight to them. For the stability on the other hand, the solution of the least absolute deviation can be affected in a large amount even at only a slight change in the data, which is not a problem in the squared case. Furthermore, with the normalization factor in the NMSE we are able to compare various lengths of ECG strips, caused by faster respectively slower rhythms that are observed. We implemented all three functions to see which is the best choice for the discrimination in our specific case. The comparison of all objective functions is calculated with our entire ECG database and given and discussed in Chapter 6.

5.1.3 Receiver Operating Characteristic

The receiver operating characteristic (ROC), also referred to as ROC curve, is a statistical tool to illustrate and assess the usefulness of a binary classification system. These systems are often used to analyze the quality and optimize diagnostic tests in medicine, for example tests to find out whether a patient does or does not have a particular disease. In consequence, the test can result in two different ways, either positive (diagnosing the disease) or negative (classified as not having the disease). In our case, the test environment is an algorithm based on a mathematical model that determines whether a patient has *one* or *the other* disease. A positive test result is represented by a regular atrial conduction, followed by a certain AV block pattern, which can describe the given RR intervals to a specified accuracy. Hence,

this positive test result leads to the diagnosis of a regular atrial tachycardia or AFlut. On the contrary, a negative result means that no regular atrial conduction and AV block pattern could be found for a sufficient objective. This leads to the conclusion the atria has to be irregular, ergo AFib. The four outcome possibilities of the test in our scenario are shown in Table 5.1.

		Actual arrhythmia	
		AFlut	AFib
Predicted	AFlut	true positive (TP)	false positive (FP)
	AFib	false negative (FN)	true negative (TN)

Table 5.1: Four outcome possibilities of the diagnostic test. Either the test environment correctly identifies AFlut, correctly rejects as AFib, or incorrectly identifies AFlut, incorrectly rejects as AFib.

Sensitivity, Specificity, and Accuracy

As a statistical measurement tool for the differentiation in a binary classification system, *sensitivity* and *specificity* are introduced in Equation 5.4. Sensitivity indicates the ability of the test to correctly diagnose AFlut, which means the probability of the predicted AFlut patients to all of those actually having the disease. On the contrary, specificity gives the probability of the properly detected AFib patients (in other words not diagnosed as AFlut).

$$\text{Sensitivity} = \frac{TP}{TP + FN} \qquad \text{Specificity} = \frac{TN}{TN + FP} \qquad (5.4)$$

Now, the whole ROC curve is visualized by plotting the sensitivity against (1-specificity) over the whole range of discrete discrimination thresholds. Actual ROC curves are displayed later on in the validation section with a negative example in Figure 5.2a or a very good one in the analysis of our approach in Figure 5.16. Further is to mention that the total accuracy of a method can also be determined within one equation. However, this reduction comes along with a loss of information compared to sensitivity and specificity.

$$\text{Accuracy} = \frac{TP + TN}{TP + TN + FP + FN} \qquad (5.5)$$

Youden Index and Area Under the Curve (AUC)

To find the optimal discrimination threshold between the two clinical pictures, one has to define a certain evaluation grid. This evaluation grid is in our case based on the objective function values that are calculated by the three possibilities of Definition 5.1. Sensitivity and specificity can then be calculated on every grid point *i*. If the threshold or cutoff value is too sensitive, obviously the diagnostic test will find a high rate of AFlut patients, but also lots of false hits of AFib patients misdiagnosed as AFlut. The same thing applies the other way

around if the test is too specific. To get this optimal threshold, the sum of sensitivity and specificity has to be maximized over all cutoff values. This correlates to the so-called *Youden Index* [161], which is given by the difference between sensitivity and (1-specificity):

$$J(i) := \text{Sensitivity}(i) + \text{Specificity}(i) - 1 \quad (5.6)$$

$$\text{Optimal cutoff} = \max_{0 \dots n} J(i), \quad i \in [0, n] \quad (5.7)$$

The overall performance of a diagnostic test, can now be measured by the *area under the ROC curve (AUC)*, which is actually calculated by the integral of the ROC curve. The following classifications can be used as an indicator for the test quality - the higher the AUC number, the better the diagnostic test [31]:

0.90 ≤ AUC ≤ 1.00: excellent

0.80 ≤ AUC < 0.90: good

0.70 ≤ AUC < 0.80: fair

0.60 ≤ AUC < 0.70: poor

0.50 ≤ AUC < 0.60: fail

5.2 Validation of Statistical Approaches

The following statistical approaches were discussed in section 3.1 in detail, has been implemented to the HEAT software package based on the literature model and are now applied to our data set.

5.2.1 RR Interval Periodicity

After an analysis of the RR interval periodicity, tested with our data set, we come to the same result as Krummen et al. in [78]. In the best case³ the RR interval periodicity results in a sensitivity of only 29% at a specificity of 89%. The AUC value of 0.55 shows the total failure of this test, which can also be seen in the ROC curve of Figure 5.2a. According to test classification of 5.1.3 this means that the RR interval periodicity test is just worthless. Hence we'd like to point out, that in fact, the differentiation of AFib and AFlut only based on the irregular irregularity of the RR intervals cannot be done at all.

5.2.2 Heart Rate Variability and Poincaré Plots

Although the RR interval periodicity is not applicable, as just pointed out, to analyze the HRV with the help of Poincaré plots actually works quite well on long time recordings, as Esperer et al. [39] showed. In order to test this method on short ECG series and then to be able to compare it to our approaches, we implemented their methods in the HEAT software package. This way, it was possible to apply this test to our data set at a ECG length of 16 RR intervals. We then searched for the specific AFlut and AFib morphology, they described. We found that

³Best solution received at an ECG length of 16 RR intervals.

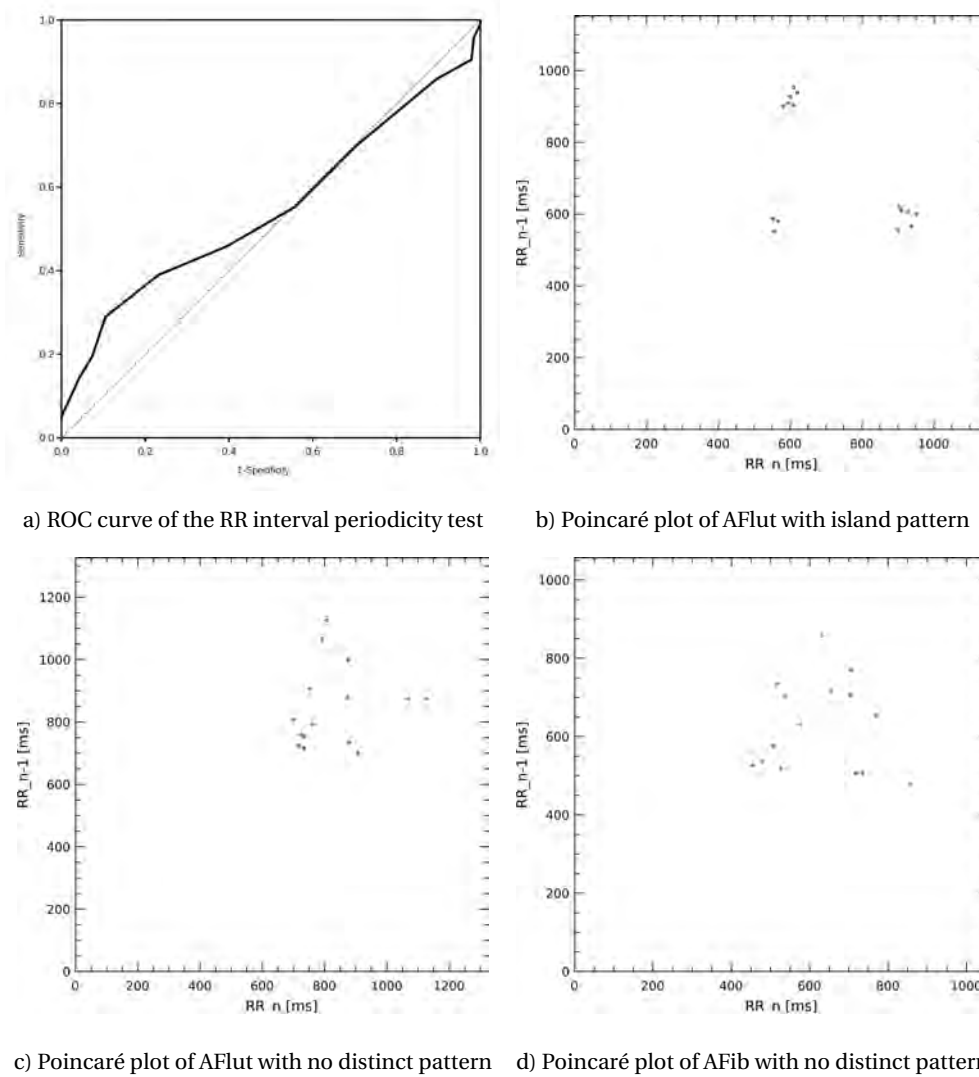


Figure 5.2: In Figure 5.2a the RR interval periodicity is displayed in a ROC curve. The curve hardly leaves the diagonal, which shows the overall failure of that test. The other three examples are Poincaré plots to analyze the HRV. Here, one can especially recognize in 5.2c AFlut compared to 5.2d AFib that there is no visual difference in the pattern at all.

64 cases indicated an AFlut *island* pattern, as exemplary displayed in Figure 5.2b. All other 316 cases could not be discriminated clearly, based on the Poincaré plots. Especially, in the case of atrial fibrillation, to recognize a certain *fan shaped* pattern, was not possible with this amount of RR intervals, see Figure 5.2d. The results showed a sensitivity of 27% and a specificity of 0%. Even if the described AFib pattern is completely ignored and just the island shape is used as a discriminator for or against AFlut (in other words no island shape equals AFib), one comes to a specificity of only 57% because of the many false positives.

Naturally, the number of data points must exceed a significant statistical number and 16 is by far not sufficient. For comparison, in a 24 hour Holter recording, there are usually about 100000 RR intervals. In conclusion, one can say that as an analyzer, visualized Poincaré plots of the HRV, are only useful in long-term ECGs, but not in clinical common, short surface ECG recordings.

5.3 Validation of Phenomenological Approaches

The various phenomenological approaches were built upon the basic AV node characteristics illustrated in Chapter 2. The according mathematical models were specifically defined in Chapter 3.3. Building on that, we implemented these models in our software package HEAT to show some real life ECG examples solved with the according models and to discuss their advantages and disadvantages.

5.3.1 Classical AV Block Type Models and the First Multilevel Approach

There are two different classical models described in this thesis, which were directly built upon the basic AV node conduction rules that arise within supraventricular tachycardias. We tested these models for one AV block level, but also extended it up to three possible block levels. This was the first approach to create a model including the combined multilevel concept. Obviously, with respect to the AV node characteristics in supraventricular tachycardias and the development process of these models, they work fine for very regular examples of typical AFlut without any changes in conduction ratio. But in particular with the extension to multiple block levels, some changes in the RR intervals could be described realistically. Figure 5.4a shows the classical linear model with two consecutive block levels that lead to variations in the RR intervals. This solution could be verified via intracardiac electrogram and the atrial cycle length was exactly found to the according AV block pattern. Nevertheless, the ventricular variations in this examples are still more or less regular, despite the MAVB.

In case of the square root model there are decreasing instead of increasing conduction increments. However, this difference between typical and atypical type I is in not the crucial component here. As we mentioned earlier, these variations which are reflected in the conduction time, are most likely to be patient dependent. The different behavior in the models can be used as refinement, or probably even be neglected if the basic model is good enough. The main problem of these two classical models though, is their inflexibility to changes in the conduction ratio, which can be seen at most of the more difficult examples of atrial tachycardia. Hence, even with the extension of multiple block levels, this model is not sufficient to explain all AV conduction characteristics.

5.3.2 Recovery Curve Approach

We implemented two of the different approaches in the HEAT software package which are based on the AV nodal recovery curve, described in Section 3.3.2. Compared to the classical models, the main advantage of this concept is that it is more flexible in the conduction pattern on one AV block level. More precisely, these models are able to explain alternating type I conduction sequences. One example for such a rhythm is given in Figure 5.3a, where the conduction pattern changes from 3 : 2 to a 2 : 1 ratio on alternating basis. In Figure 5.3b, a 6 : 5 block is described in which one can see the another effect of the exponential function. There is a decrease in the interval length, starting with the first conducted beat. In this case, it is followed by an increase at the last conducted beat within one block cycle, which is caused by the double exponential function given by Shrier et al. This effect could explain some of the atypical form of the type I block pattern, as illustrated in this specifications in Chapter 2.

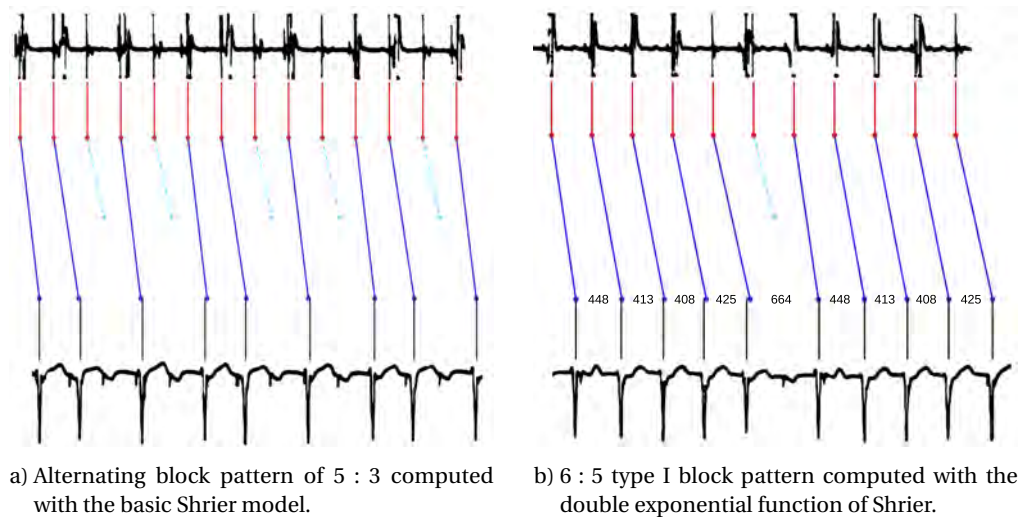


Figure 5.3: Solutions computed with the recovery curve model of Shrier, which was implemented in the HEAT software package. Both examples adapted from Shrier et al.[132]. On the left-hand side, there is an alternating AV block pattern of 3 : 2 and 2 : 1, which results in a total conduction ration of 5 : 3. This solution was computed with the basic Shrier model, however with different parameters (see also text). On the right-hand side, the typical exponential decrease, followed by an increase of conduction interval length of the recovery curve models is illustrated. This solution was simulated with the double exponential function of Shrier.

Figures 5.3a was computed with the basic Shrier model function of Equation 3.24, including one exponential term. However, this model was not able to reproduce the desired AV conduction pattern with the specified parameters by Shrier et al. As they described in their publication, this model had some inaccuracies for the measured patient specific parameters.

Nevertheless, we enumerated these parameters and were able to find a pretty good solution with the given atrial cycle length for this example. The main difference between the two Shrier models is similar to the one in the classical models. In fact, with the double exponential function more or less the atypical type I could be explained, while the basic Shrier model fits rather to the typical type I definition, given in Chapter 2.

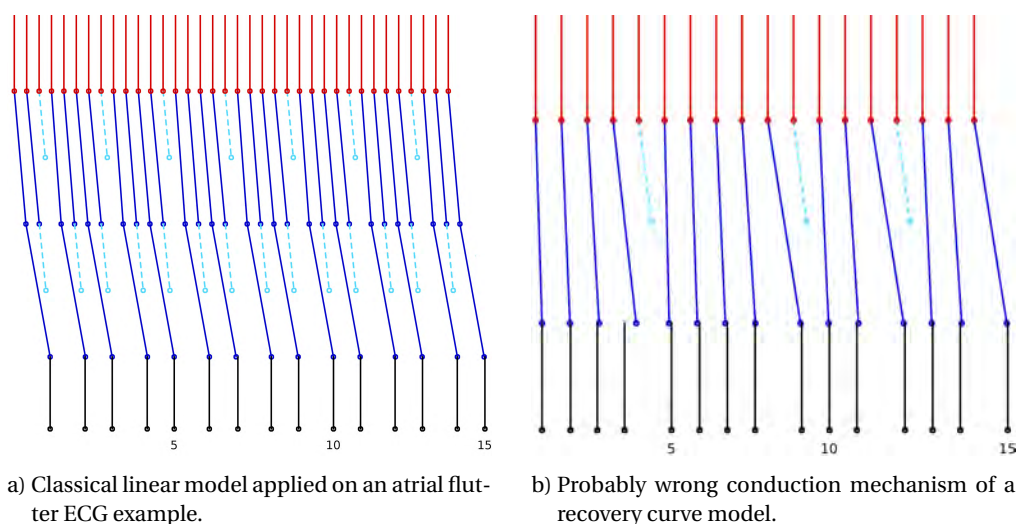


Figure 5.4: On the left-hand side, the atrial cycle length of 256 ms was exactly found with the linear model applied on two AV block levels. It shows a 5 : 4 type I block followed by a 2 : 1 conduction block. The right-hand side figure shows a probably false conduction mechanism of recovery curve model, found with the double exponential Shrier model via enumeration. Further details are explained in the text.

However, for both Shrier models applies that they did not have the desired precision. As previously stated in the discussion of Section 3.3.2, the biggest problem with this model is its strong dependency on the atrial cycle length. We did an extensive analysis of these two models at various test examples and came to the same conclusion. For some individual examples it works quite well with the ability of displaying the alternating phenomenon. Applied on further real life examples, however, this approach does not display all of the conduction phenomena of the second-degree AV block correctly, even when we do *not* take MAVB examples into account. Figure 5.4b shows a case where in fact, a solution was found by enumeration with the double exponential Shrier model, but also the problem of this model becomes obvious. One can see that although such changes in conduction ratio could be described by the sudden prolongation of the conduction time, it is most unlikely to be the correct conduction mechanism when we keep the medical background of Chapter 2 in mind. Supporting this negative example, there is also the fact that this special kind of conduction only work for this particular case, while most of the atypical AFlut examples could not be described by the recovery curve models.

5.4 Detailed Validation of the HEAT Algorithm

In this section, we are finally going to analyze the fundamental achievements of this dissertation in detail. We use various data sets specified in the Verification Requirements Section 5.1 to validate the HEAT Algorithm and put it to the acid test at all kinds of real life example. Additionally, we compare our method against other algorithms and data sets from literature to get a further and comparable impression of its performance. Numerous possible kinds of AV blocks are shown of these examples and confirmed with intracardiac recordings. Altogether, we want to prove the underlying medical theory and mathematical models which we developed in this thesis, in the best possible way. All numerical results are also summarized and collected for a better analysis overview in Table 6.1 and 6.2 in the following Chapter 6.

5.4.1 HEAT Validation Against Other Data Sets

There are several papers which focus on the AFlut versus AFib discrimination done by physicians, as well as papers that try to explain the complex processes in the AV node [14, 24, 75, 78, 79, 131]. The according challenges were described in Chapter 2, as well as the additional difficulties that arise with MAVB. As an additional validation for our algorithm, we now present results from HEAT applied to the ECG examples of those publications, as far as we could extract proper ECG data.

Knight et al. - Electrocardiographic Differentiation of AFlut from AFib by Physicians [75]

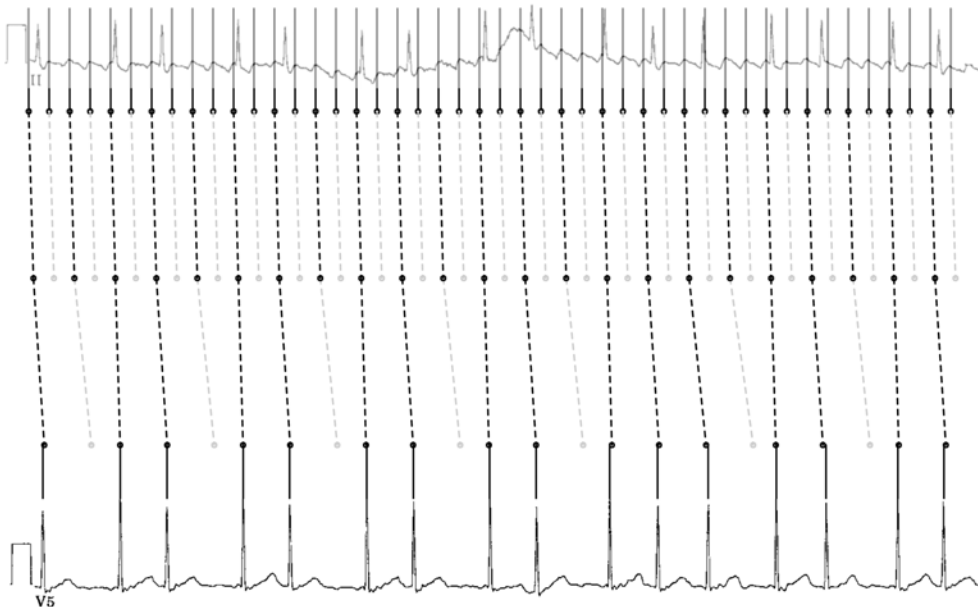


Figure 5.5: Atrial Flutter from Knight et al. correctly diagnosed by the HEAT Algorithm.

In this paper, Knight et al. showed the frequent misdiagnosis of physicians in the discrimination of AFlut from AFib. The details of this paper were described in Section 2.1.2. Even though there were only three ECG examples used, they presented an overall misdiagnosis of over one-third, including experts like cardiologists. The HEAT Algorithm, on the other hand, reached a sensitivity and specificity of both 100%. Furthermore and even more impressive, we can show at the example ECG of atrial flutter in Figure 5.5 that the HEAT Algorithm was able to find the correct solution including the exact atrial rate. In this example one can see with a simple view at the figure that the calculated atrial rate of 218ms fits perfectly to the P waves of the presented ECG. The computed solution indicates a MAVB with 2 : 1 conduction on the first level, followed by a varying type I block. To summarize, the HEAT Algorithm was able to get an improved result of 52 % in comparison to the physicians in the paper.

Kosowsky et al. - Multilevel Atrioventricular Block [77]

This paper is one of the essential publications about the MAVB and was presented in the discussion of Section 2.3. We extracted 10 surface ECGs with atrial flutter cases, which Kosowsky et al. all describe in the paper with various multilevel AV blocks. In this section, we show one example out of the paper of solutions calculated by the HEAT Algorithm. Another exemplary solutions of this data set are shown in Appendix B.

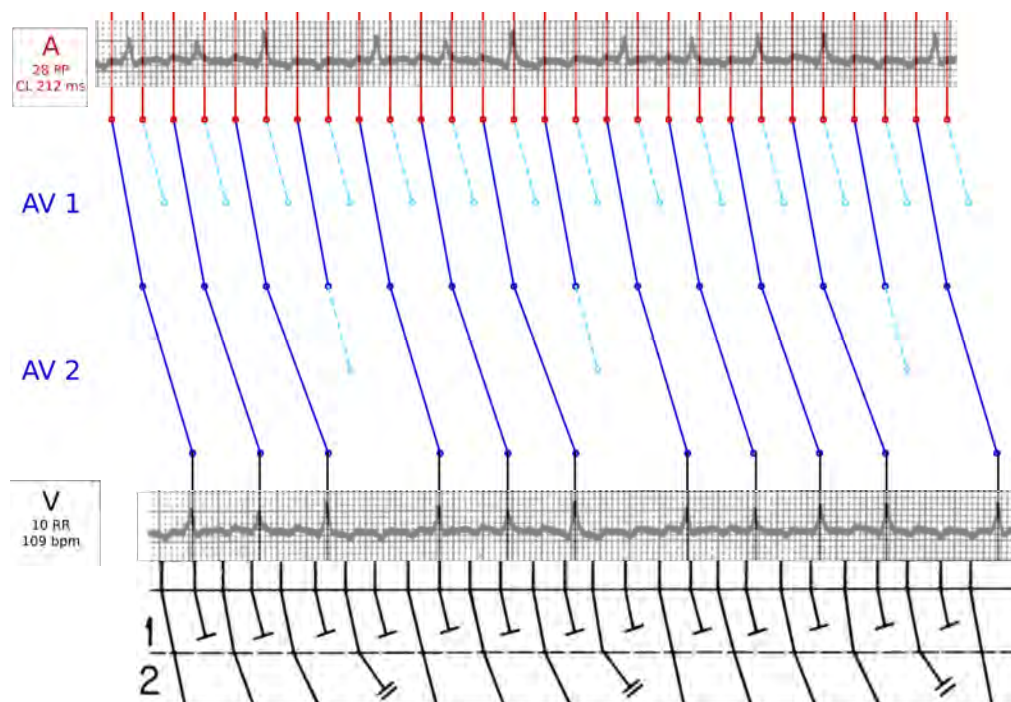


Figure 5.6: MAVB 2a solution calculated by the HEAT Algorithm of Kosowsky’s “Figure 1” [77].

In Figure 5.6 the HEAT Algorithm computed the same solution as suggested by Kosowsky. At the top of this figure, the calculated atrial rate is superimposed over the given ECG lead to compare to the P waves which equals exactly the described atrial rate of 212 ms. At the bottom, the original ECG can be seen to verify the HEAT input data of the RR intervals. Besides, the MAVB pattern presented by Kosowsky et al. is shown below the ventricular level. Clearly, it can be seen that the MAVB type found by the HEAT Algorithm of a 2 : 1 block on the first and a varying type I block on the second level, also correlates to the pattern as described in the paper. In total, the HEAT Algorithm was able to solve 9/10 of these MAVBs, despite the bad ECG quality and the little number of RR intervals acting as input data.

Slama et al. - Multilevel Block in the Atrioventricular Node During Atrial Tachycardia and Flutter Alternating with Wenckebach Phenomenon [134]

As discussed in Section 2.3 and 2.4, Slama et al. investigated very interesting facts about the conduction in the AV node and MAVB theory. They described several examples of their data set in detail, including the intracardially measured atrial cycle length and the according AV block pattern. All studied patients suffered from atrial flutter or regular atrial tachycardia with absolute regular atrial rhythm. In patients with a restored sinus rhythm, who were successfully treated by atrial stimulation, the fast atrial rhythm was reproduced by incremental atrial pacing [134].

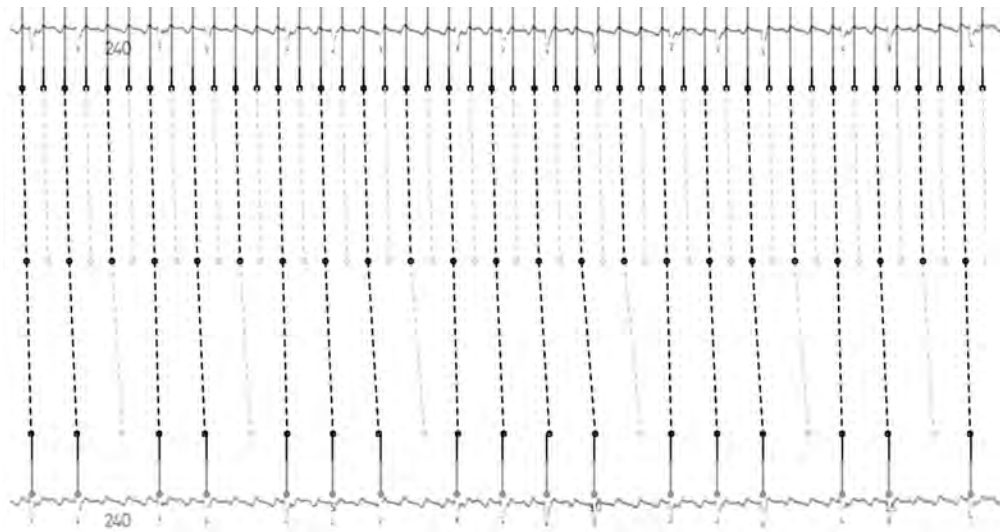


Figure 5.7: MAVB 2a solution calculated by the HEAT Algorithm of Slama's "Figure 1", which was presented in [134].

We extracted 15 different examples from the paper, on the one hand, to build an additional validation data set. However, this was done not only to prove the successful AFlut recognition of the HEAT Algorithm but especially to show its quality by reproducing the described AV

block type. Additionally, it can be proved whether, or in which cases, the HEAT Algorithm is able to compute the correct atrial rhythm exactly. In this paragraph, three different kinds of multilevel AV block types computed by the HEAT Algorithm are shown. Further figurative solutions of this data set are illustrated and can be reviewed in Appendix B. Besides, the detailed validation of all ECGs that could be extracted of the paper of Slama et al. is described in Table 5.2.

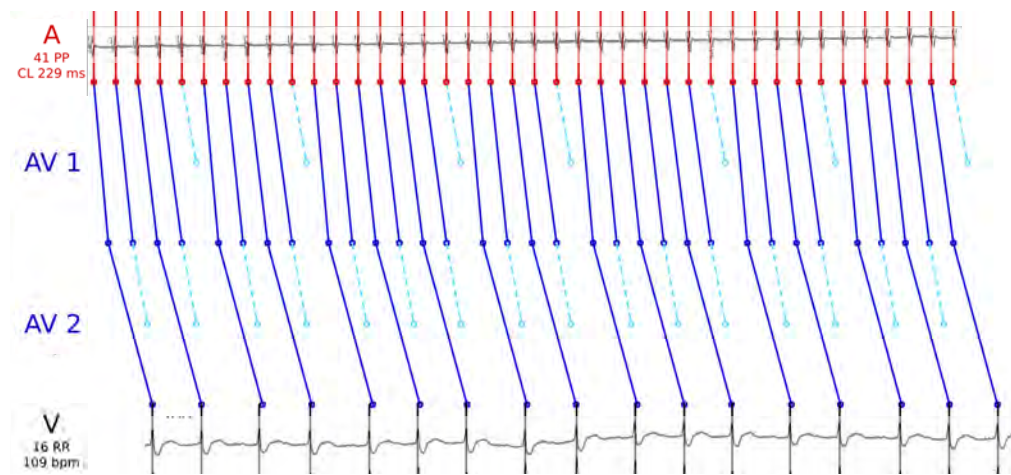


Figure 5.8: MAVB 2b solution calculated by the HEAT Algorithm of Slama’s “Figure 4” [134].

Figure 5.7 shows a MAVB 2a with a 2 : 1 block on the first level and a varying type I block on the second. The atrial rate was correctly calculated by the HEAT Algorithm at 240 ms, which equals exactly the measured atrial rhythm that was described in the paper. At the bottom of the figures, the original ECG can be seen with the input data of the RR intervals. The computed AV block type is described in the middle, while at the top the calculated atrial rate is superimposed over the ECGs P waves for comparison. The second two level type of a MAVB 2b is described in Figure 5.8. The HEAT Algorithm computed a solution with a varying type I block on the first level and a 2 : 1 block on the second precisely like described by Slama et al. Although the atrial rhythm for this example was not denoted in the paper, one can see at the intracardiac signal that it was correctly found at 229 ms by the superimposed intracardiac over the calculated atrial signal. As in example 4, the atrial rate is not specified in the paper in ECG 5a and 5c. Nevertheless, the superimposed solution in the surface ECG lead can be checked visually in these cases. In all of these specific examples the computed atrial cycle length fits perfectly to the P waves or the intracardiac signal. This can be reviewed in Figure 5.8 as described above or in Appendix B in the case of Figure B.3 and B.4.

Finally, to come to the validation of the HEAT Algorithm by means of this data set, the analysis is explicitly listed in Table 5.2. As mentioned above, all examples came with a totally regular atrial rhythm exactly measured by intracardiac (IC) electrogram or respectively given by atrial pacing. There are some atrial flutter examples where a correct solution was found but the atrial rate was missed. On the one hand, this can be explained with too little input

data with the available RR intervals, to compute the fitting atrial cycle length. Most of the times, these examples are rather simple AV block cases with a 2 : 1 conduction ratio, as e.g. in ECG 7b. In these cases the correct atrial cycle length with the according AV block is in the solution set, but due to the regularity of the examples the algorithm just finds another atrial rhythm with a better objective function value based on the specified model and parameters.

ECG	Length	Gold Std.	AA	Solved	AA Correct	Block Type
1	16 RR	IC	240 ms	yes	yes	MAVB 2a
2	9 RR	IC	220 ms	yes	yes	MAVB 2a
3	10 RR	IC	330 ms	yes	no	MAVB 2b
4	16 RR	IC	229 ms	yes	yes	MAVB 2b
5a	20 RR	Surface ECG ⁴	300 ms	yes	yes	2 : 1
5b	20 RR	Surface ECG	n.a.	yes	no	MAVB 2b
5c	16 RR	Surface ECG	295 ms	yes	yes	MAVB 2a
6a	14 RR	IC	250 ms	yes	no	MAVB 3
6b	9 RR	IC	200 ms	yes	no	MAVB 3
7a	8 RR	IC	545 ms	yes	(no)	5 : 4
7b	7 RR	IC	353 ms	yes	no	2 : 1
7c	15 RR	IC	316 ms	yes	no	MAVB 2b
7d	9 RR	IC	273 ms	yes	yes	MAVB 2a
7e	8 RR	IC	261 ms	yes	yes	MAVB 2b
7f	12 RR	IC	207 ms	yes	yes	2 : 1 / 2 : 1

Table 5.2: The complete validation data set of ECGs presented by Slama et al. [134] and the calculated solutions by the HEAT Algorithm. Further information is given in the text.

Furthermore, it should be mentioned that in Slama's ECG 7a the correct one level solution with a 5:4 block was found as best solution from the HEAT Algorithm. The wrong atrial cycle length is in this case only caused by the defined parameter settings. We fixed the upper bound for the atrial cycle length at 400 ms as described in Section 4.2.3, where also the reasons for this were explained in detail. Hence, we excluded this case completely in the calculation of the correctly found atrial cycle lengths. For the two three level examples, the HEAT Algorithm found a two level solution. Again, this could come from the short ECG length which leads to another AV block type. Nevertheless, the most important thing in all of these solutions is that they were diagnosed correctly as regular atrial tachycardia or AFlut. In fact, with our approach we were able to find the correct diagnosis for *all* specified examples. The HEAT Algorithm was also able to compute the correct multilevel AV block types in many examples as well as in 57 % the exact atrial cycle length, despite the short ECG lengths. This result further proves the quality of the HEAT Algorithm and of our approach in total.

⁴For the examples denoted as "surface ECG", the intracardiac measurements were just not specifically stated in the paper.

Masé et al. - Nodal Recovery, Dual Pathway Physiology, and Concealed Conduction Determine Complex AV Dynamics in Human Atrial Tachyarrhythmias [98]

This paper was not explicitly described so far, but mentioned in Section 3.3 when we discussed the recovery curve approaches. Masé et al. modeled the AV node dynamics in a dual pathway approach also based on the recovery curve model. They also mentioned the prevalent difficulties in understanding the AV node processes that arise in atrial tachycardias. As an additional validation from literature, we extracted one ECG example that was given in their paper including the intracardiac signal. In Figure 5.9, one can clearly see the correct solution including the atrial cycle length. Masé et al. described also they same number and pattern of blocked atrial waves that lead to the ventricular block pattern in total as 3 : 1 at the beginning and 5 : 1 at the end of the ECG. However, with our approach realized in the HEAT Algorithm and based on the medical concept of the MAVB concept as well as further specifically defined assumptions, we are once more able to explain the processes in the AV node.

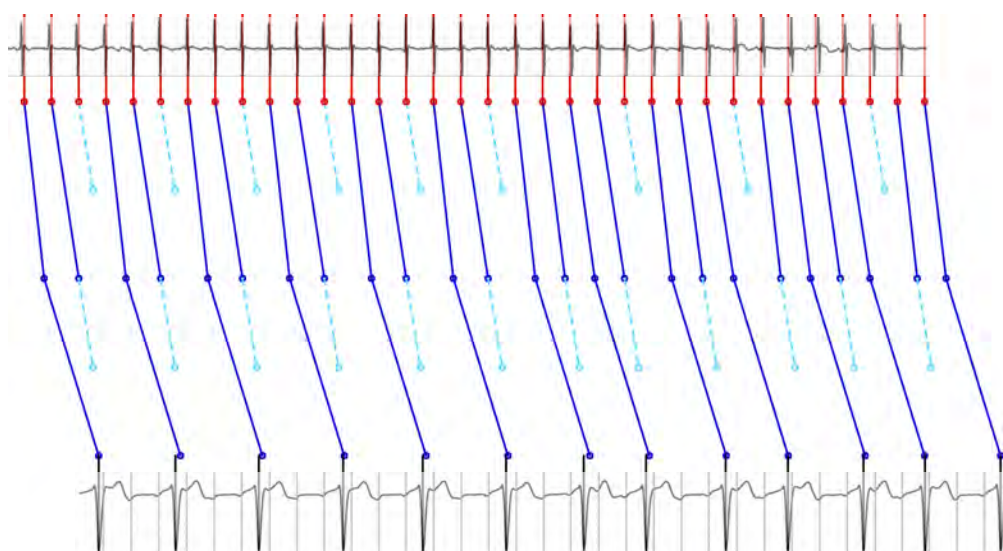


Figure 5.9: MAVB 2b solution calculated by the HEAT Algorithm extracted from Masé [98].

Morrison et al. - Computer Detection of Atrial Flutter [108] - (Glasgow Algorithm)

To compare HEAT to other ECG interpretation algorithms, described in Section 4.1.2, was not possible on our data set, because we obviously couldn't implement all other approaches. Nevertheless, we tried to find accessible data sets to compare the different approaches. Unfortunately, the only available data set we could extract was given by the algorithms publication in case of the Glasgow algorithm. Here, Morrison et al. show three ECGs, of which their "newly upgraded" Glasgow algorithm fails to detect two out of three. One of the exam-

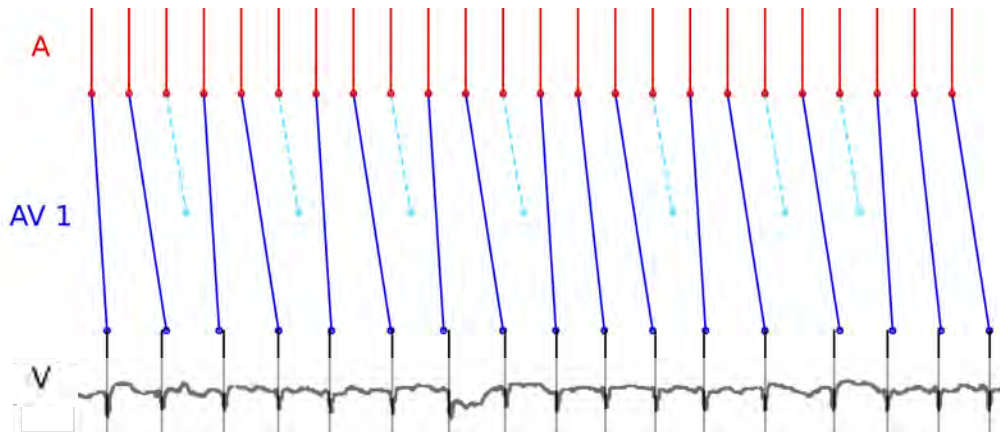


Figure 5.10: One level solution calculated by the HEAT Algorithm of Morrison's Figure 3a [108]. The figure shows an atrial flutter example with a varying type I AV block.

ples was an AFlut with 2 : 1 AV block. In Figure 5.10, the correct solution of the second atrial flutter example is shown with a varying type I block. We are aware that this data set is rather small and they showed it to illustrate the still occurring trouble the Glasgow algorithm has. Nevertheless, the HEAT Algorithm is able to solve all of these problems causing examples easily. Hence, we can conclude in this case that the HEAT Algorithm improves the Glasgow software by 200 % based on this data set.

5.4.2 Validation Against Heidelberg University Hospital Data Set

In this section, we present the enormous data set of 380 ECGs which we collected at the Heidelberg University Hospital with the highest possible gold standard of intracardiac measurements. Hereby, we illustrate additional AFlut cases which further confirm our presented theory of the MAVB, while we are also able to validate the quality of the HEAT algorithm once more. As mentioned in the Verification Requirements of Section 5.1, this data set was randomly extracted and includes typical as well as atypical AFlut ECG examples, besides the AFib cases.

First of all, it can be noted that the MAVB is a rather common phenomenon. Nearly all of the 190 AFlut patients suffered from a MAVB with more than one level, based on our assumptions about the AV node characteristics of Chapter 2. Here, the HEAT Algorithm was not only able to achieve an outstanding discrimination result between the two arrhythmias, presented in the following, but also to compute the exact atrial cycle length in over 52% of the AFlut cases. This result on a such high number of test cases clearly confirms our developed combined multilevel concept of the AV node. We further investigated that two active AV block levels seem to be the most common type by far. Especially, the MAVB 2a with a continuous 2 : 1 block on the first level and a varying or constant type I on the second level could be detected most frequently. This was also confirmed by the exact atrial cycle length that could be calculated by the HEAT algorithm in conjunction with the MAVB 2a.

Furthermore, also the other two level types of MAVB 2b and 2c could be confirmed. However, the distinction between these two is probably not so clear as these types are rather similar. In fact, all two level types are able to vary in their specific kind over a longer time period, which is totally conform with our theory developed in the previous chapters. Besides, we determined that the MAVB 2c can actually be seen as a kind of mixture between the other two. More on that topic is given in the specific examples in the following. Moreover, the MAVB 3 could be verified for several examples. To be more specific, in about 10% of the total number of AFlut test cases a MAVB 3 occurred and could be computed by the HEAT Algorithm exactly to the millisecond. This knowledge also accords to discussed assumption that the MAVB 3 is rarer than the other block types. There are also MAVB 3 examples presented in this section in the following.

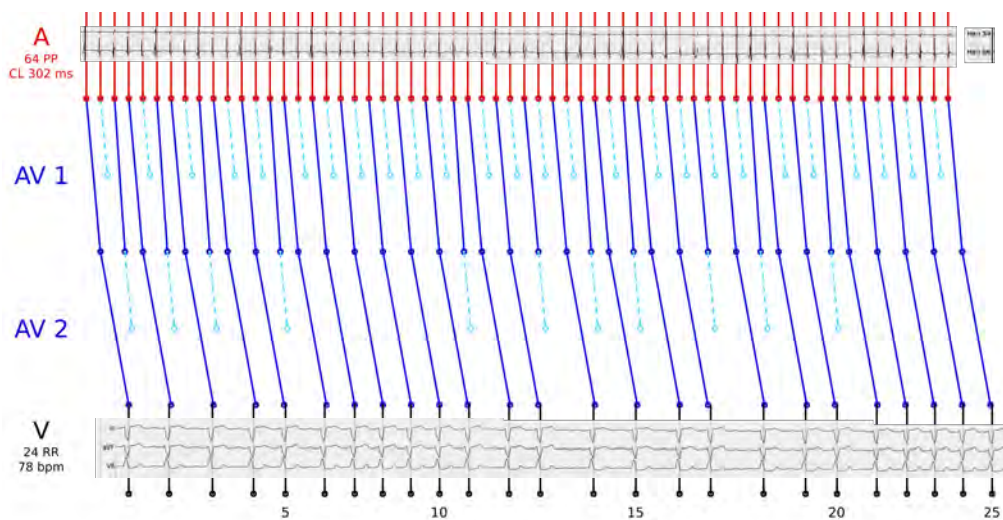


Figure 5.11: MAVB 2c computed by the HEAT Algorithm of an Example including intracardiac measurements from the HD University Hospital data set.

We now would like to present some more interesting MAVB examples of this data set in detail. First, another case of the MAVB 2a can be examined in Appendix B as we already presented this kind of blocking pattern earlier. Nonetheless, we would like to highlight in this Figure B.7 that the P waves are almost not visual in the surface ECG of lead (V6). Thus can be concluded that other approaches using signal processing methods, as other algorithms, would very likely have problems in detecting the regular atrial rhythm due to the facts discussed in Section 4.1.3. The same problem with the missing P waves can be observed in the surface ECG leads of Figure 5.11. The difficulty to recognize AFlut in this ECG is aggravated by the fact that the RR intervals are extremely irregular. The HEAT Algorithm however, computed a MAVB 2c solution for this patient of which we can strongly assume to be the correct AV block type. The correctly calculated atrial cycle length of 302 ms can be checked at the superimposed intracardiac leads of Halo 3/4 and Halo 5/6 on the top of the figure.

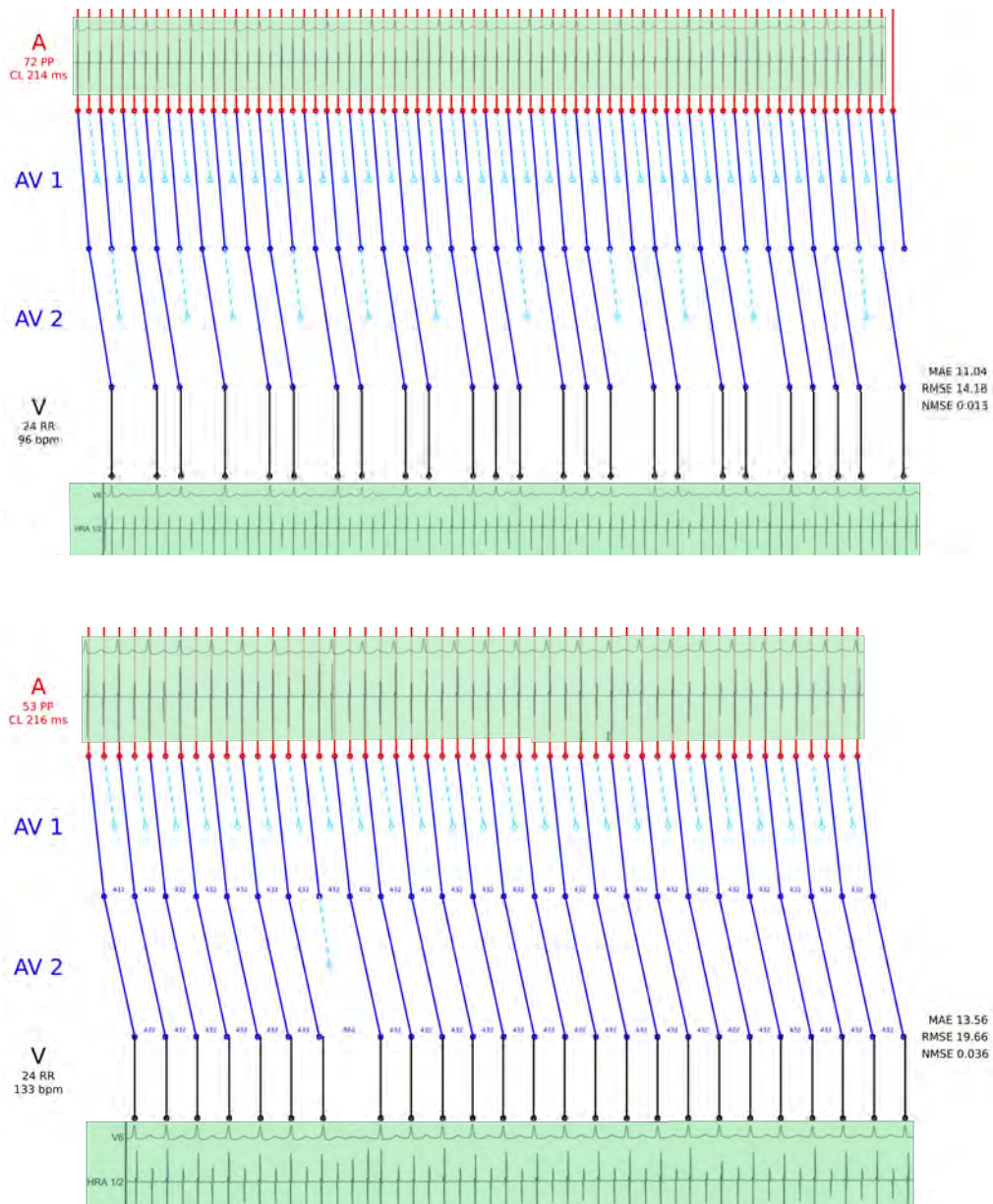


Figure 5.12: Special kind of MAVB 2c with one block level turning from active to inactive. In the first ECG clearly a MAVB 2a is visible described by a type I block on the second level. A few seconds later on the bottom ECG recording, this block level turns almost completely inactive. Further description is given in the text.

We would like to especially emphasize the next AFlut case. This example verifies not only the whole MAVB concept, but in particular our theory that singular AV block levels can become active or inactive. Furthermore, it also proves our basic assumption that the conduction mechanism arises from the same rather than from two distinct electrophysiologic mechanisms. Thus, the *combined* as well as the *multilevel* part are verified by this case. Now, the ECG in Figure 5.12 is continuously recorded which means that the beginning of the ECG at the bottom, proceeds directly at the end of the ECG at the top. It can be seen that slight variations in the atrial cycle length can occur over a longer recording time period despite a “regular” rate. And while the atrial cycle length changes from 214 ms to 216 ms, also the AV block levels are adjusted. In the first part there is a MAVB 2a with a varying type I block on the second level. A few seconds of recording later, the second level changes into an almost continuous 1 : 1 conduction with just one blocked signal within 24 RR intervals. In conclusion, this level becomes inactive most likely due to the slight slowing of the atrial rate of 2 ms. This example furthermore indicates that the MAVB 2c can be seen as kind of connecting link between MAVB 2a and 2b.

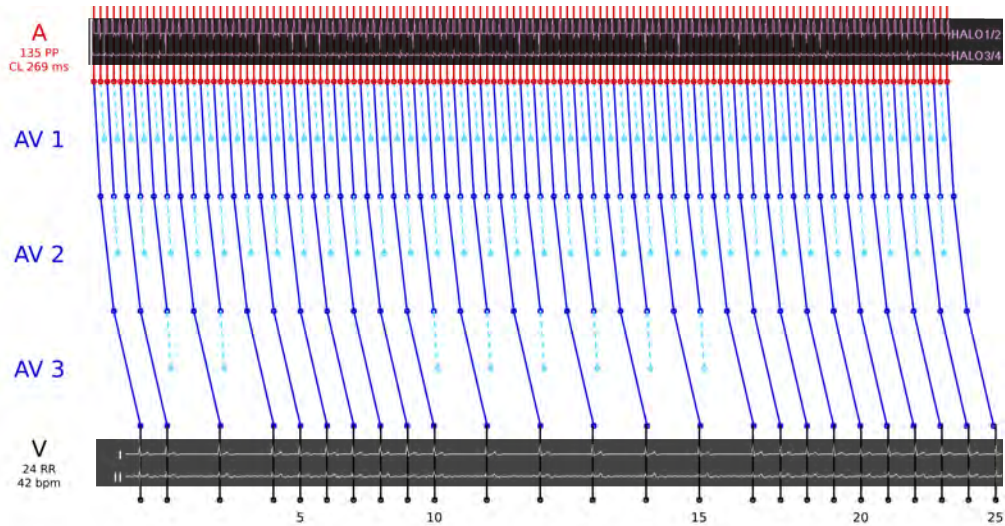


Figure 5.13: MAVB 3 with two levels continuously blocking with a 2 : 1 pattern and the third level changing between 1 : 1 and 2 : 1 conduction.

Next, the particular case of a MAVB 3 is presented for the first time at two specific examples. Despite the extremely slow heart rate of $42 \frac{\text{beats}}{\text{min}}$ illustrated in the ECG of Figure 5.13, the patient suffers from atrial flutter with $223 \frac{\text{beats}}{\text{min}}$ within the atria. This can be explained by three active AV block levels. In this case, the first two levels are blocking continuously with a 2 : 1 ratio and the third level varies between active and inactive. Once more, the HEAT Algorithm was able to compute the atrial cycle exactly length to the millisecond. Figure 5.14 is even more interesting due to the variations in conduction ratio on every block level which also lead to a MAVB 3. Here, several changes between 2 : 1 and 3 : 2 conduction ratio appear

on the first level. As we assumed in our theoretical concept about the conduction mechanisms of the AV node, one can clearly see that these changes on the first level consequently result in changes on the subsequent levels. Similar to the examples before, our *combined multilevel* concept is furthermore verified due to the exactly computed atrial cycle length and in these two particular cases for three block levels. Besides, further solution examples out of the Heidelberg University Hospital data set can be examined in Appendix B.

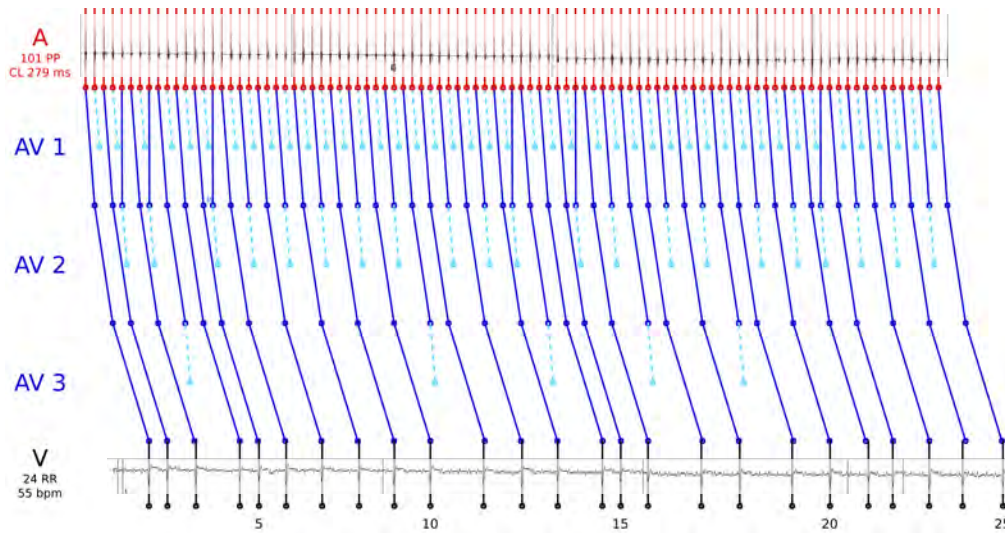


Figure 5.14: MAVB 3 with one level of varying 2 : 1 / 3 : 2 blocking followed by 2 levels with a changing 1 : 1 / 2 : 1 conduction.

5.4.3 Validation Summary

After these diverse real life ECG examples of various kinds of multilevel AV blocks, we would like to analyze the HEAT Algorithm more on the whole but also applied on the Heidelberg University Hospital data set. As mentioned earlier, we examined ECG lengths from 5 to 24 RR intervals and calculated the best possible discrimination values for each ECG length. Therefore, we computed the ROC curve as well as the solution spreading of depending on various objective function values. Additionally, we used all three different objective functions to calculate the solution values to determine which one provides the best possible discrimination result between AFlut and AFib. However, it was exposed by the analysis of various objective functions that although there can be slight variations seen in the discrimination results, no significant difference could be identified in their quality.

For the various number of RR intervals the Youden index $J(i)$, which was specified in Section 5.1.3, shows the quality of the discrimination between the two arrhythmias. It could be established that starting from a length of 8 RR intervals $J(i) > 0.50$ which equals a sensitivity and specificity from each 0.75. Below that number, although the correct AFlut result can be

computed, there are still a lot of false positives obviously. However, the discrimination result constantly improves with an increasing ECG length and hence the additional information. As we already discussed, this goes on until a certain point where the ECG is eventually too long and even slight variations within the atria despite a “regular” atrial rhythm, make the underlying model assumptions invalid. In conclusion the best results have been determined in the ECG range of 16 to 23 RR intervals with constantly $J(i) > 0.60$.

Final Discrimination Result of the HEAT Algorithm

To be more specific, the HEAT Algorithm managed to reach a Youden value of $J(i) = 0.68$, a sensitivity of 0.81, and a specificity of 0.87 at number of 22 RR intervals. These good discrimination results can be observed in solution spreading in Figure 5.15. Here, the vertical dashed line shows the optimal cutoff value that guarantees the best discrimination. Furthermore, this solution leads to a total accuracy of 84%.

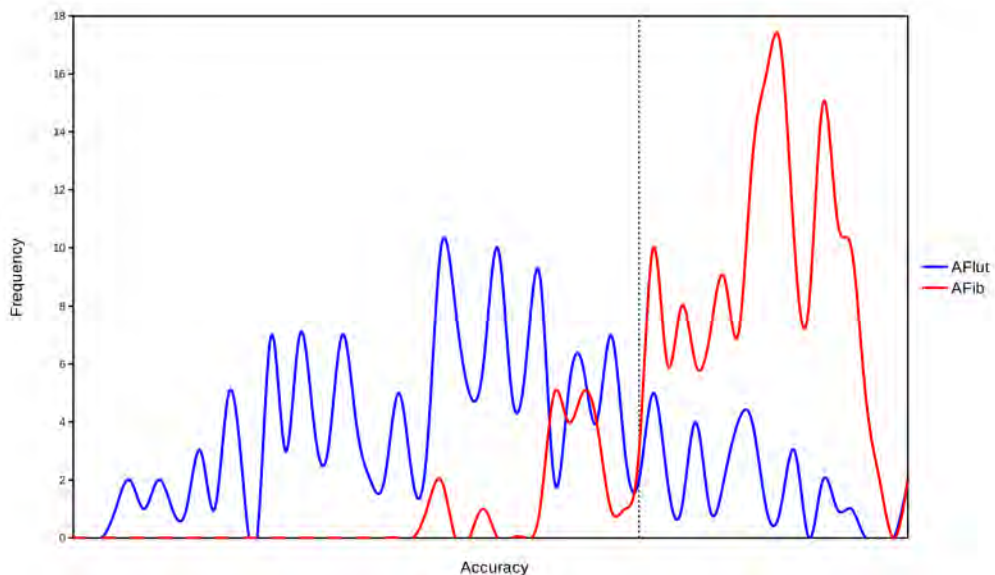


Figure 5.15: Solution spreading of the objective function values of the HEAT Algorithm applied on the HD University Hospital data set.

In Figure 5.16, the ROC curve shows the HEAT Algorithm applied on the Heidelberg University Hospital data set. In this curve, the consistently outstanding performance of our approach is validated. With an Area Under the Curve (AUC) value of 0.90, the quality of our approach can especially be demonstrated in total. According to the classification indicator of diagnostic tests, presented in Section 5.1.3, the HEAT Algorithm is classified as *excellent*. Finally, we would like to draw the attention to the fact that all of these impressive results were not only calculated within real-time but within 1 to 3 seconds. The variation only depends on the complexity of the underlying RR input data. In conclusion, this means that we

managed to reduce the enormous complexity of the underlying inverse simulation problem drastically by means of our model and algorithmic optimization.

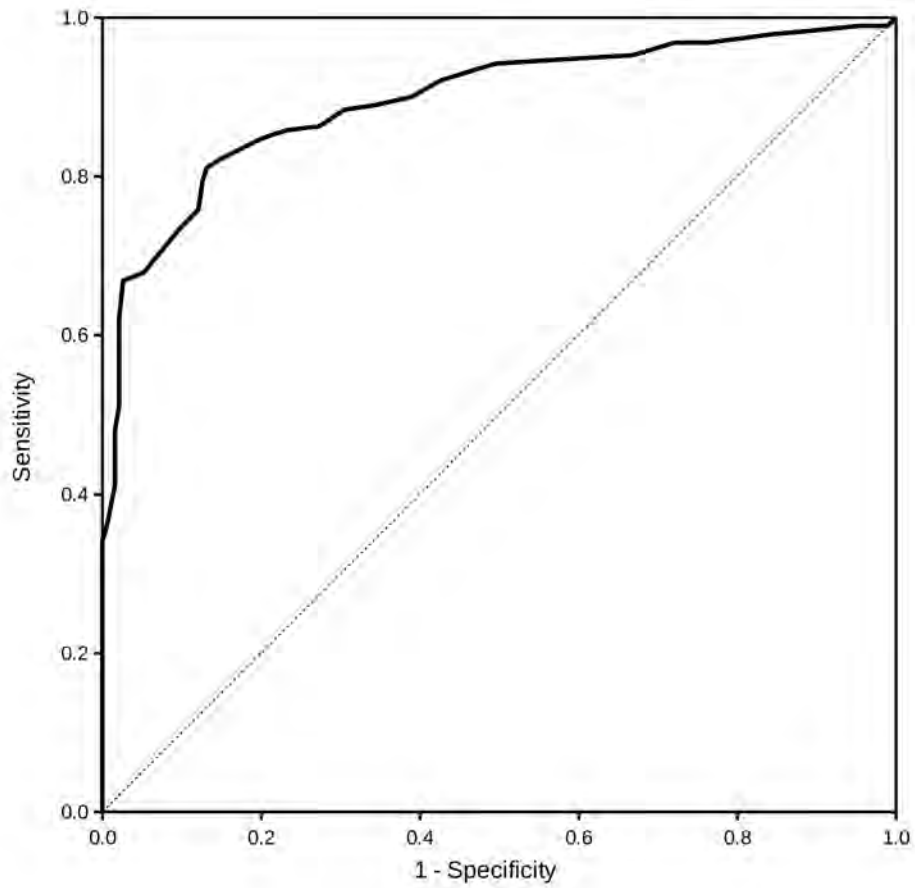


Figure 5.16: ROC curve of the HEAT Algorithm applied on the HD University Hospital data set.

Chapter 6

Summary

In this final chapter, we would like to summarize the mathematical improvements and contributions that were developed in this thesis by an algorithmic approach to the inverse simulation of cardiac arrhythmia. Furthermore, we illustrate the gained medical insight especially about the complex behavior of the AV node characteristics. We managed to create an entirely novel mathematical model as well as an algorithmic concept that is able to explain most of the AV node characteristics easier, more precise and effective. Besides, possible areas of application of the Heidelberg Electrocardiogram Analysis Tool (HEAT) Software Package are examined. We also recapitulate the HEAT Algorithm in comparison to other approaches on the topic of discriminating regular atrial tachycardias including AFlut from AFib. Finally, we especially want to highlight the impact that the accomplished mathematical innovations could have in medical application, on the health care system, and in particular and most important on the patients.

We explored the functionality and dynamics of the human heart as well as the complex conduction characteristics between atria and ventricles in detail. To approach the existing discrimination problem, various modeling techniques from different perspectives were analyzed. In particular, we investigated statistical as well as first principle methods on a cellular basis and showed why our approach of a phenomenological model is superior. We also tested statistical methods at our data set of the Heidelberg University Hospital. The results and the drastic improvements of our approach compared to these methods are illustrated in Table 6.2. Additionally, existing phenomenological models from literature were examined, while we also tested multiple specifically developed approaches.

Based on this, we established an entirely new concept to model atrioventricular dynamics in order to describe the electrical processes in the human heart more complete and better in detail. While this kind of mathematical model can be easily simulated forward if all patient-specific model parameters were known, in our context of an inverse simulation though a non-standard optimization problem arises. The combined combinatorial and nonlinear nature together with variable dimensions on different block levels make this problem class highly difficult. Nevertheless, we managed to drastically reduce the complexity of the existing discrimination problem which leads to an enormous run time acceleration, providing a diagnostic result within real-time. In particular, the HEAT Algorithm is able to compute a highly reliable diagnostic result within a run time of only 1 to 3 seconds.

One further unique feature of the HEAT Algorithm is that the analysis occurs solely based on the input data of RR intervals, without any additional ECG information. As described in Chapter 4, most of the existing algorithms need much more information for their rhythm analysis. Here lies one of the major advantages of our approach. Not only is the data acquisition less error-prone for example against ECG artifacts, which are common especially

in patients with cardiac arrhythmias, but it also makes a whole new area of application accessible. This can be all kinds of ECG hardware that produce a standard 12-lead ECG to devices that only return a *single-lead* ECG recording. These are for example implantable ECG recorders or modern attachments to mobile devices, or else. Even less input data is gained, when using the pulse curve, respectively the pulse signal. This could also be a further area of application for the HEAT software package. This would add devices like blood pressure monitors, modern mobile devices itself, and much more to the input data acquisition possibilities. However, it still needs to be determined whether the pulse curve is accurate enough as measurement for the RR intervals.

Finally, we would like to present the outstanding numerical results we achieved with the mathematical tools developed in this thesis. To validate the HEAT Algorithm, we established the world's largest database with verified cases of the considered cardiac arrhythmia. We verified our software package not only against this data set but also at other databases that were received from literature. This way we were able to compare our approach on the specific AFlut / AFib discrimination problem with physicians as well as other computerized algorithms. The results are summarized in Table 6.1. Here, the "AA correct" column not only shows the percentage of the correctly diagnosed AFlut examples, but additionally where the HEAT Algorithm was able to compute the exact atrial cycle length to the millisecond. In conclusion, this clearly confirms our developed *combined multilevel concept* of the AV node as well as the specific MAVB types we defined. Furthermore, the HEAT Algorithm applied on the huge Heidelberg University Hospital data set accomplished a discrimination result between the two arrhythmia of 0.81% sensitivity and 0.87% specificity. In addition, the quality of our approach can especially be demonstrated at the Area Under the Curve (AUC) value of 0.90. According to the classification indicator of diagnostic tests[31], the HEAT Algorithm is therefore classified as *excellent*.

To summarize, we developed, implemented and evaluated a specifically tailored solution algorithm that outperforms standard approaches by orders of magnitude with respect to run time, sensitivity and specificity. In consequence, our software package, including a mobile app, is able to assist a physician with a diagnostic result right at the patient's bedside. One important result of this thesis is clearly that the developed mathematical tools are able to solve this medical application problem from start to finish. In consequence, the mathematical basis creates a better understanding of the AV node mechanisms, which could lead to correctly diagnosed and potentially cured patients.

Data Set & Source	# Data (AFlut/AFib)	Gold Standard	HEAT Sens. / Spec.	HEAT Accuracy	HEAT A.A Correct	HEAT Improvement
Morrison et al. [108]	3 (2/1)	Experts	1.0 / 1.0	100 %	n.a.	200 %
Knight et al. [75]	3 (1/2)	Experts	1.0 / 1.0	100 %	100 %	52 %
Kosowsky et al. [77]	10 (10/0)	Surface ECG	0.9 / -	90 %	n.a.	-
Slama et al. [134]	15 (15/0)	IC	0.93 / -	93 %	55 %	-
HD University Hospital	380 (190/190)	IC	0.81 / 0.87	84 %	52 %	-

Table 6.1: This table shows the HEAT Algorithm applied on various kinds of data sets. Further description is given in the text or the according sections in Chapter 5 of the Numerical Results.

Method & Source	Data Set (AFlut/AFib)	Sens. / Spec.	Accuracy	AUC	HEAT Improvement
Glasgow Algorithm [108]	Morrison et al. (2/1)	0.5 / 0.0	33 %	n.a.	-
HEAT Algorithm	Morrison et al. (2/1)	1.0 / 1.0	100 %	1.0	200 %
RR Interval Periodicity [78]	HD Hospital (190/190)	0.29 / 0.89	58 %	0.55	45 %
HRV and Poincaré Plots [39]	HD Hospital (190/190)	0.27 / 0.0	14 %	n.a.	500 %
HEAT Algorithm	HD Hospital (190/190)	0.81 / 0.87	84 %	0.90	-

Table 6.2: This table shows other approaches for the discrimination of AFlut from AFib in comparison to the HEAT Algorithm. Further description is given in the text or the according sections in Chapter 5 of the Numerical Results.

Algorithm A.2: Second Shrier version of the AV nodal recovery curve models.**Input:** m incoming signals A_i , conduction constant α , refractory time θ , patient dependent constants $\hat{\beta}$, Δ , τ_{rec} , τ_{fat} , AV conduction time at the first beat AV_1 **Output:** n conducted signal time points V_j **begin**

$$V_1 = A_1 + AV_1$$

$$VA_1 = -AV_1$$

$$j = 2$$

$$AA_l = 0$$

for $i = 2$ **to** m **do**

$$AA_l = AA_l + AA_{i-1}$$

if $AA_l + VA_{j-1} > \theta$ **then** /* Signal can be processed */

$$AV_j = \alpha + \hat{\beta} \cdot \exp\left(\frac{-VA_{j-1}}{\tau_{\text{rec}}}\right) + \Delta \cdot \exp\left(\frac{-VA_{j-1}}{\tau_{\text{fat}}}\right)$$

$$V_j = A_i + AV_j$$

$$VA_j = -AV_j$$

$$j = j + 1$$

$$AA_l = 0$$

else /* Signal can not be processed */

$$VA_{j-1} = VA_{j-1} + (A_i - A_{i-1})$$

$$n = j - 1$$

Appendix B

Solutions

In this Appendix we show further solutions computed by the HEAT Algorithm. The examples are from different data sets, all described in this thesis and named at each Figure. At the bottom of the figures, the original ECG can be seen with the input data of the RR intervals for the algorithm. The computed AV block type is described in the middle, while at the top, the calculated atrial rate is superimposed over the ECGs P waves for comparison.



Figure B.1: HEAT solution of Kosowsky's ECG "Figure 4" presented in [77]. The example shows a 2 level block with a 2 : 1 block on the first level and a varying type I block on the second. The atrial rate was correctly calculated by the HEAT Algorithm at 217 ms which can be seen at the top of the figure where the computed atria is superimposed exactly over the P waves of the ECG.

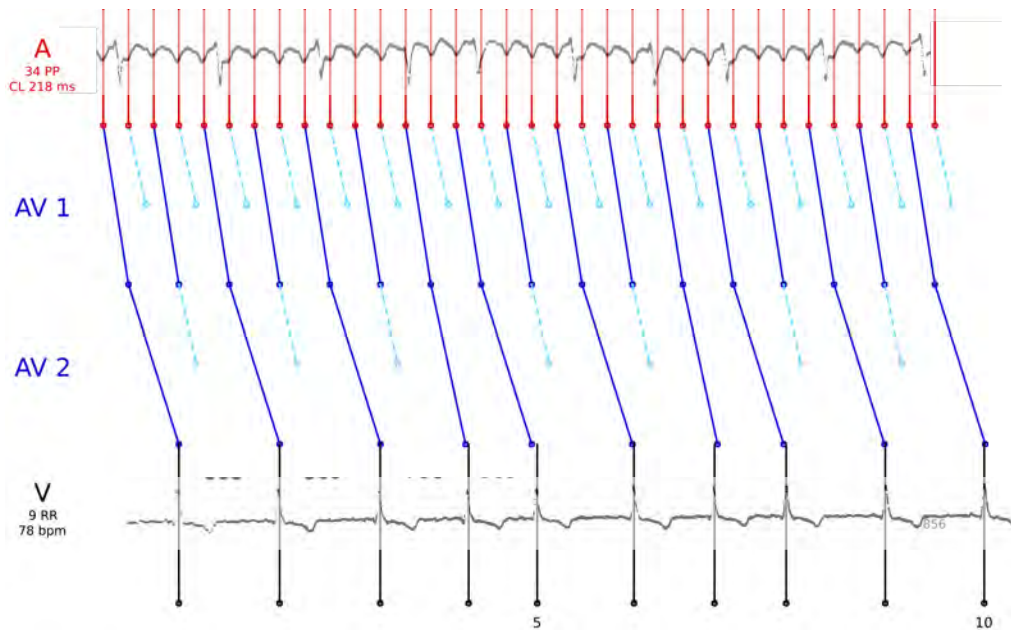


Figure B.2: HEAT solution of Slama's ECG "Figure 2" presented in [134]. The figure shows a 2 level block with a 2 : 1 block on the first level and a varying type I block on the second. The atrial rate was correctly calculated by the HEAT Algorithm at 218 ms. This fits quite good to the 220 ms described in the paper and are actually completely exact as it can be seen at the superimposed atrial excitations.

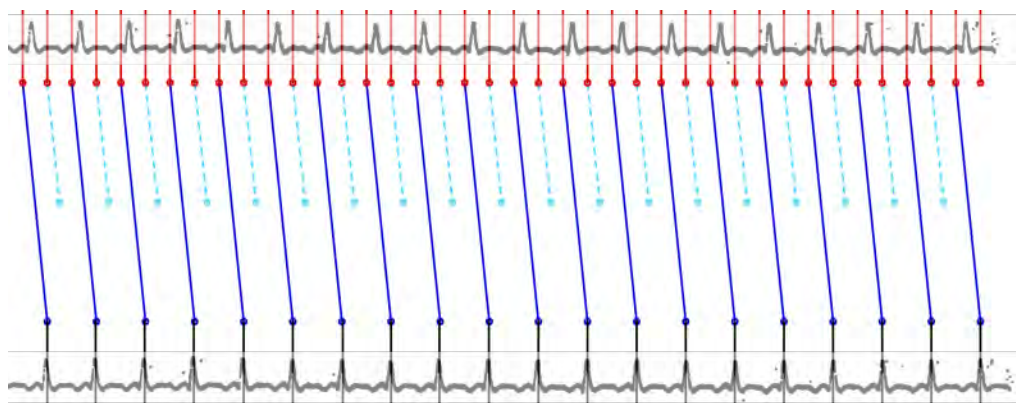


Figure B.3: HEAT solution of Slama's ECG "Figure 5a" presented in [134]. The figure shows a continuous 2 : 1 block on one level. The atrial rate was correctly calculated by the HEAT Algorithm at 300 ms, which equals exactly the P waves as can be seen in the superimposed ECG.



Figure B.4: HEAT solution of Slama's ECG "Figure 5c" presented in [134]. The figure shows a 2 level block with a 2 : 1 block on the first level and a varying type I block on the second. The atrial rate was correctly calculated by the HEAT Algorithm at 295 ms, which equals exactly the P waves as can be seen in the superimposed ECG.



Figure B.5: HEAT solution of Slama's ECG "Figure 7f" presented in [134]. The figure shows a 2 level block with each 2 : 1 conduction. The atrial rate was correctly calculated by the HEAT Algorithm at 207 ms, which equals the $290 \frac{\text{beats}}{\text{min}}$ described in the paper.

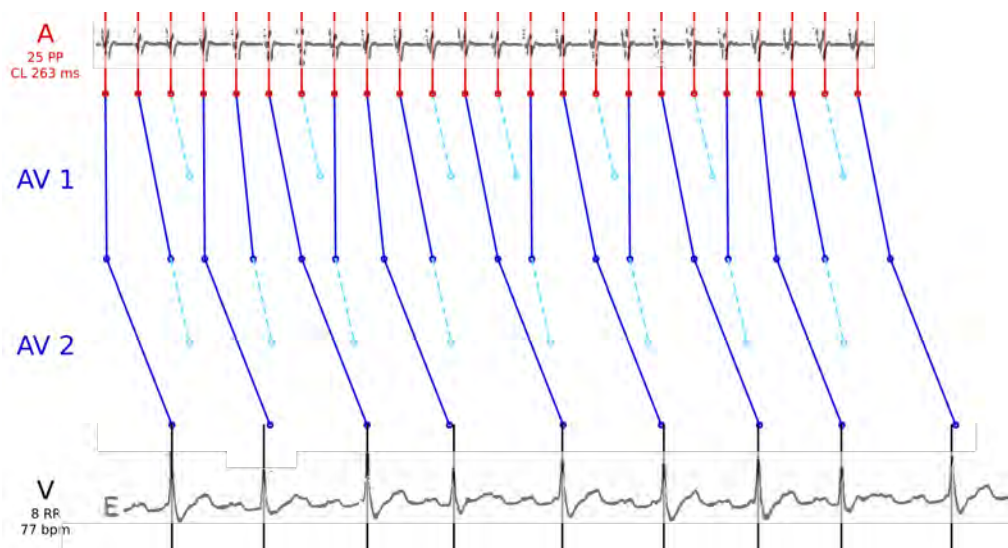


Figure B.6: HEAT solution of Slama's ECG "Figure 7e" presented in [134]. The figure shows a 2 level block with a type I block on the first level and a continuous 2 : 1 block on the second. The atrial rate was correctly calculated by the HEAT Algorithm at 263 ms, with a deviation of only 2 ms. As it can be seen in the superimposed intracardiac signal this deviation is negligible, as the signals are almost exactly equal.

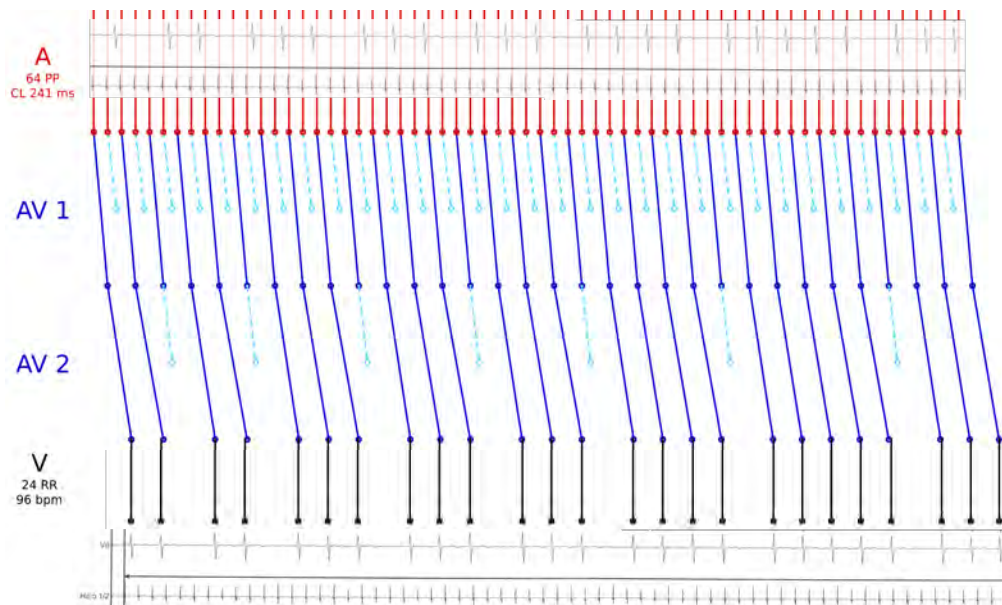


Figure B.7: MAVB 2a calculated by the HEAT Algorithm of an AFlutter example the HD University Hospital data set. There is a continuous 2 : 1 block on the first level followed by a varying type I conduction on the second. The HEAT algorithm computed the exact atrial cycle length of 241 ms.

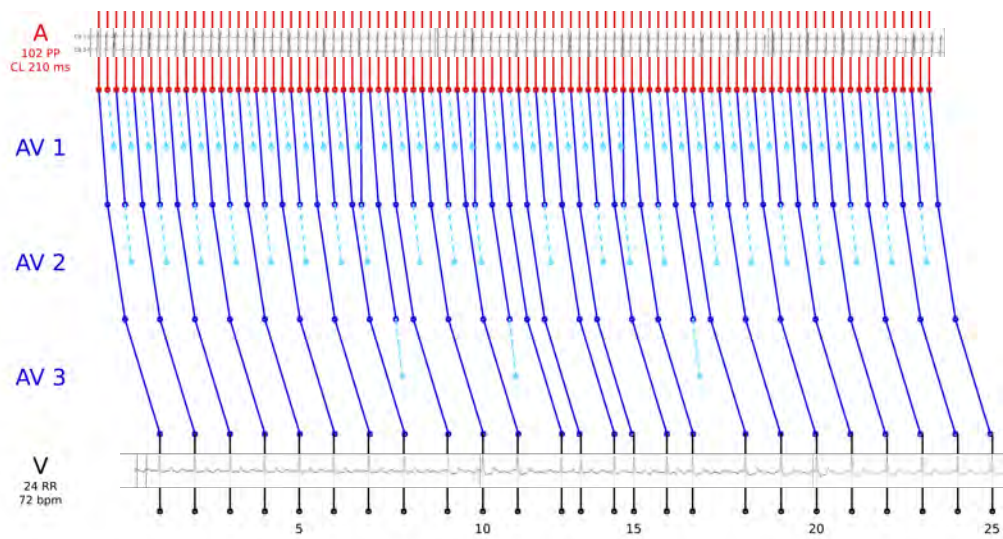


Figure B.8: MAVB 3 calculated by the HEAT Algorithm of an AFLut example the HD University Hospital data set. There is a continuous 2 : 1 block on the first level followed by two varying 1 : 1 / 2 : 1 conduction levels. The HEAT algorithm computed the exact atrial cycle length of 210 ms.

Danksagung

Ich möchte allen danken, die zum Entstehen und Gelingen dieser Arbeit beigetragen haben, dazu gehört meine Arbeitsgruppe in Magdeburg, Andreas Potschka und Christian Kirches, sowie meine Heidelberger Kollegen, und die EU¹. Ich danke Johannes Schlöder und Georg Bock für einen Platz im Mathematikon, und Tillmann Lang für die gute Zeit im Studium.

Eberhard Scholz danke ich besonders für seine Ideen und seine medizinische Kompetenz, ebenso Clemens Zeile und Felix Bernhardt für Ihre enorme Unterstützung. Sie und alle anderen wissen hoffentlich wofür ich Ihnen dankbar bin, ich weiß es auf jeden Fall.

Meinen Eltern und meinem Bruder Marcus danke ich für ihren bedingungslosen Rückhalt, mit dem Sie mir nicht nur mein Studium und diese Doktorarbeit ermöglicht haben, sondern auch sonst immer für mich da sind.

Besonders hervorheben möchte ich meinen Professor und Mentor Sebastian Sager, dessen großartige Unterstützung mich die letzten Jahre und auf dem Weg zu dieser Arbeit begleitet hat und der es durch seine offene und herzliche Art zu einem Vergnügen macht Teil seiner Arbeitsgruppe sein zu dürfen.

Mein letzter und wichtigster Dank gehört meiner Freundin Julla, für ihre Inspiration, Motivation, Geduld, und Liebe.

Heidelberg, im Februar 2018

Florian Kehrle

¹This project has received funding from the European Research Council (ERC) under the European Unions Horizon 2020 research and innovation programme (grant agreement No 647573), which is gratefully acknowledged.

Bibliography

- [1] P. S. Addison. Wavelet transforms and the ECG: a review. *Physiological Measurement*, 26:R155–R199, 2005.
- [2] M. AlGhatrif and J. Lindsay. A brief review: History to understand fundamentals of electrocardiography. *Journal of Community Hospital Internal Medicine Perspectives*, 2, 2012.
- [3] R. H. Anderson, S. Y. Ho, and A. E. Becker. Anatomy of the Human Atrioventricular Junctions Revisited. *The Anatomical Record*, 260:81–91, 2000.
- [4] R. H. Anderson, V. M. Christoffels, and A. F. Moorman. Controversies concerning the anatomical definition of the conduction tissues. *The Anatomical Record. Part B, New Anatomist*, 280:8–14, 2004.
- [5] R. H. Anderson, J. Yanni, M. R. Boyett, N. J. Chandler, and H. Dobrzynski. The anatomy of the cardiac conduction system. *Clinical Anatomy*, 22:99–113, 2009.
- [6] L. Aschoff. Referat über die Herzstörungen in ihren Beziehungen zu den Spezifischen Muskelsystem des Herzens. In *Verhandlungen der deutschen Pathologischen Gesellschaft*, volume 14, pages 3–35, 1910.
- [7] C. Auffray and D. Noble. Origins of Systems Biology in William Harveys Masterpiece on the Movement of the Heart and the Blood in Animals. *International Journal of Molecular Sciences*, 10:1658–1669, 2009.
- [8] S. S. Barold. 2:1 Atrioventricular block: Order from chaos. *The American Journal of Emergency Medicine*, 19(3):214–217, 2001.
- [9] S. S. Barold and H. D. Friedberg. Second degree atrioventricular block - a matter of definition. *The American Journal of Cardiology*, 33(2):311–315, 1974.
- [10] S. S. Barold and D. Hayes. Second-degree atrioventricular block: A reappraisal. *Mayo Clinic Proceedings*, 76:44–57, 2001.
- [11] S. S. Barold and B. Lüderitz. John hay and the Earliest Description of Type II Second-Degree Atrioventricular Block. *The American Journal of Cardiology*, 87(12):1433–1435, 2001.
- [12] C. S. Beck, W. Pritchard, and S. Feil. Ventricular fibrillation of long duration abolished by electric shock. *JAMA*, 135:985–989, 1947.
- [13] M. Besoain-Santander, A. Pick, and R. Langendorf. A-V conduction in auricular flutter. *Circulation*, 2(4):604–616, 1950.

- [14] F. Bogun, D. Anh, G. Kalahasty, E. Wissner, C. B. Serhal, R. Bazzi, W. Weaver, and C. Schuger. Misdiagnosis of atrial fibrillation and its clinical consequences. *The American Journal of the Medical Sciences*, 117(9):636–642, 2004.
- [15] G. E. Burch and N. P. de Pasquale. *A History of Electrocardiography*. Norman Publishing, 1964.
- [16] H. Calkins, R. Canby, R. Weiss, G. Taylor, P. Wells, L. Chinitz, S. Milstein, S. Compton, K. Oleson, L. Sherfese, J. Onufer, and W. A. I. I. Group. Results of catheter ablation of typical atrial flutter. *The American Journal of Cardiology*, 94(4):437–442, 2004.
- [17] H. Calkins, K. H. Kuck, R. Cappato, J. Brugada, A. J. Camm, S.-A. Chen, H. J. Crijs, J. Ralph J. Damiano, D. W. Davies, J. DiMarco, J. Edgerton, K. Ellenbogen, M. D. Ezekowitz, D. E. Haines, M. Haissaguerre, G. Hindricks, Y. Iesaka, W. Jackman, J. Jalife, P. Jais, J. Kalman, D. Keane, Y.-H. Kim, P. Kirchhof, G. Klein, H. Kottkamp, K. Kumagai, B. D. Lindsay, M. Mansour, F. E. Marchlinski, P. M. McCarthy, L. Mont, F. Morady, K. Nademanee, H. Nakagawa, A. Natale, S. Nattel, D. L. Packer, C. Pappone, E. Prys-towsky, A. Raviele, V. Reddy, J. N. Ruskin, R. J. Shemin, H.-M. Tsao, and D. Wilber. 2012 HRS/EHRA/ECAS expert consensus statement on catheter and surgical ablation of atrial fibrillation: Recommendations for patient selection, procedural techniques, patient management and follow-up, definitions, endpoints, and research trial design. *Heart Rhythm Journal*, 9(4):632–696.e21, 2012.
- [18] A. Castellanos, P. R. Fernandez, A. Interian, M. M. Cox, and R. J. Myerburg. Dynamics of atrioventricular nodal conduction ratios during conversion of 2 : 1 into 3 : 1, 4 : 1 and 5 : 1 atrioventricular block. *The American Journal of Cardiology*, 68(9):979–981, 1991.
- [19] A. Castellanos, M. M. Cox, P. R. Fernandez, A. Interian, M. Mayor, T. Ravina, and R. J. Myerburg. Mechanisms and dynamics of episodes of progression of 2:1 atrioventricular block in patients with documented two-level conduction disturbances. *The American Journal of Cardiology*, 70:193–199, 1992.
- [20] A. Castellanos, A. Interian, M. M. Cox, and R. J. Myerburg. Alternating wenckebach periods and allied arrhythmias. *Pacing and Clinical Electrophysiology: PACE*, 12:2285–2300, 1993.
- [21] A. Castellanos, F. Moleiro, N. Saoudi, A. Interian, and R. J. Myerburg. Dynamics of, and alternating wenckebach periods during, 4:1 and 6:1 atrioventricular block. *The American Journal of Cardiology*, 76:523–525, 1995.
- [22] A. Castellanos, F. Moleiro, J. A. Pastor, A. Interian, and R. J. Myerburg. Reverse alternating Wenckebach periods and other modes of regression of $\geq 8:1$ to 2:1 atrioventricular block. *The American Journal of Cardiology*, 82(4):528–531, 1998.
- [23] A. Castellanos, J. Diaz, A. Interian, and R. J. Myerburg. Wenckebach’s periods or alternating wenckebach’s periods during 4:1 atrioventricular block? *Journal of Electrocardiology*, 38:157–159, 2005.

- [24] J. M. Davidenko and L. S. Snyder. Causes of errors in the electrocardiographic diagnosis of atrial fibrillation by physicians. *Journal of Electrocardiology*, 40:450–466, 2007.
- [25] E. O. R. de Medina, R. Bernard, P. Coumel, A. Damato, C. Fisch, D. Krikler, N. Mazur, F. Meijler, L. Mogensen, P. Moret, Z. Pisa, and H. Wellens. Who/isc task force. Definition of terms related to cardiac rhythm. *American Heart Journal*, 95:796–806, 1978.
- [26] P. Denes, L. Levy, A. Pick, and K. M. Rosen. The incidence of typical and atypical A-V Wenckebach periodicity. *American Heart Journal*, 89(1):26–31, 1975.
- [27] DESTATIS. Die 10 häufigsten todesursachen. Technical report, Statistisches Bundesamt Wiesbaden, 2017.
- [28] D. DiFrancesco and D. Noble. A model of cardiac electrical activity incorporating ionic pumps and concentration changes. *Philosophical Transactions of the Royal Society B: Biological Sciences*, 307(1133):353–398, 1985.
- [29] E. Donoso, L. N. Adler, and C. K. Friedberg. Unusual forms of second-degree atrioventricular block, including Mobitz Type-II block, associated with the Morgagni-Adams-Stokes syndrome. *American Heart Journal*, 67(2):150–157, 1964.
- [30] E. H. Du Bois-Reymond. *Untersuchungen über thierische elektricität*. G. Reimer, 1848.
- [31] I. G. Duncan. *Healthcare Risk Adjustment and Predictive Modeling*. ACTEX Publications, 2011.
- [32] D. Echt, P. R. Liebson, B. Mitchell, R. W. Peters, D. Obias-Manno, A. H. Barker, D. Arensberg, A. Baker, L. Friedman, L. Greene, M. L. Huther, D. W. Richardson, and et al. Mortality and morbidity in patients receiving encainide, flecainide, or placebo. The Cardiac Arrhythmia Suppression Trial. *The New England Journal of Medicine*, 324(12):781–788, 1991.
- [33] W. Einthoven. Über die Form des menschlichen Electrocardiogramms. *Pflügers Archiv für die gesamte Physiologie*, 60:101–123, 1895.
- [34] W. Einthoven. Galvanometrische registratie van het menscheijk electrocardiogram. *Herinneringsbudendedl Professor S.S. Rosenstein*, pages 101–107, 1902.
- [35] W. Einthoven. Le Telecardiogramme. *Arch Inc. de Physiol.*, 4:132–164, 1906. Translated into English: *Am Heart J*. 1957;53:602–615.
- [36] N. El-Sherif, B. Scherlag, and R. Lazzara. Pathophysiology of second degree atrioventricular block: A unified hypothesis. *The American Journal of Cardiology*, 35(3):421–434, 1975.
- [37] N. El-Sherif, J. Aranda, B. Befeler, and R. Lazzara. Atypical wenckebach periodicity simulating mobitz ii av block. *British Heart Journal*, 40(12):1376–1383, 1978.
- [38] K. A. Ellenbogen and K. Kaszala. *Cardiac Pacing*. Wiley-Blackwell, 2002.

- [39] H. Esperer, C. Esperer, and R. Cohen. Cardiac arrhythmias imprint specific signatures on lorenz plots. *Annals of Noninvasive Electrocardiology*, 13:44–60, 2008.
- [40] R. Fischer, G. Kleina, B. Widiger, L. Hoy, and C. Zywietz. Discrimination between atrial flutter and atrial fibrillation by computing a flutter index. *Computing in Cardiology*, 32:81–84, 2005.
- [41] W. Forßmann. Die Sondierung des Rechten Herzens. *Klinische Wochenschrift*, 8(45): 2085–2087, 1929.
- [42] H. S. Friedman, J. A. C. Gomes, and J. I. Haft. An analysis of Wenckebach periodicity. *Journal of Electrocardiology*, 8(4):307–315, 1975.
- [43] B. W. Fye. A History of the Origin, Evolution, and Impact of Electrocardiography. *The American Journal of Cardiology*, 73(13):937–949, 1994.
- [44] L. Galvani. De viribus electricitatis in motu musculari commentarius. *Bononiensi scientiarum et artium instituto atque academia commentarii of Bologna*, 7:363–418, 1791. Translation: Commentary on the effect of electricity on muscular motion.
- [45] L. Gerardo-Giorda, M. Perego, and A. Veneziani. Optimized schwarz coupling of bidomain and monodomain models in electrocardiology. *ESAIM: Mathematical Modelling and Numerical Analysis*, 45:309–334, 2011.
- [46] M. Gertsch. *The ECG Manual: An Evidence-Based Approach*. Springer London, 2008.
- [47] E. Goldberger. A simple, indifferent, electrocardiographic electrode of zero potential and a technique of obtaining augmented, unipolar, extremity leads. *American Heart Journal*, 23(4):483–492, 1942.
- [48] E. Goldberger. The aVR, aVL, and aVF leads. A simplification of standard electrocardiography. *American Heart Journal*, 24:378–396, 1942.
- [49] J. Granada, W. Uribe, P.-H. Chyou, K. Maassen, R. Vierkant, P. N. Smith, J. Hayes, E. Eaker, and H. Vidaillet. Incidence and predictors of atrial flutter in the general population. *Journal of the American College of Cardiology*, 36(7):2242–2246, 2000.
- [50] E. Grandi, S. V. Pandit, N. Voigt, A. J. Workman, D. Dobrev, J. Jalife, and D. M. Bers. Human atrial action potential and Ca^{2+} model: sinus rhythm and chronic atrial fibrillation. *Circulation Research*, 109(9):1055–1066, 2011.
- [51] W. Harvey. *On the Motion of the Heart and Blood in Animals*, volume 38, part 3 of *The Harvard Classics*. New York: P.F. Collier & Son, 1909–14. Originally published in 1628. Translated from latin to english by Robert Willis.
- [52] J. Hay. Bradycardia and cardiac arrhythmias produced by depression of certain functions of the heart. *Lancet*, 1:138–143, 1906.
- [53] G. Healthcare. Marquette 12SL ECG Analysis Program, 2008. Physician Guide.

- [54] H. Heiss. Werner Forßmann: A german problem with the nobel prize. *Clinical Cardiology*, 15(7):547–549, 1992.
- [55] D. Hilgemann and D. Noble. Excitation-contraction coupling and extracellular calcium transients in rabbit atrium: reconstruction of basic cellular mechanisms. *Proceedings of the Royal Society of London B: Biological Sciences*, 230(1259):163–205, 1987.
- [56] A. Hollman. *Thomas Lewis: Pioneer Cardiologist and Clinical Scientist*. Springer, 1997.
- [57] B. L. Hoppe, A. Kahn, G. Feld, A. Hassankhani, and S. Narayan. Separating atrial flutter from atrial fibrillation with apparent electrocardiographic organization using dominant and narrow F-wave spectra. *Journal of the American College of Cardiology*, 46:2079–2087, 2005.
- [58] W. J. Hucker, V. P. Nikolski, and I. R. Efimov. Optical mapping of the atrioventricular junction. *Journal of Electrocardiology*, 38:121–125, 2005.
- [59] P. A. Iaizzo. *Handbook of Cardiac Anatomy, Physiology, and Devices*. Humana Press, 2005.
- [60] S. Inada, Hancox, H. Zhang, and M. Boyett. One-dimensional mathematical model of the atrioventricular node including atrio-nodal, nodal, and nodal-his cells. *Biophysical Journal*, 97:2117–2127, 2009.
- [61] T. C. A. S. T. C. Investigators. Preliminary report: effect of encainide and flecainide on mortality in a randomized trial of arrhythmia suppression after myocardial infarction. *The New England Journal of Medicine*, 321(6):406–412, 1989.
- [62] T. C. A. S. T. I. Investigators. Effect of the antiarrhythmic agent moricizine on survival after myocardial infarction. *The New England Journal of Medicine*, 327:227–233, 1992.
- [63] T. N. James. Connecting pathways between the sinus node and A-V node and between the right and the left atrium in the human heart. *American Heart Journal*, 66(4):498–508, 1963.
- [64] A. H. Janardhan, W. Li, V. V. Fedorov, M. Yeung, M. J. Wallendorf, R. B. Schuessler, and I. R. Efimov. A novel low-energy electrotherapy that terminates ventricular tachycardia with lower energy than a biphasic shock when antitachycardia pacing fails. *Journal of the American College of Cardiology*, 60(23):2393–2398, 2012.
- [65] P. Jorgensen. A mathematical model of human atrioventricular nodal function incorporating concealed conduction. *Bulletin of Mathematical Biology*, 64:1083–1099, 2002.
- [66] M. E. Josephson. *Clinical Cardiac Electrophysiology: Techniques and Interpretations*. Lippincott Williams & Wilkins, 3rd edition, 2001.
- [67] M. E. Josephson. *Clinical Cardiac Electrophysiology: Techniques and Interpretations*. Lippincott Williams & Wilkins, 4th edition, 2008.

- [68] W. H. Jr. *Die Thätigkeit des Embryonalen Herzens und deren Bedeutung für die Lehre von der Herzbewegung beim Erwachsenen*. Arbeiten aus der medicinischen Klinik zu Leipzig, 1893.
- [69] S. Kadambe, R. Murray, and G. F. Boudreaux-Bartels. Wavelet transform-based QRS complex detector. *Transactions on Biomedical Engineering*, 46:838–848, 1999.
- [70] A. M. Katz. *Physiology of the Heart*. Lippincott Williams & Wilkins, 5th edition, 2011.
- [71] L. N. Katz and A. Pick. *Clinical Electrocardiography*. Lea & Febiger, 1956.
- [72] R. Kaufmann and C. J. Rothberger. Der Übergang von Kammerallorhythmien in Kammer-Arhythmie in klinischen Fällen von Vorhofflattern, Alternans der Reizleitung. *Zeitschrift für die gesamte experimentelle Medizin*, 57(1):600–640, 1927.
- [73] K. Kettering, V. Dörnberger, R. Lang, R. Vonthein, R. Suchalla, R. F. Bosch, C. Mewis, B. Eigenberger, and V. Kühkamp. Enhanced detection criteria in implantable cardioverter defibrillators: Sensitivity and specificity of the stability algorithm at different heart rates. *Pacing and Clinical Electrophysiology*, 24:1325–1333, 2001.
- [74] A. Khawaja, J. Litwin, T. Auzinger, W. O'Rourke, T. Devine, A. Furlong, C. Lehmann, and R. Fischer. Analyzing the delineation precision of Hannover ECG System (HES[®]): A validation study. *Computing in Cardiology*, 38:617–620, 2011.
- [75] B. Knight, G. Michaud, S. Strickberger, and F. Morady. Electrocardiographic differentiation of atrial flutter from atrial fibrillation by physicians. *Journal of Electrocardiology*, 32:315–319, 1999.
- [76] W. Koch. Weitere Mitteilungen über den Sinusknoten des Herzens. In *Verhandlungsband der Deutschen Pathologischen Gesellschaft*, volume 13, pages 85–92, 1909.
- [77] B. Kosowsky, P. Latif, and A. Radoff. Multilevel atrioventricular block. *Circulation*, 54:914–921, 1976.
- [78] D. Krummen, G. Feld, and S. Narayan. Diagnostic accuracy of irregularly irregular RR intervals in separating atrial fibrillation from atrial flutter. *The American Journal of Cardiology*, 98:209–214, 2006.
- [79] D. Krummen, M. Patel, H. Ngyen, G. Ho, D. Kazi, P. Clopton, M. Holland, S. Greenberg, G. Feld, M. Faddis, and S. Narayan. Accurate ECG diagnosis of atrial tachyarrhythmias using quantitative analysis: A prospective diagnostic and cost-effectiveness study. *Journal of Cardiovascular Electrophysiology*, 21:1251–1259, 2010.
- [80] R. T. H. Laennec. *De l'Auscultation Médiante ou Traité du Diagnostic des Maladies des Poumons et du Coeur*. Brosson & Chaudé, Paris, 1819.
- [81] R. Langendorf. Concealed a-v conduction: The effect of blocked impulses on the formation and conduction of subsequent impulses. *American Heart Journal*, 35(4):542–552, 1948.

- [82] R. Langendorf and L. N. Katz. Unusual arrhythmias due to multiple sites of conduction delay in the a-v junction in cases with a subsidiary ventricular pacemaker located above the bifurcation of the common bundle. *American Heart Journal*, 24(1):31–40, 1942.
- [83] R. Langendorf and A. Pick. Concealed conduction: Further evaluation of a fundamental aspect of propagation of the cardiac impulse. *Circulation*, 13(3):381–399, 1956.
- [84] G. Lee, P. Sanders, and J. M. Kalman. Catheter ablation of atrial arrhythmias: State of the art. *Lancet*, 380(9852):1509–1519, 2012.
- [85] P. P. Leite, V. Bortelli, F. S. de Brito, and R. Andretto. Experimental selective blocks of the internodal conduction pathways in the dog. *Rev. Fac. Med. Vet. Zootec. Univ. S. Paulo*, 13:421–458, 1976.
- [86] F. A. Y. Leon, R. Chuquimia, D. Wu, P. Denes, R. C. Dhingra, C. Wyndham, and K. M. Rosen. Alternating Wenckebach periodicity: A common electrophysiologic response. *The American Journal of Cardiology*, 36(6):757–764, 1975.
- [87] T. Lewalter and B. Lüderitz. *Herzrhythmusstörungen - Diagnostik und Therapie*. Springer, 6th edition, 2010.
- [88] S. T. Lewis and A. M. Master. *Observations upon conduction in the mammalian heart: A-V conduction*. Unknown, 1926.
- [89] T. Lewis. A lecture on the evidences of auricular fibrillation, treated historically. *Br Med J*, 1:57–60, 1912.
- [90] C. Li, C. Zheng, and C. Tai. Detection of ECG characteristic points using wavelet transforms. *Transactions on Biomedical Engineering*, 42:21–28, 1995.
- [91] J. Li, S. Inada, J. E. Schneider, H. Zhang, H. Dobrzynski, and M. R. Boyett. Three-dimensional computer model of the right atrium including the sinoatrial and atrioventricular nodes predicts classical nodal behaviours. *PLOS ONE*, 9(11):e112547, 2014.
- [92] Life in the Fastlane. Atrial fibrillation, 2017. <http://lifeinthefastlane.com/ecg-library/atrial-fibrillation>.
- [93] Life in the Fastlane. Atrial flutter with 4:1 block, 2017. <http://lifeinthefastlane.com/ecg-library/atrial-flutter>.
- [94] L. Littmann and R. H. Svenson. Atrioventricular alternating Wenckebach periodicity: Conduction patterns in multilevel block. *The American Journal of Cardiology*, 49(4):855–862, 1982.
- [95] P. W. Macfarlane. ECG waveform identification by digital computer. *Cardiovascular Research*, 5:141–146, 1971.

- [96] B. C. Mani and B. B. Pavri. Dual atrioventricular nodal pathways physiology: A review of relevant anatomy, electrophysiology, and electrocardiographic manifestations. *Indian Pacing Electrophysiol Journal*, 14(1):12–25, 2014.
- [97] R. Manusama, C. Timmermans, F. Limon, S. Philippens, H. J. Crijns, and L.-M. Rodriguez. Catheter-based cryoablation permanently cures patients with common atrial flutter. *Circulation*, 109(13):1636–1639, 2004.
- [98] M. Masè, L. Glass, M. Disertori, and F. Ravelli. Nodal recovery, dual pathway physiology, and concealed conduction determine complex AV dynamics in human atrial tachyarrhythmias. *The American Journal of Physiology-Heart and Circulatory Physiology*, 303:H1219–H1228, 2012.
- [99] C. Matteucci. Sur un phenomene physiologique produit par les muscles en contraction. *Annales de chimie et de physique*, 6:339–341, 1842.
- [100] T. Mazgalev and P. J. Tchou. *Atrial-AV Nodal Electrophysiology: A View from the Millennium*. Wiley, 2000.
- [101] T. N. Mazgalev, S. Y. Ho, and R. H. Anderson. Anatomic-Electrophysiological Correlations Concerning the Pathways for Atrioventricular Conduction. *Circulation*, 103:2660–2667, 2001.
- [102] C. Mendez and G. Moe. Some characteristics of transmembrane potentials of av nodal cells during propagation of premature beats. *Circulation Research*, 19:933–1010, 1966.
- [103] J. Meredith and J. Titus. The Anatomic Atrial Connections Between Sinus and A-V Node. *Circulation*, 37:566–579, 1968.
- [104] M. Mirowski, M. Mower, A. Langer, M. Heilman, and J. Schreibman. A chronically implanted system for automatic defibrillation in active conscious dogs. Experimental model for treatment of sudden death from ventricular fibrillation. *Circulation*, 58:90–94, 1978.
- [105] W. Mobitz. Über die unvollständige Störung der Erregungsüberleitung zwischen Vorhof und Kammer des menschlichen Herzens. *Zeitung für die gesamte experimentelle Medizin*, 41:180–237, 1924.
- [106] G. K. Moe, J. B. Preston, and H. Burlington. Physiologic Evidence for a Dual A-V Transmission System. *Circulation Research*, 4:357–375, 1956.
- [107] J. G. Mönckeberg. Beiträge zur normalen und pathologischen Anatomie des Herzens. In *Verhandlungen der deutschen Pathologischen Gesellschaft*, volume 14, pages 64–71, 1910.
- [108] S. Morrison and P. W. Macfarlane. Computer detection of atrial flutter. *Annals of Non-invasive Electrocardiology*, 5:358–364, 2000.

- [109] D. Noble. A modification of the Hodgkin-Huxley equations applicable to Purkinje fibre action and pacemaker potentials. *The Journal of Physiology*, 160(2):317–352, 1962.
- [110] D. Noble. Modeling the heart. *The Journal of Physiology*, 19:191–197, 2004.
- [111] D. Noble. From the Hodgkin-Huxley axon to the virtual heart. *The Journal of Physiology*, 280(1):15–22, 2007.
- [112] D. Noble, A. Garny, and P. J. Noble. How the Hodgkin-Huxley equations inspired the cardiac physiome project. *The Journal of Physiology*, 590(Pt 11):2613–2628, 2012.
- [113] Open Source Computer Vision. Canny edge detection, 2018. https://docs.opencv.org/3.1.0/da/d22/tutorial_py_canny.html.
- [114] OpenStax College. *Anatomy & Physiology*. OpenStax CNX, July 2017. <http://cnx.org/contents/14fb4ad7-39a1-4eee-ab6e-3ef2482e3e22@7.1:126>.
- [115] OpenStax College. *Anatomy & Physiology*. OpenStax CNX, July 2017. <http://cnx.org/contents/14fb4ad7-39a1-4eee-ab6e-3ef2482e3e22@7.1:127>.
- [116] PhysioControl. Glasgow 12-lead ECG Analysis Program, 2009. Physician Guide.
- [117] P. Podziemski and J. J. Zebrowski. A simple model of the right atrium of the human heart with the sinoatrial and atrioventricular nodes included. *Journal of Clinical Monitoring and Computing*, 4:481–498, 2013.
- [118] M. Potse, B. Dubé, J. R. A. Vinet, and R. Gulrajani. A comparison of monodomain and bidomain reaction-diffusion models for action potential propagation in the human heart. *IEEE Transactions on Bio-medical Engineering*, 53:2425–2435, 2006.
- [119] J.-L. Prevost and F. Battelli. Sur quelques effets des décharges électriques sur le cœur des mammifères. *Acad. Sci. Paris, FR*, 129:1267–1268, 1899. Translation: On the effects of electric shocks on the hearts of mammals.
- [120] P. M. Rautaharju. The birth of computerized electrocardiography: Hubert V. Pipberger (1920-1993). *Cardiology Journal*, 14(4):420–421, 2007.
- [121] B. Reddy, B. Taha, S. Swiryn, R. Silberman, and R. Childers. Prospective evaluation of a microprocessor-assisted cardiac rhythm algorithm: results from one clinical center. *Journal of Electrocardiology*, 30:28–33, 1998.
- [122] D. C. Reddy. *Biomedical Signal Processing: Principles and Techniques*. McGraw-Hill, 2005.
- [123] H. Reuter. The dependence of slow inward current in Purkinje fibres on the extracellular calcium-concentration. *The Journal of Physiology*, 192(2):479–492, 1967.
- [124] B. J. Roth. *Bidomain Model*. Scholarpedia, July 2017. http://www.scholarpedia.org/article/Bidomain_model.

- [125] S. M. Salerno, P. C. Alguire, and H. S. Waxman. Competency in interpretation of 12-lead electrocardiograms: A summary and appraisal of published evidence. *Annals of Internal Medicine*, 138:751–760s, 2003.
- [126] D. Sánchez-Quintana and S. Y. Ho. Anatomy of cardiac nodes and atrioventricular specialized conduction system. *Revista Española de Cardiología*, 56(11):1085–1092, 2003.
- [127] N. Saoudi, F. Cosio, A. Waldo, S. A. Chen, Y. Iesaka, M. Lesh, S. Saksena, J. Salerno, and W. Schoels. A classification of atrial flutter and regular atrial tachycardia according to electrophysiological mechanisms and anatomical bases. A statement from a joint expert group from the working group of arrhythmias of the European Society of Cardiology and the North American Society of Pacing and Electrophysiology. *European Heart Journal*, 22(14):1162–1182, 2001.
- [128] S. Schmieder, G. Ndrepepa, J. Dong, B. Zrenner, J. Schreieck, M. A. Schneider, M. R. Karch, and C. Schmitt. Acute and long-term results of radiofrequency ablation of common atrial flutter and the influence of the right atrial isthmus ablation on the occurrence of atrial fibrillation. *European Heart Journal*, 24:956–962, 2003.
- [129] E. P. Scholz, F. Kehrlé, S. Vossel, A. Hess, E. Zitron, H. A. Katus, and S. Sager. Discriminating atrial flutter from atrial fibrillation using a multilevel model of atrioventricular conduction. *Heart Rhythm Journal*, 11(5):877–884, 2014.
- [130] J. B. Shea and W. H. Maisel. Cardioversion. *Circulation*, 106:e176–e178, 2002.
- [131] A. Shiyovich, A. Wolak, L. Yacobovich, A. Grosbard, and A. Katz. Accuracy of diagnosing atrial flutter and atrial fibrillation from a surface electrocardiogram by hospital physicians: Analysis of data from internal medicine departments. *The American Journal of the Medical Sciences*, 340(4):271–275, 2010.
- [132] A. Shrier, H. Dubarsky, M. Rosengarten, M. R. Guevara, S. Nattel, and L. Glass. Prediction of complex atrioventricular conduction rhythms in humans with use of the atrioventricular nodal recovery curve. *Circulation*, 76(6):1196–1205, 1987.
- [133] B. Singh and M. V. Williams. The effect of amiodarone, a new anti-anginal drug, on cardiac muscle. *British Journal of Pharmacology*, 39(4):657–676, 1970.
- [134] R. Slama, J. F. Leclercq, M. Rosengarten, P. Coumel, and Y. Bouvrain. Multilevel block in the atrioventricular node during atrial tachycardia and flutter alternating with wenckebach phenomenon. *British Heart Journal*, 42(4):463–470, 1979.
- [135] R. Slama, C. Sebag, G. Motte, and J. Leclercq. Double wenckebach phenomenon in atrioventricular node and his bundle. electrophysiological demonstration in a case of atrial flutter. *British Heart Journal*, 45:328–330, 1981.
- [136] M. Small. *Dynamics of Biological Systems*. Chapman & Hall/CRC Mathematical and Computational Biology. Chapman and Hall/CRC, 2012.

- [137] H. A. Snellen. *Willem Einthoven (1860-1927) Father of Electrocardiography*. Kluwer Academic Publishers, 1994.
- [138] D. H. Spodick. Seven-cycle wenckebach period without atypical features. *American Heart Hospital Journal*, 2(1):64, 2004.
- [139] F. W. Stallmann and H. v. Pipberger. Automatic recognition of electrocardiographic waves by digital computer. *Circulation*, 9:1138–1143, 1961.
- [140] B. Surawicz, H. Uhley, R. Borun, M. Laks, L. Crevasse, K. Rosen, W. Nelson, W. Mandel, P. Lawrence, L. Jackson, N. Flowers, J. Clifton, J. Greenfield, and E. R. D. Medina. The quest for optimal standardization of terminology and interpretation. *American Heart Journal*, 41(1):130–145, 1978.
- [141] C. Sánchez, A. Corrias, A. Bueno-Orovio, M. Davies, J. Swinton, I. Jacobson, P. Laguna, E. Pueyo, and B. Rodríguez. The Na^+/K^+ pump is an important modulator of refractoriness and rotor dynamics in human atrial tissue. *The American Journal of Physiology-Heart and Circulatory Physiology*, 302(5):1146–1159, 2012.
- [142] B. Taha, S. Reddy, Q. Xue, and S. Swiryn. Automated discrimination between atrial fibrillation and atrial flutter in the resting 12-lead electrocardiogram. *Journal of Electrocardiology*, 33:123–125, 2000.
- [143] M. Talajic, D. Papadatos, C. Villemaire, L. Glass, and S. Nattel. A unified model of atrioventricular nodal conduction predicts dynamic changes in wenckebach periodicity. *Circulation Research*, 68:1280–1293, 1991.
- [144] S. Tawara. *Das Reizleitungssystem des Säugetierherzens: Eine anatomisch-histologische Studie über das Atrioventrikulärbündel und die Purkinjeschen Fäden*. Gustav Fischer, 1906.
- [145] C. Thorel. Vorläufige Mitteilung über eine besondere Muskelverbindung zwischen der Cava superior und dem Hisschen Bündel. *Münchener medizinische Wochenschrift*, 56: 2159, 1909.
- [146] C. Thorel. Über den Aufbau des Sinusknotens und seine Verbindung mit der Cava superior und den Wenckebachschen Bündeln. *Münchener medizinische Wochenschrift*, 57:183, 1910.
- [147] A. L. H. und Andrew F. Huxley. A quantitative description of membrane current and its application to conduction and excitation in nerve. *The Journal of Physiology*, 117(4): 500–544, 1952.
- [148] H. v. Pipberger, E. d. Freis, L. Taback, and H. L. Mason. Preparation of electrocardiographic data for analysis by digital electronic computer. *Circulation*, 21:413–418, 1960.
- [149] K. Velten. *Mathematical Modeling and Simulation: Introduction for Scientists and Engineers*. Wiley-VCH, 2008.

- [150] E. Vigmond, R. W. dos Santos, A. Prassl, M. Deo, and G. Plank. Solvers for the cardiac bidomain equations. *Progress in Biophysics and Molecular Biology*, 96(1–3):3–18, 2008.
- [151] R. A. von Kölliker and H. Müller. Nachweis der negativen Schwankung des Muskelstroms am natürlich sich contrahirenden Muskel. In *Verhandlungen der Physikalisch-Medizinischen Gesellschaft in Würzburg*, volume 6, pages 528–533, 1856.
- [152] A. D. Waller. A demonstration on man of electric changes accompanying the heart's beat. *Journal Physiology*, 8:229–234, 1887.
- [153] Y. Watanabe and L. Dreifus. Second degree atrioventricular block. *Cardiovascular Research*, 1:150–158, 1967.
- [154] K. F. Wenckebach. Zur analyse des unregelmässigen pulses. *Zeitschrift für Klinische Medizin*, 37:475–488, 1899.
- [155] K. F. Wenckebach. Beiträge zur Kenntnis der menschlichen Herztätigkeit. *Archiv für Anatomie und Physiologie*, 1:297–354, 1906.
- [156] K. F. Wenckebach. Beiträge zur Kenntnis der menschlichen Herztätigkeit. *Archiv für Anatomie und Physiologie*, 2:1–24, 1907.
- [157] K. F. Wenckebach and H. Winterberg. *Die unregelmäßige Herztätigkeit*. Wilhelm Engelmann, 1927.
- [158] WHO. World health factsheets 2017. Technical report, World Health Organisation, 2017.
- [159] M. V. Williams. Classification of anti-arrhythmic drugs. In E. Sandfte, E. Flensted-Jensen, and K. Olesen, editors, *Symposium on Cardiac Arrhythmias*, pages 449–472, 1970.
- [160] N. F. Wilson, F. E. Johnston, A. G. Macleod, and P. S. Barker. Electrocardiograms that represent the potential variations of a single electrode. *American Heart Journal*, 9: 447–458, 1934.
- [161] W. Youden. Index for rating diagnostic tests. *American Cancer Society*, 3:32–35, 1950.
- [162] D. P. Zipes and J. Jalife. *Cardiac Electrophysiology: From Cell to Bedside*. W.B. Saunders Co., 4th edition, 2004.
- [163] D. P. Zipes and J. Jalife. *Cardiac Electrophysiology: From Cell to Bedside*. W.B. Saunders Co., 6th edition, 2013.
- [164] D. P. Zipes, M. Akhtar, P. Denes, R. W. DeSanctis, A. Garsm, L. S. Gettes, M. E. Josephson, J. W. Mason, R. J. Myerburg, J. N. Ruskin, H. J. J. Wellens, C. Fisch, H. T. Dodge, H. P. Dustan, J. W. Kennedy, T. J. Reeves, and S. L. Weinberg. Guidelines for clinical intracardiac electrophysiologic studies a report of the american college of cardiology/american heart association task force on assessment of diagnostic and therapeutic cardiovascular procedures (subcommittee to assess clinical intracardiac electrophysiologic studies. *Journal of the American College of Cardiology*, 14(7):1827–1842, 1989.

- [165] D. P. Zipes, J. P. Dimarco, P. C. Gillette, W. M. Jackman, R. J. Myerburg, S. H. Rahimtoola, J. L. Ritchie, M. D. Cheitlin, A. Garson, R. J. Gibbons, R. P. Lewis, R. A. O'Rourke, T. J. Ryan, and R. C. Schlant. Guidelines for clinical intracardiac electrophysiological and catheter ablation procedures. a report of the american college of cardiology/american heart association task force on practice guidelines (committee on clinical intracardiac electrophysiologic and catheter ablation procedures), developed in with collaboration the north american society of pacing and electrophysiology. *Journal of the American College of Cardiology*, 26(2):555–573, 1995.

Nomenclature

Throughout this dissertation, number spaces are denoted in uppercase blackboard style (\mathbb{N} , \mathbb{R} , \mathbb{Z}). Uppercase calligraphic style is used for sets ($\mathcal{A}, \mathcal{B}, \mathcal{T}$) which are usually including actual time points. On the other hand, overlined uppercase calligraphic style ($\overline{\mathcal{A}}, \overline{\mathcal{C}}$) is used for sets of time intervals or durations.

All symbols and variables are generally used in the same purpose, which is explained on the following pages. One exception hereof are the variables of Section 3.2. For these, we kept the common notation for simplicity reasons. These variables are explained in their corresponding section of the First Principle Models.

List of Symbols

\triangle	End of a definition, lemma, or theorem
\square	End of a proof

Black Board Symbols

\mathbb{N}	Set of natural numbers (including zero)
\mathbb{R}	Set of real numbers

Greek Symbols

α	Regular signal conduction time through the AV node Present in normal sinus rhythm as well as in all various block types
$\hat{\alpha}_{\#Level}$	Maximum possible conduction constant on a specific AV block level
$\alpha_{2:1}$	Specific conduction constant for which a 2 : 1 block appears
Δ_j	Conduction Increment Varying increment to the basic conduction time in type I blocks
$\Delta_{(n+1):n}$	Specific conduction increment for which a $(n + 1) : n$ block cycles appears
θ	Absolute refractory period
β	Facilitation parameter
$\hat{\beta}$	Facilitation parameter
δ	Facilitation parameter
τ_{rec}	Recovery time constant
τ_{fat}	Fatigue time constant
τ_{fac}	Facilitation time constant

Roman Symbols

A	Atrial level
A_i	Atrial Input - Time point of the i th atrial signal in the considered ECG sector
AA	Atrial Cycle Length - Time interval between two consecutive atrial excitations in case of a regular atrial rhythm
AV	Atrioventricular level
AV_j	Entire conduction time from the atria to the ventricles, at the j th conducted beat within a block cycle.
AV_i^{II}	Input signal time of a specific AV block level, in this case the second, at the i th incoming signal.
AV_j^{II}	Conduction time of a specific AV block level, in this case the second, at the j th conducted signal.
C_m	Membrane capacity
$CS_{1/2}$	Electrograms obtained between the distal pair of electrodes of the coronary sinus catheter
$CS_{3/4}$	Electrograms obtained between the proximal pair of electrodes of the coronary sinus catheter
E_m	Equilibrium potential across a cell's membrane
F	Faraday constant
I_m	Total membrane current
I_i	Current density carried by ions
k	Conducted signal counter within one block cycle
m	Number of incoming signals
n	Number of conducted signals
R	Universal gas constant
T	Absolute temperature (temperature in Kelvin)
t	Time in ms (unless noted otherwise)
V	Ventricular level
V	The difference of the membrane potential from the inside to the outside of the cell (only in Section 3.2)
V_j	Time point of the j th ventricular signal in the considered ECG sector
$VV_j^{I, II}$	Ventricular Interval - The j th ventricular interval within one cycle of a type I, respectively type II block
$VV_n^{I, II}$	Ventricular Block Pause - Produced by the nonconducted signal at the end of every cycle of a type I, respectively type II block

List of Figures

- 1.1 Willem Einthoven using the first table-model electrocardiograph. 6
- 1.2 Werner Forßmann catheterizing himself. 8
- 1.3 Internal anatomy of the human heart. 10
- 1.4 The electrical conduction system of the heart. 12
- 1.5 Action potentials in the different regions of the heart. 17
- 1.6 Action potential of a cardiac muscle cell. 18
- 1.7 Action potential of a sinoatrial pacemaker cell. 19
- 1.8 Placement of the 12-lead ECG electrodes. 20
- 1.9 Exemplary ECG of a normal cardiac cycle. 21
- 1.10 Standard 12-lead surface ECG print of a male athlete. 22
- 1.11 ECG example of typical atrial flutter and atrial fibrillation. 26
- 1.12 Various reentry locations and dimensions of supraventricular tachycardias. 28
- 1.13 Conduction graph from the atria to the ventricles. 29
- 1.14 Approximate area of application of a catheter ablation therapy. 32

- 2.1 Exemplary surface ECGs and intracardiac recordings from AFib and AFlut. 36
- 2.2 Conduction graph of a typical type I block. 40
- 2.3 Conduction graph of a type II block. 43
- 2.4 Conduction graph of an advanced second-degree block. 44
- 2.5 Visual description of a multilevel AV block. 45
- 2.6 5 : 1 2nd-degree AV block described by a MAVB of three consecutive block levels. 48

- 3.1 Mechanisms of the intracellular calcium ion movements. 57
- 3.2 Impact of parameter \hat{g}_{Na} on the solution of Noble equations. 61

- 4.1 Overview of the HEAT software package. 81
- 4.2 Visual description of the AV block process with MAVB at increased atrial rate. 85
- 4.3 Possible level combinations of a MAVB implemented in the HEAT Algorithm. 93

- 5.1 Diagnostic workflow of our approach. 105
- 5.2 ROC curve of RR interval periodicity test and Poincaré Plots of the HRV. 109
- 5.3 Solutions computed with the recovery curve model of Shrier. 111
- 5.4 Classical linear model and wrong recovery curve conduction mechanism. 112
- 5.5 Atrial Flutter from Knight et al. correctly diagnosed by HEAT. 113
- 5.6 MAVB 2a solution calculated by the HEAT Algorithm of Kosowsky's "Figure 1". 114
- 5.7 MAVB 2a solution calculated by the HEAT Algorithm of Slama's "Figure 1". 115
- 5.8 MAVB 2b solution calculated by the HEAT Algorithm of Slama's "Figure 4". 116
- 5.9 MAVB 2b solution calculated by the HEAT Algorithm extracted from Masé. 118
- 5.10 One level solution calculated by the HEAT Algorithm of Morrison's Figure 3a. 119
- 5.11 MAVB 2c computed by the HEAT Algorithm. 120
- 5.12 MAVB 2c block with one level changing from active to inactive. 121

- 5.13 MAVB 3 computed by the HEAT Algorithm. 122
- 5.14 MAVB 3 computed by the HEAT Algorithm. 123
- 5.15 Solution spreading of the objective function values of the HEAT Algorithm. 124
- 5.16 ROC curve of the HEAT Algorithm. 125

- B.1 HEAT solution of Kosowsky's ECG "Figure 4". 133
- B.2 HEAT solution of Slama's ECG "Figure 2". 134
- B.3 HEAT solution of Slama's ECG "Figure 5a". 134
- B.4 HEAT solution of Slama's ECG "Figure 5c". 135
- B.5 HEAT solution of Slama's ECG "Figure 7f". 135
- B.6 HEAT solution of Slama's ECG "Figure 7e". 136
- B.7 MAVB 2a calculated by the HEAT Algorithm of an AFlut example. 137
- B.8 MAVB 3 calculated by the HEAT Algorithm of an AFlut example. 138

List of Tables

- 1.1 Conduction velocity and pacemaker rate of the cardiac conduction system. 14
- 1.2 Standard limb leads. 20

- 3.1 Basic variables and descriptions for a classical AV block type model. 64
- 3.2 Additional variables and descriptions for a recovery curve model. 67
- 3.3 Basic variables and definitions for the combined multilevel model. 71

- 4.1 Diagnosis variety of the different algorithms. 79
- 4.2 Possible input data for discrimination between AFlut and AFib. 79
- 4.3 Feasible sets of the combined multilevel model parameters. 87

- 5.1 Outcome possibilities of the diagnostic test. 107
- 5.2 ECGs presented by Slama and used as validation data set for the HEAT Algorithm. 117

- 6.1 HEAT Algorithm applied on various data sets. 129
- 6.2 HEAT Algorithm compared to other approaches. 129

List of Acronyms

A	atria
ACC	American College of Cardiology
AFib	atrial fibrillation
AFlut	atrial flutter
AH	atrial-His
AHA	American Heart Association
AN	atrionodal
AP	action potential
ARP	absolute refractory period
AT	atrial tachycardia
ATP	adenosine triphosphate
AV	atrioventricular
aVF	augmented voltage foot
aVL	augmented voltage left
aVR	augmented voltage right
AVNRT	AV nodal reentry tachycardia
AUC	Area Under the Curve
CL	cycle length
CS	coronary sinus
DC	direct-current
e.g.	for example (<i>exempli gratia</i>)
ECG	electrocardiogram
et al.	and others (<i>et alii</i>)
FDA	U.S. Food and Drug Association
FP	false positive
FN	false negative
FRP	functional refractory period
H	His
HD	Heidelberg
HEAT	Heidelberg Electrocardiogram Analysis Tool
HES	Hannover ECG System
HV	His-ventricular
HRA	high right atrium
HRV	heart rate variability
i.e.	that is (<i>id est</i>)
ICD	implantable cardioverter defibrillator
IC	intracardiac
LA	left arm

LL	left leg
LSQ	method of least squares
MAE	mean absolute error
MAVB	Multilevel AV Block
n.a.	not available
N	nodal
NH	nodal-His
NMSE	normalized mean squared error
PAC	Premature Atrial Contraction
PJC	Premature Junctional Contraction
PVC	Premature Ventricular Contraction
PV	pulmonary vein
PVI	pulmonary vein isolation
RA	right arm
RMSE	root mean squared error
RFA	radiofrequency ablation
ROC	receiver operating characteristic
RRP	relative refractory period
RVA	right ventricular apex
S	stimulation
SA	sinoatrial
SR	sarcoplasmic reticulum
STFT	short-time Fourier transform
SV	spatial velocity
SVT	supraventricular tachycardia
TP	true positive
TN	true negative
V	ventricles
VT	Ventricular Tachycardia
WHO	World Health Organization
WPW	Wolff-Parkinson-White